Seismic Upgrade of Flat-Plate Slab-Column Connections using Carbon Fiber Reinforced Polymer Stirrups

by

Andrew D. Stark, B.A., B.S.

Thesis

Presented to the Faculty of the Graduate School of

The University of Texas at Austin

in Partial Fulfillment

of the Requirements

for the Degree of

Master of Science in Engineering

The University of Texas at Austin

August, 2003

Seismic Upgrade of Flat-Plate Slab-Column Connections using

Carbon Fiber Reinforced Polymer Stirrups

Approved by
Supervising Committee:

Oguzhan Bayrak, Supervisor

James O. Jirsa

To my parents for their love and support over the years

Acknowledgements

Dr. Oguzhan Bayrak, of the University of Texas at Austin, supervised this research project. Dr. Bayrak provided me with the opportunity to work with him at Ferguson Structural Engineering Laboratory. His advice, research proficiency and personable nature have made working on this project an invaluable experience. It has been a pleasure working with him.

I gratefully acknowledge my fellow research colleague Baris Binicci, Ph.D. candidate at the University of Texas at Austin. Baris shared his knowledge and assistance over many blackboard sessions, long days in the lab and late nights with the data acquisition system. I am indebted to him for all he has offered throughout the duration of this research project.

Dr. James O. Jirsa, of the University of Texas at Austin, was the second reader for this study. Dr. Jirsa's expertise in reinforced concrete flat-plate structures and earthquake engineering has truly aided the development of this thesis.

I would like to thank the Ferguson Structural Engineering Laboratory staff for their assistance. Blake Stasney, Mike Bell, and Denis Fillip and Eric Schell

Abstract

Seismic Upgrade of Flat-Plate Slab-Column Connections using Carbon Fiber Reinforced Polymers

Andrew D. Stark, Master's of Science in Civil Engineering

The University of Texas at Austin, 2003

Supervisors: Dr. Oguzhan Bayrak

Flat-plate concrete structures provide an economical structural system that is unique to concrete. However, the slab-column connections can exhibit brittle behavior under lateral displacement reversals imposed by strong ground motions. Brittle behavior is exacerbated when the gravity shear load is greater than or equal to 40% of the connection shear capacity. The addition of carbon fiber reinforced polymer (CFRP) stirrups positioned radially around the slab-column interface is an effective way of increasing the drift capacity and ductility of the connection.

Tests have been conducted at the University of Texas at Austin studying the behavior of flat-plate slab-column connections. Test specimens were square having 2.44 m lengths, 114 mm thickness, and a 305 mm square column. Connections were upgraded by stitching CFRP stirrups in two different patterns around the slab-column interface through cored holes in the slab thickness; a novel technique developed during the course of the research summarized herein. Any remaining voids were filled with two-part epoxy. Specimens were tested

under combined gravity and lateral loads. A hydraulic ram and load maintainer were used to simulate gravity load conditions. Lateral displacement excursions were imposed using a hydraulic actuator.

During the tests, flexural cracks were observed in a patterns around the slab-column interface, on each specimen. Punching shear failure initiated in the control specimens at lateral drift-ratios of 2.3% and 2.4%. Upgraded specimens had significant flexural yielding at lateral drifts of 8%, and did not fail in shear. In some specimens, the lateral load displacement ductility factor increased up to 200% and the joint rotation ductility factor increased up to 350%, when the slab-column connection was upgraded. The energy dissipated in CFRP upgraded slab-column connections were more than 10 times greater than that dissipated in the control specimen. It was concluded that the innovative CFRP stirrup upgrade technique of slab-column connections, developed during the course of the study, was structurally effective.

Table of Contents

ix

List of Tables

List of Figures

CHAPTER 1

Introduction

1.1 INTRODUCTION

Flat-plate reinforced concrete structures are unique structural systems. These systems consist of slabs supported by columns, and are ideal for residential or office occupancy because floor-to-floor inter-story heights are low and construction economy is high. The gravity load design of flat-plate structures is well understood; however, when subjected to earthquake induced lateral loads, slab-column connection behavior is not clearly understood. Furthermore, methods to upgrade or rehabilitate deficient slab-column connections are not well established. There is a clear need to develop simple and reliable upgrade techniques for deficient slab-column connections, where a major design concern is preventing a punching shear failure at the slab-column interface. Preventing punching shear failure is paramount because this brittle failure mechanism can lead to the progressive collapse of flat-plate structures.

When subjected to earthquake induced reversed-cyclic lateral loads, flat-plate structures can exhibit brittle behavior. Flat-plate structural systems are flexible and generally have low energy dissipation capacities. When a seismic event occurs, inclined shear cracks may form through the slab, around the slab-column connection, due to reversed-cyclic lateral displacement excursions. This type of loading degrades slab-column connections, and can initiate a punching shear failure. Punching shear failure occurs more rapidly when the gravity shear stress acting on the connection approaches $0.133\sqrt{f_c^{'}}$ MPa ($1.6\sqrt{f_c^{'}}$ psi) [23]. An increase in gravity load is critical for interior connections because it places the

greatest amount of shear stress on these connections. It is therefore imperative to control lateral displacement of flat-plate structural systems or provide shear reinforcement at the slab-column connections to allow displacements to increase without affecting shear capacity.

1.2   STATEMENT OF THE PROBLEM

Flat-plate structural systems have exhibited brittle seismic response during past earthquakes. This is evidenced by the Baybridge Office Plaza collapse during the 1989 Loma Prieta Earthquake [18] and the Bullocks Department Store collapse during the 1994 Northridge Earthquake [19].   In regions of high seismic risk, flat-plate structural systems are considered primary lateral force resisting system (LFRS) only in low-rise construction, but can be coupled with moment frames or shear walls in other cases. In moderate to low seismic regions, the primary LFRS (in coupled structural systems) is assumed to resist seismic induced lateral loads; so, flat-plate components have been designed considering gravity load conditions only. However, sufficient slab-column ductility is needed to undergo lateral displacements imposed by a seismic event. This may be a problem for flat-plate floor systems coupled with special moment resisting frames in regions of high seismicity, because significant lateral displacement capacity is needed due to the flexibility of the structural system. The seismic performance of some flat-plate structures built in the 1960s and 1970s reflected the omission of lateral displacement effects on slab-column connections in coupled, flat-plate structural systems.

To address known seismic deficiencies, ACI 318-95 [2] included prescriptive detailing requirements and placed vertical load limits on flat-plate framing systems. However, methods to upgrade or rehabilitate existing deficient flat-plate structures are not well defined. FEMA 310 [11] and FEMA 356 [12]

2

are documents that assist with the evaluation existing structures and guide the retrofit design process. Many deficient flat-plate structures exist, however mitigation is only required when deficiencies are identified due to a change in occupancy. When rehabilitation is warranted, loads defined by the FEMA 356 provisions could possibly lead to a change in the original design loads. This reflects changes in maximum earthquake ground motion maps by NEHRP [22], in 1997. Imposing larger unbalanced moments on an existing flat-plate structure may require increased slab-column connection capacity, even when flat-plate moment frames are not the primary lateral force resisting system.

Current methods of locally upgrading flat-plate slab-column connections can be complicated and change the dynamic response of the original structure. Providing shear reinforcement at slab-column connections can help mitigate punching shear failure. Typical connection upgrades involve attaching steel plates around the slab-column interface or adding concrete to the columns below the bottom slab face. However, constructing these systems to be compatible with the existing structure is complex and in turn, expensive. In addition, these methods can increase the overall stiffness of an existing structure, which may lead to increased seismic design loads. A simple method of providing shear reinforcement to flat-plate slab-column connections that does not significantly change the seismic response of the structure is therefore needed.

1.3   OBJECTIVES OF THE STUDY

The objectives of this study are as follows:

- Study the inelastic behavior of flat-plate slab-column connections designed according to ACI 318-02 and ACI 318-63 requirements and assess the impact of continuous compression reinforcement in slab-column

connections on the seismic response and residual gravity load carrying capacity of each system;

- More specifically, to perform an evaluation of interior, flat-plate, slab-column connections, upgraded with CFRP stirrups, under the maximum gravity shear stress permitted by section 21.12.6.8 of ACI 318-02, for seismic applications.

1.4   THESIS ORGANIZATION

Four test specimens were constructed to accomplish the objectives of the study. Each test specimen had equivalent dimensions, designed at half-scale from a prototype structure. Test specimens included two control specimens, denoted C-02 and C-63, and two specimens with upgraded connection regions, denoted A4-S and B4-S. The design and construction of the test specimens will be discussed in chapter 2.

The test setup was constructed such that seismic loading conditions could be simulated. Each test specimen was subjected to a constant gravity shear load applied in combination with progressively increased lateral drift-cycles that simulated seismic load conditions. The shear due to applied gravity load was equal to forty percent of the two-way shear resistance provided by concrete at the critical perimeter of the control specimens in this study. All specimens were instrumented to measure and record the displacements, rotations and loads that acted on the structure during testing. The test protocol of this study is further discussed in chapter 3.

Results from the slab tests are presented and discussed in chapter 4. Lateral load-displacement behavior, unbalanced moment-connection rotation behavior and residual gravity load capacity of the test specimens are discussed. Evaluation of each specimen was based on strength and stiffness degradation and

4

a set of ductility parameters defined in chapter 4. A summary and conclusions will be presented in chapter 5.

1.5 PREVIOUS RESEARCH

Many experiments have been performed flat-plate connection response to gravity and lateral loads. Previous research has lead to the development of current design guidelines and procedures. An extensive review of literature revealed the fact that no experiments have been performed on interior slab-column connections upgraded using carbon fiber shear stirrups. The background, design principals and a literature survey of simulated seismic testing of flat-plate slab-column connections will now be discussed.

1.5.1 Background Information

Design provisions for flat-plate structural systems are presented in ACI 318-02 [1] and the ACI-ASCE Committee 352 Report [4]. These documents provide a basis for determining the limit states of two-way slab systems. Moehle, Kreger and Leon [20] presented commentary on the ACI-ASCE Committee 352 Report as it applies to slab-column connection design. This paper discussed the differences between beam-column and slab-column joints, and design recommendations were offered. The content of these documents will be further discussed in this section because the information directly relates to the current study.

The connection region of flat-plate structural systems differs from that of beam-column framing. A typical beam-column joint is defined as the volume of concrete common to both the beam and column. In flat-plate structural systems, the shared volume of concrete between the slab and column is small and very well confined, so joint failure is not common [20]. Therefore, assuming the columns are properly detailed, the weak link of flat-plate connections is at a perimeter

located at a distance from the face of column. Section 11.12.1.2 of ACI 318-02 defines the critical perimeter for two-way slabs, b_o, to be located half the depth of the slab, $d/2$, from the face of the column. The connection region in flat-plate construction is therefore the volume of slab contained within the critical perimeter and common to the column and slab. The slab-column connection region and critical perimeter are shown in Figure 1.1 (a) and (b).

(a) Slab-column connection region

(b) Critical perimeter
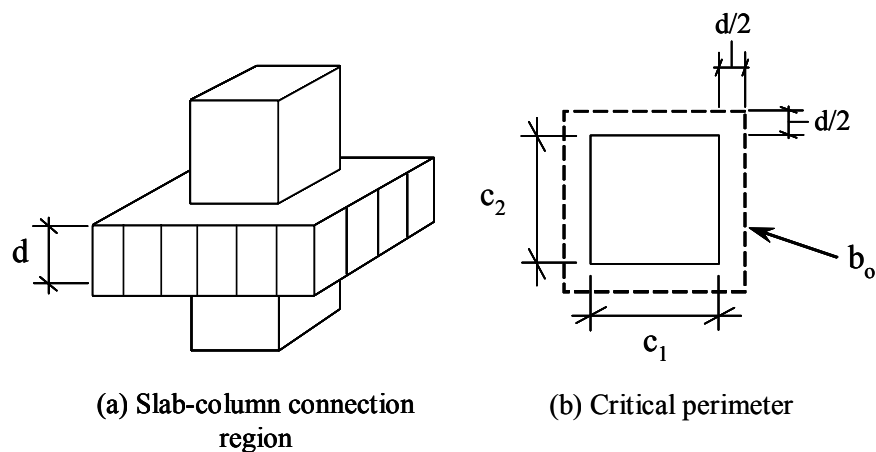
Figure 1.1 (a) Slab-column Connection Region and (b) Critical Perimeter

The two-way shear resistance provided by concrete at the critical perimeter is defined by three equations in section 11.12.2.1 of ACI-318-02, defined in equations (1.1) through (1.3).

$$V_c = \left(2 + \frac{4}{\beta_c}\right) \cdot \sqrt{f_c'} \cdot b_o \cdot d \qquad\qquad (1.1)$$

$$V_c = \left(2 + \frac{\alpha_s d}{b_o}\right) \cdot \sqrt{f_c'} \cdot b_o \cdot d \qquad\qquad (1.2)$$

$$V_c = 4 \cdot \sqrt{f_c'} \cdot b_o \cdot d \qquad\qquad (1.3)$$

Where,

f_c' = concrete strength (psi);

b_o = two-way slab critical perimeter;

d = slab depth;

β_c = ratio of c_1 to c_2 (see Figure 1.1(a)); and,

α_s = 40 for interior columns, 30 exterior columns and 20 edge columns.

The shear demand at each column location in a flat-plate structure must be less than the minimum shear resistance provided by equations (1.1) through (1.3). For the square, interior slab-column connections, slab and column dimensions used in this study, equation (1.3) governs shear strength.

Gravity loads and unbalanced moments influence shear demand acting on slab-column connection regions. Shear stresses develop on the face of the critical perimeter from gravity loads acting within the tributary area of a slab-column connection region, as shown in Figure 1.2(a). When unbalanced moment is present, shear stresses are distributed along the critical perimeter. This distribution is assumed to be linear and increases the magnitude of the stress acting on the connection region, as displayed in Figure 1.2(b) [20].

(a) Stress distribution from gravity loading

(b) Stress distribution from combined gravity loads and unbalanced moments
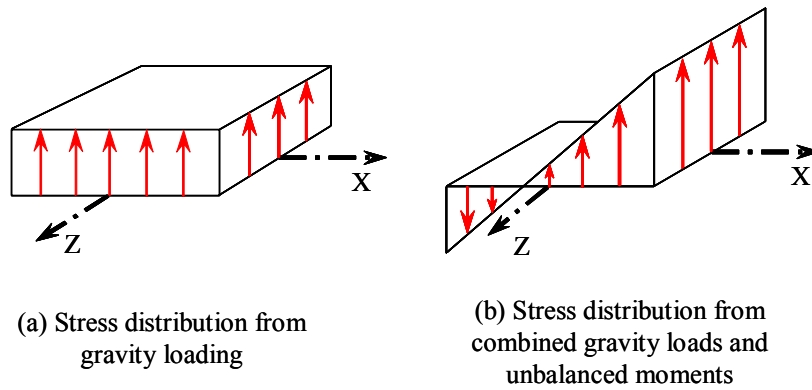
Figure 1.2 Vertical Stress Distributions acting on a Two-Way Slab at the Critical Perimeter

Section 11.12.6.2 of ACI 318-02 defines the shear demand acting on a flat-plate slab-column connection due to combined gravity load and unbalanced moment. This is shown in equation (1.4).

$$v_n = \frac{V_g}{b_o \cdot d} + \frac{\gamma_v \cdot M_{u_x}}{J_{c_x}} + \frac{\gamma_v \cdot M_{u_z}}{J_{c_z}} \qquad (1.4)$$

$$\gamma_v = 1 - \frac{1}{1 + \frac{2 \cdot \sqrt{\beta_{cr}}}{3}} \qquad (1.5)$$

Where,

v_n = shear stress

V_g = gravity shear force acting on the connection;

M_{ux}, M_{uy} = unbalanced moments acting about the x-axis and y-axis;

J_{cx}, J_{cy} = property of the critical section similar to the polar moment of inertia (section R11.12.6.2 of ACI 318-02);

C = perpendicular distance from the edge of the critical perimeter to the centerline of the column;

γ_v = portion of unbalanced moment (acting on critical region) transferred in shear;

β_{cr} = ratio of the perpendicular lengths of the critical perimeter.

Equation (1.4) assumes the stress distribution created by shear and unbalanced moment transfer varies linearly within the connection. Shear stresses induced by gravity loads are accounted for in the first term in equation (1.4). Unbalanced moment is accounted for in final two terms of Equation (1.4). Mu_x and Mu_z are unbalanced moments acting on the axes shown in Figure 1.2. Biaxial moments are accounted for in Equation (1.4) because tests showed this type of loading adversely affected the shear capacity of flat-plate connections [23]. When unbalanced moments act on a flat-plate connection, a portion of the unbalanced moment is transferred in flexure, γ_v, and the remaining unbalanced moment is transferred in shear, γ_v. γ_v is defined in equation (1.5) and varies based on the aspect ratio of the critical perimeter of the slab-column connection. For square columns, γ_v is equal to 0.4

The gravity shear acting on the flat-plate connections should be limited for use in seismic design. Tests have shown, [23], the amount of gravity load acting on a flat-plat slab-column connection directly affects lateral load response of flat-plate structures. As the ratio of V_g/V_o increases, the lateral deformation capacity of flat-plate connection decreases. For this reason, section 21.12.6.8 limits the V_g/V_o ratio to 40%.

1.5.2 Simulated Seismic Testing of Flat-Plate Slab-Column Connections

The behavior of flat-plate slab-column connection subjected to combined axial and lateral loads has been widely researched. The research reviewed for this study includes single bay tests on flat-plate connections by Morrison, Hirasawa and Sozen [21], Pan and Moehle [23]; shear reinforced slab-column connections by Islam and Park [15]; and repaired slab-column connections by Ebead and Marzouk [8], Farhey, Moshe and Yankelevsky [10]. The physical properties of each test specimen are listed in Table 1.1 for reference. General test protocol, results and conclusions will be presented. All presented ductility factors are calculated as the ratio of the approximate yield deformation to the deformation corresponding to a 20% decrease in the maximum lateral load, on the descending branch of the average backbone curve (see section 4.3 for further explanation).

Table 1.1 Geometric Properties of Previously Tested Specimens

Researcher	l_1 (in)	l_2 (in)	t (in)	d_{ave} (in)	c_1 (in)	c_2 (in)	h (in)
Morrison and Sozen	72	72	3.11	2.36	12	12	44
Pan and Moehle	144	144	4.84	4.07	10.8	10.8	72
Islam and Park	108	90	3.5	2.75	9	9	60
Ebead and Marzouk	74.8	74.8	5.9	5	9.8	9.8	61.8
Farhey, *et al*	106	106	3.1	2.64	7.9	11.8	62.2

*1 in = 25.4 mm

1.5.2.1 Morrison, Hirasawa and Sozen [21]

Interior flat-plate slab-column assemblages were tested by Morrison, Hirasawa and Sozen [21]. The effect of the amount of longitudinal steel on seismic response was investigated. Specimens were constructed at one-third scale of a prototype structure, with the dimensions listed in Table 1.1. Reinforcement ratios varied from 0.5-1.3% for the specimens in this study. Specimens were tested vertically, where a steel beam having three hinges was attached to the ends

of each specimen, connected to the laboratory floor using vertical struts. A horizontal actuator was positioned at the top of the column to apply lateral load. Each specimen was loaded laterally until failure, with two specimens having an additional gravity shear load of 14.3 kN (3.2 kips) and 28.6 kN (6.4 kips), corresponding to V_g/V_o ratios of 0.05 and 0.15.

Results showed increasing ρ did not increase the lateral load capacity of the connection. As ρ increased over 1%, the resulting unbalanced moment was less than that calculated using the effective width defined in ACI 318 code. Furthermore, tests showed that there was a limit to the effectiveness of the connection to resist lateral loads. At connection rotations greater than 0.03 radians, it was noted that cracking was significant and punching failure occured. It was also reported that the addition of dead load acting on the column reduced the lateral load and deformation capacities, but no correlation was developed.

1.5.2.2 *Pan and Moehle [23]*

Pan and Moehle [23] conducted biaxal lateral load tests of flat-plate connections under variable gravity loads. Test specimens were constructed at 40% scale of a prototype structure (to conform to laboratory dimensions), having a reinforcement ratio of 0.72% across the ACI effective width. Specimens were positioned on supports consisting of four vertical struts connected directly to the slab edges. Gravity load was applied by stacking lead blocks on top of the slab face until the desired slab-column connection shear was attained. Lateral load was applied using horizontal actuators, in perpendicular directions, at the top of the column. Specimens were tested at V_g/V_o ratios of 22% and 35%.

The key finding in these tests was that the level of applied gravity load on flat-plate connection was one of the most influential factors that affected the lateral deformation capacity of the connection. As the ratio of V_g/V_0 approached

0.4, flat-plate slab-column connections exhibited poor ductility when subjected to both biaxial and uniaxial lateral loads. Results showed that reducing V_g/V_0 from 0.4 to 0.2 resulted in an increased drift capacity of 200%. The increased gravity load also produced more flexural cracks around the connection, prior to lateral loading. This was found to reduce the lateral stiffness, and confirmed a one-third stiffness reduction factor recommended by Vanderbuilt and Corley [28].

1.5.2.3 Islam and Park [15]

Islam and Park [15] performed flat-plate connection tests reinforced with cranked bars, shear-heads and closed stirrups. Specimens were constructed at half scale from a prototype structure, with dimension listed in Table 1.1 and reinforcement ratios of 1.07%. The test frame consisted of attaching beams to the slab edges transverse to the direction of loading and connecting the beams to the laboratory floor using four vertical struts. Unbalanced moment on the slab-column connection was simulated by displacing vertically paired struts in opposite directions. Gravity loads were applied by suspending 200 lb (890 N) blocks from the top face of the slab, corresponding to a 25% V_g/V_o ratio.

Results showed that test specimens had an increase in unbalanced moment capacity, but no significant increase in ductility, when reinforced with cranked bars and shear-heads. However, connections reinforced with closed stirrups showed increased ductility and strength. The addition of closed stirrup shear reinforcement had two benefits: *(i)* they provided additional shear strength to the slab-column critical section; and, *(ii)* they confined longitudinal reinforcing bars, which increased available ductility. Cranked bars and shear heads did not perform either function. They provided supplementary longitudinal reinforcement to strengthen the specimens, but did not supply shear resistance

12

when the diagonal tension cracks formed across the critical perimeter due to reversed-cyclic loading.

1.5.2.4 Ebead and Marzouk [8]

Ebead and Marzouk [8] performed simulated seismic tests on specimens with repaired flat-plate connections. Longitudinal reinforcement ratios of 0.5 – 1.0% were used, with dimensions defined in Table 1.1. Specimens were repaired by coring holes and bolting steel plates to each side of the slab. Epoxy was injected into the holes to achieve continuity. Specimens were tested with the columns positioned horizontally. A steel frame provided reaction points for the applied gravity and simulated lateral loads. Two vertical actuators applied opposing loads to each end of the column to generate unbalanced moments. The tests were performed with a gravity load equal to 50% of the shear capacity of the control specimen.

Test results showed an increase in drift capacity up to 76% when specimens were repaired by fixing steel plates around the slab-column connection. This repair system also improved the energy dissipation capacity of the slab-column connection. The unbalanced moment capacity of the repaired specimens increased 15% over the control specimens in the study. However, the additional steel plates increased the initial stiffness of the repaired specimens 1.7 times that of the average control specimen stiffness.

1.5.2.5 Farhey, Moshe and Yankelevsky [10]

Farhey, Moshe and Yankelevsky [10] tested a method for repairing severely damaged flat-plate connections. Test specimens were constructed at two-thirds scale of the model structure, with a reinforcement ratio of 0.58% over the ACI effective width. Test specimens were supported by channels along the edges transverse to the direction of loading and supported by vertical struts. Gravity and

13

lateral loads were then applied to the bottom column section. Four unrepaired specimens were constructed and tested until failure. Cracked and crushed concrete was then removed from the specimen, the column was straightened and concrete was replaced. One-half inch holes were drilled through the slab thickness for bolting steel plates. After fixing the plates, voids between the steel and concrete were caulked so pressure injected so epoxy could be applied. Initially, V_g/V_o ratios of 26% and 30% were applied to the test specimens, increasing to 50% after the specimens were repaired.

Test results showed that the unbalanced moment capacity was three times greater than that of the initial specimens, with an applied V_g/V_o ratio at 0.5. Initially, test specimens exhibited punching shear failures at drift ratios of 0.8-1.0%. Repaired specimens did not fail when subjected to simulated seismic loading; however, lateral load ceased to be applied at 2.8% inter-story drift, i.e. the researchers ran out of actuator stoke capacity. The greatest lateral stiffness increase was 4 times that of the initial flat-plate test specimen, as a result of the repair scheme.

1.5.3   Research Significance

Flat-plate connections are susceptible to a punching shear failure when subject to combined gravity and lateral loads. This behavior is exacerbated when the V_g/V_o ratio at the critical perimeter of the connection exceeds 0.4. When large gravity shears are expected, shear reinforcement can be added to strengthen flat-plate connections. The reviewed methods of upgrading and repairing flat-plate structures involve the use of large steel plates fastened by steel bolts and epoxy. Other methods of strengthening flat-plate connections involve adding concrete capitols or steel collars to the columns of the structure [13]. Each of these strengthening techniques is complicated and significantly increases the lateral

14

stiffness of the connection. If the lateral stiffness of the connection is increased, any increase in lateral deformation or connection rotation capacity may be nullified because the seismic loads also increase.   In addition, the lateral deformations of flat-plate structures (caused by a seismic event) may be too large due to the flexibility of the structural system.   Flat-plate structural systems are therefore considered secondary LFRS in high seismic risk regions.   However, when a flat-plate structural system is considered secondary LFRS, the slab-column connection must have the lateral displacement capacity to displace with the structure during a seismic event. A simple method of increasing the shear strength and lateral displacement capacity of existing flat-plate structures, without significantly increasing the lateral stiffness of the original system, is therefore needed.

CHAPTER 2

Test Specimens

2.1 INTRODUCTION

In chapter 2, the design and construction of the test specimens in the study is described. A prototype structure was designed after which the test specimens are modeled. Specimens were then constructed to complete the experimental phase of the study.

2.2 PROTOTYPE STRUCTURE

A four-story, flat-plate concrete structure, located in a moderate seismic zone, was chosen as the prototype structure. The IBC 2000 [14] was the building code were used to define loads acting on the structure and all structural components were designed according to ACI 318-02 [1]. Figure 2.1 shows the plan and elevation of the prototype structure. A 3.1 m (10 ft) floor clear-height was chosen, with column spacing of 4.9 m (16 feet) on center. For the interior frames, gravity and lateral load combinations induced the largest stresses on flat-plate slab-column connections. Detailed calculations can be found in Appendix A.1.

The prototype structure was assumed to have office occupancy, with a live load of 2.39 kPa (50 *psf*) and a partition load of 0.96 kPa (20 *psf*). A trial slab thickness of 203 mm (8 in) was chosen from table 9.5(c) in ACI 318-02 for slabs without drop panels, to determine the dead load of the structure. Preliminary column sizes were chosen such that the column load would be below the balance point of the axial load-moment interaction diagram. This was approximated by

16

designing for 30% of P_o, using a column reinforcement ratio of 1% and a 27.6 MPa (4000 *psi*) concrete strength were assumed.

Plan   **Elevation**

Figure 2.1 Plan and Elevation of Prototype Structure

Load combinations specified by IBC 2000 include effects from dead, live wind and earthquake loads. Because the study was conducted with the specific intention of testing reversed-cyclic lateral loads, the effects of wind are neglected. To calculate design moments, gravity and lateral load cases were analyzed separately and combined in the appropriate load combination.

Gravity moments were calculated using the Direct Design Method in section 13.6 of ACI 318-02. IBC 2000 was used to calculate lateral loads. Seismic accelerations were chosen from the NEHRP *Maximum Earthquake Ground Motion* maps [22], near St. Louis, MO. This resulted in a seismic design category classification of C, so the equivalent lateral force procedure could be used to calculate and distribute lateral story shears. Earthquake moments were computed using a two dimensional interior frame, modeled in SAP 2000 [27]. Column properties were chosen from the dimensions specified in the preliminary

calculations. Beams were modeled using an effective slab width derived by Pecknold [24], and a thickness as specified by ACI 318-02.

Prototype structural components were designed using ACI 318-02. Slab thickness was determined from the preliminary calculations. Concentric punching shear was checked at an interior connection for the load combination considering dead and live loads. Sufficient shear resistance was provided by the minimum slab thickness specified in table 9.5(c) in ACI 318-02, so the final slab thickness was chosen to be 203 mm (8 in).

Reinforcement ratios were determined from the moment envelope developed using the IBC 2000 load combinations. Table 2.1 lists the reinforcement ratios for the column and middle strips. The ACI minimum reinforcement ratios controlled the flexural steel design for the middle strip of the top mat of steel and the column and middle strips for the bottom mat of steel. The distance C + 3H is the effective width of the column strip participating in the resistance of unbalanced moment, defined in section 13.5.3.2 of ACI 318-02. Detailing requirements are further discussed in section 2.3.1.

Preliminary column designs were checked to ensure strength exceeded the unbalanced moment. A 508 by 508 mm (20 by 20 in) column with a 1% reinforcement ratio was chosen for the preliminary calculations.

Table 2.1 Prototype Structure Slab Reinforcement Ratios

STEEL LOCATION	SLAB ZONE	DIMENSION (in)*	ρ (%)
TOP STEEL	COLUMN STRIP	96	0.99
	C + 3H	44	1.30
	ONE-HALF REMAINING AREA	26	0.73
	MIDDLE STRIP	96	0.60
	ONE-HALFAREA	48	0.60
BOTTOM STEEL	COLUMN STRIP	96	0.60
	MIDDLE STRIP	96	0.60
	ONE-HALFAREA	48	0.60

*1 in = 25.4 mm

2.3   TEST SPECIMENS

Test specimens were scaled to nominally one-half of the prototype structure. The reinforcement ratios from the prototype structure design (listed in Table 2.1) were used for each test specimen. Control specimen C-63 was detailed according to ACI 318-63 [1] code provisions, where discontinuous longitudinal steel was placed through the connection region. Control specimen C-02 was detailed in accordance with the provisions of section 21.12.6 of ACI 318-02. These provisions are as follows:

(i) 50% of the negative reinforcement of the column strip must be place in a zone (C + 3H) about the column centerline;

(ii) 25% of the negative reinforcement of the column strip must be continuous;

19

(iii) 50% of the positive reinforcement in the middle strip and all of the reinforcement in the column strip must be continuous.

Both upgraded specimens had equivalent details to control specimen C-02. Test specimens A4-S and B4-S included upgraded slab-column connections, where A4 and B4 denote the geometrical configuration of each upgrade pattern. Slab-column connection upgrade design is discussed in section 2.4.

2.3.1 Slab Design

Test specimen slabs were designed and constructed using scaled dimensions of the prototype structure. A slab thickness of 114 mm (4.5 in) was chosen for the test specimen design. An additional 13 mm (0.5 in) was added to the test slab thickness to assure proper concrete placement. The slab lengths were constructed to be 2.8 m (112 in) square. These dimensions included an additional 0.4 m (16 in) of length in each direction from the half-scale, centerline-to-centerline, prototype structure dimensions. The additional slab length was added to provide area to connect each specimen to the laboratory strong floor and to develop the longitudinal bars outside the test region and. The test setup will be further discussed in section 3.2.

Test specimens C-02, A4-S and B4-S were detailed according to section 21.12.6 of ACI 318-02, using the nominal reinforcement ratios specified in section 2.2. All longitudinal reinforcement used in the test slabs was no. 4 bars. Figure 2.2 shows a detail of the bottom and top mats of flexural reinforcement and Table 2.1 lists a rebar schedule. All longitudinal reinforcement was equally placed in perpendicular directions. Flexural steel was developed using a 180 degree hook with a longitudinal bar passing through the center. The additional steel bar passing through the 180 degree hooks is not a code requirement, but was

placed to assure the reinforcement anchorage. This detail is shown in Figure 2.3. Test Specimen C-63 had the same anchorage details as specimens C-02, A4-S and B4-S, except the bottom mats of steel are discontinuous through the column centerlines in both directions. Bottom mat steel reinforcement details for control specimens C-63 and C-02 are shown in Figure 2.4.
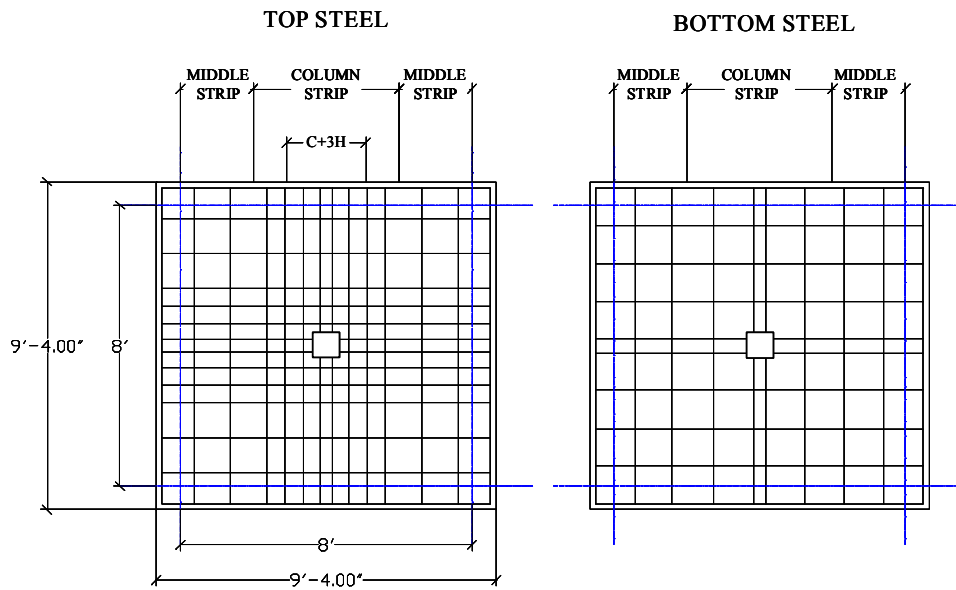
Figure 2.2 Test Specimen Top and Bottom Mats of Longitudinal Reinforcement

Table 2.2 Test Specimen Rebar Schedule

STEEL LOCATION	SLAB ZONE	DIMENSION (IN)*	ρ (%)	NUMBER OF BARS
TOP STEEL	COLUMN STRIP	48	1.03	8
	C + 3H	26	1.42	6
	ONE-HALF REMAINING	11	0.56	1
	MIDDLE STRIP	48	0.51	4
	ONE-HALFAREA	24	0.51	2
BOTTOM STEEL	COLUMN STRIP	48	0.51	4
	MIDDLE STRIP	48	0.51	4
	ONE-HALFZONE	24	0.51	2

*1 in = 25.44 mm
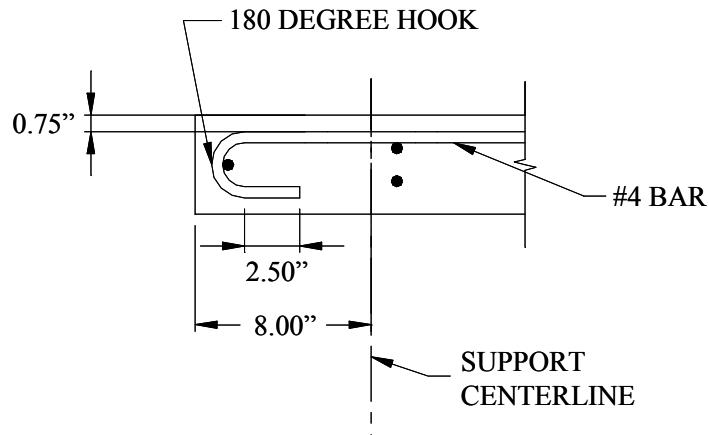
Figure 2.3 Re-bar Anchorage Detail

22

(a)   (a)
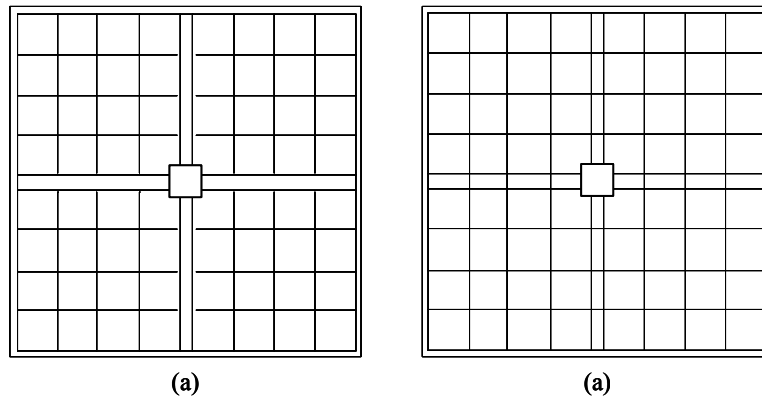
Figure 2.4 Bottom Steel Reinforcement Details (a) Control C-63; and (b) Control C-02

2.3.2 Column

Steel column sections were chosen for the test specimen design. Building monolithic concrete test specimens would have complicated construction because raised formwork and multiple concrete pours would be required. Use of a steel column allowed test specimens to be constructed simply and assembled quickly. The steel columns consisted of a W10x88 welded to a 305 by 305 mm (12 by 12 in) base plate. A W10x88 provided room to weld the section to the base plate and bolt the column section to the concrete slab. Eight bolts were fastened through holes created in each slab to attach the steel columns to the test slabs. This is shown in Figure 2.5. To assure uniform surface, grout was applied to the top slab face prior to positioning the column sections. Bolts were tightened until no visible gaps existed between the bottom column base-plate section and the bottom slab face. Test specimen construction will be further discussed in section 3.4.1.

23

Figure 2.5 Steel Column to Concrete Slab Connection

The steel column section was chosen by matching the stiffness of a typical column in the prototype structure. It should be noted that the use of steel columns in the tests of this study may alter the behavior of the slab-column joint. However, if the overall behavior of a typical test specimen in this study exhibits similar performance compared with monolithic, concrete specimens reported in literature, the value of using steel columns in flat-plate connection tests can be better appreciated. In the following sections, the behavior of steel versus concrete columns for use in flat-plate slab-column testing will be discussed.

2.3.2.1 Sectional Analysis

A 305 by 305 mm (12 by 12 in) concrete column and a steel column with a base plate were chosen as the potential column sections. Figure 2.6 shows a detail of the two cross-sections. The sectional analysis program RCCOLA [25] was used to construct an axial-moment interaction diagram for the concrete column. This is shown in Figure 2.7. Results from sectional analysis showed that a concrete column should remain elastic during the flat-plate connection tests. While each specimen was loaded, the lateral capacity was controlled by the flexural strength of the slab. The unbalanced moment capacity of the slab was

24

calculated to be 51.5 kN-m (456 kip-in), or equivalently, 25.8 kN-m (228 kip-in) applied to each column. This moment was well below the flexural strength of the concrete column sections. Figure 2.7 also displays the moment-axial load interaction controlled by concrete shear strength [25]. This analysis showed that the moment corresponding to the theoretical unbalanced yield moment of the slab was also below the moment causing shear cracking on the potential concrete section, i.e. shear was not critical for this case.
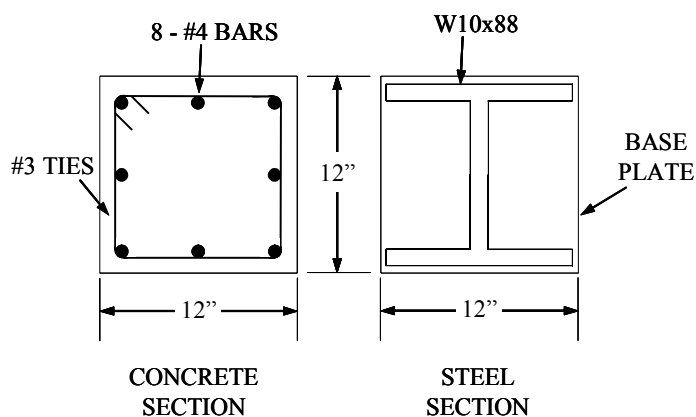
Figure 2.6 Concrete and Steel Column Sections

The cracking moment of the section was calculated to be 15.4 kN-m (136.6 kip-in). At this load level, flexural slab cracking would have a more significant influence on the lateral displacement of the test specimen than the loss in stiffness that occurred from flexural cracking of the column. For the case of the steel column section, the moment generated by lateral loads was below the yield moment of the W10x88 section.

Moment (kip-in)

228 kip-in applied moment based on slab capacity.

— M-N (Initial Section)

— Shear Controlled M-N Interaction

Moment (kN-m)
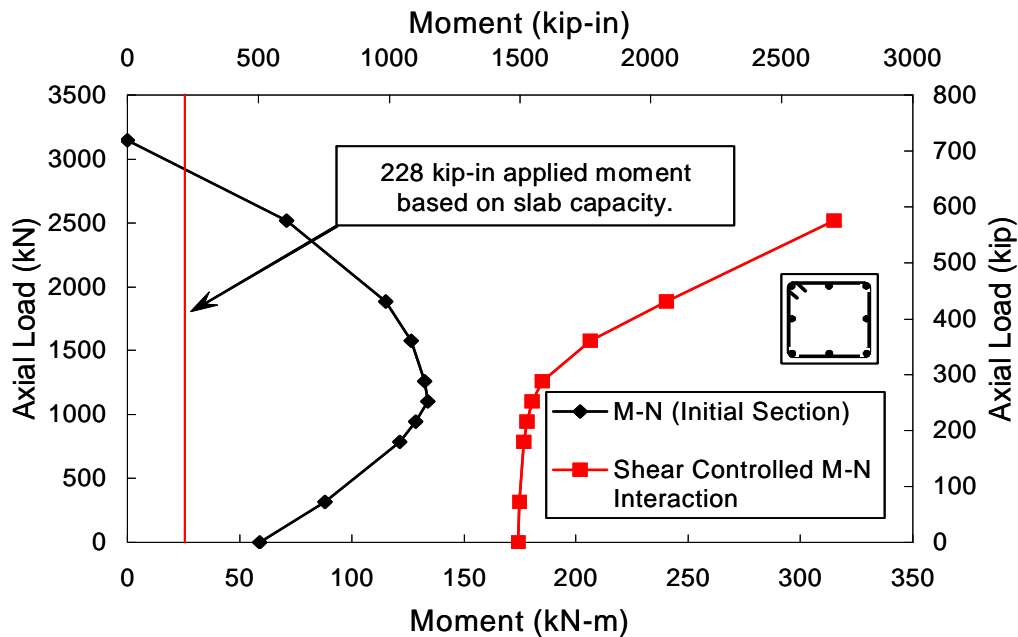
Figure 2.7 Concrete Section Axial Load-Moment Interaction Diagram

2.3.2.2 Stiffness Analysis

SAP2000 Nonlinear [27] was used to model and analyze the lateral stiffness of a test specimen using concrete and steel columns. Slab properties for input to SAP2000 were based on the effective beam width parameters of Pecknold [24], Allen and Darvall [5], and on an explicit transverse torsional model proposed by Cano and Klinger [6]. In each model, the inertia of the uncracked slab section was multiplied by the one-third factor recommended by Vanderbuilt and Corley [28], which accounted for slab cracking and inelastic effects. Model flexibilities were calculated by applying a unit point load to the corresponding position of the lateral ram in the computer model. Flexibilities were verified by hand calculations using the stiffness method. Detailed calculations can be found in Appendix A.2.

Lateral stiffness models using both steel and concrete columns, as well as the backbone curve of control specimen C-02 are shown in Figure 2.8. The elastic behavior of the test specimen with a steel column was accurately modeled by Cano and Klinger's [6] method. The effective width models derived by Allen and Darvall [5] yield close results, but had slightly greater stiffness than the actual results. Table 2.3 lists the differences in each model when using steel versus a concrete column and compares the steel column results with the actual backbone curve. In each case, modeling the initial lateral stiffness of the system with steel column produces 10% to 15% greater stiffness than that of a concrete column. Due to the accuracy of the model of Cano and Klingner [6], the stiffness difference should be closer to 10%. These results show that a steel column should produce greater lateral stiffness, it is also apparent that the slab would control the overall behavior of the test specimen. Reported test results ([15], [20] and [21]) also indicated that minimal column cracking occurred, verified with pictorial evidence.

Table 2.3 Stiffness Differences Between Computer Models and Test Results

Stiffness Model	Percent Stiffness Difference	
	Steel Column vs. Concrete Column	Steel Column Model vs. C-02 Results
Effective Width (Allen and Darvall)	13.4	17.3
Transverse Torsional (Cano and Klingner)	10.5	1.0
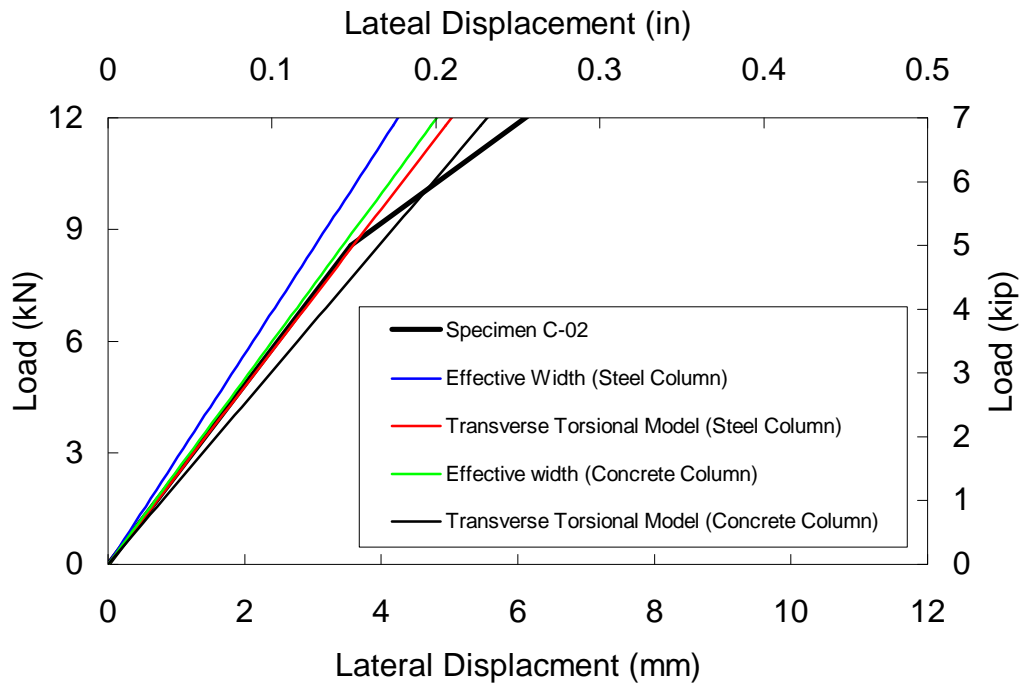
Figure 2.8 Comparison of Modeled and Actual Lateral Load versus Displacement

2.3.2.3 Comparison with Data from Literature

Previous test results have shown that columns of flat-plate connection tests effectively remained elastic. Table 2.4 lists the physical properties from previous flat-plate connection tests. Morrison, Hirasawa and Sozen [21] reported that the columns were much stronger than the slab, negligibly contributing to the lateral displacement of the system. Pan and Moehle [22] stated that the columns remained essentially elastic during tests. Results from Islam and Park [15] stated that cracking at the column slab interface occurred causing increased lateral deformation of the system. However, the reinforced concrete columns remained uncracked along the length of the columns.

Table 2.4 Physical Properties of Reported Interior Flat-Plate Connection Tests

Researcher	l_1 (in)	l_2 (in)	t (in)	d_{ave} (in)	c_1 (in)	c_2 (in)
Current Study	112	112	4.5	3.75	12	12
Morrison and Sozen	72	72	3.11	2.36	12	12
Robertson and Lee	114	78	4.5	3.7	10	10
Researcher	f_y (ksi)	f_c (ksi)	V_g/V_0	t/l_1	c_1/l_1	rho % (l')
Current Study	60	4.5	0.4	0.0469	0.125	1.42
Morrison and Sozen	48.6	4.9	0.035	0.0432	0.167	1.31
Robertson and Lee	60	5.1	0.25	0.0395	0.0877	0.83
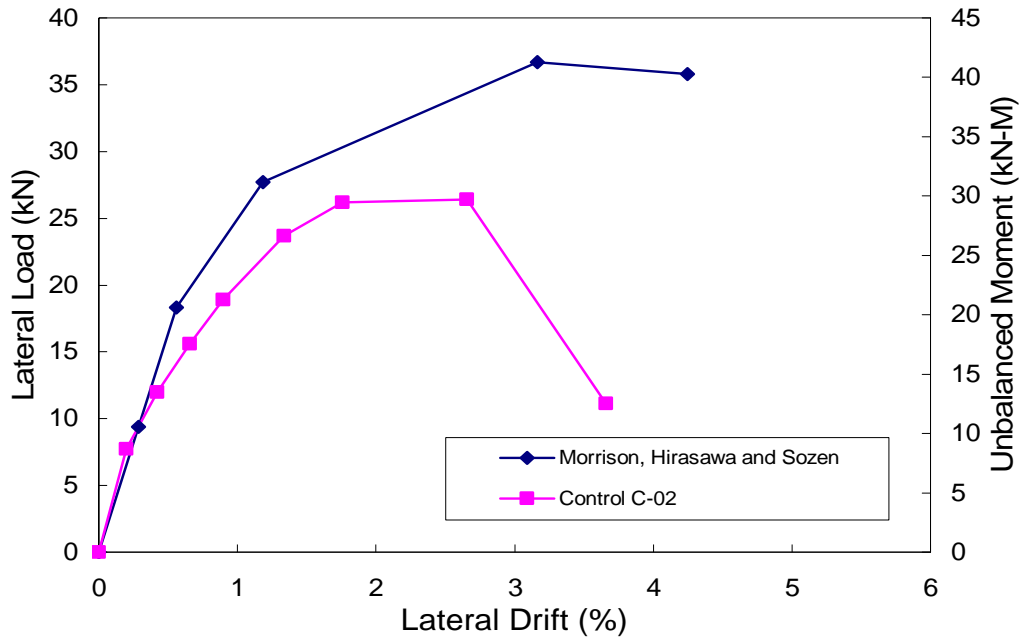
Figure 2.9 Backbone Curve Comparison

Figure 2.9 shows the backbone curves from flat-plate connection tests from Morrison, Hirasawa and Sozen [21], and the present study. The test specimen of Morrison, *et al*, had similar properties to the current study (Table 1.1), but had significantly less gravity shear applied to the specimen. Figure 2.1 shows that the two specimens had similar initial stiffnesses. The backbone curve

29

of the present study had a slightly greater stiffness, which can be attributed to a larger slab thickness to span ratio. The effect of gravity shear was also shown as the backbone curve from the Morrison test specimen did not degrade as rapidly.

The elastic load-deformation cycles from Lee and Robertson [26] and the present study are presented in Figure 2.10. The physical properties of the Lee and Robertson specimen are listed in Table 2.4. Figure 2.10 shows the hysteretic response of each specimen was similar. Area under the load-deformation curves for the first four cycles are listed in Table 2.5. The total energy dissipated through the first four cycles by the test specimen of the present specimen C-02 tested during this study was greater than that of Lee and Robertson by 15%. On the other hand, the V_g/V_o ratio was greater in this study, so more damage, and therefore more energy dissipation, can be expected during the early stages of the test. Also, when significant inelastic deformation occurred, most, if not all, of the energy would be dissipated in the slab. Hence, the differences between the two tests become even smaller.

Table 2.5 Hysteresis Comparisons, First Four Cycles

Cycle No.	Present Study		Hysteresis (kip-inches)‡	Lee and Robertson		Hysteresis (kip-inches)
	Average backbone			Average backbone		
	Load (kips)*	Displacement (in)†		Load (kips)	Displacement (in)	
1	1.93	0.14	0.22	2.02	0.23	0.17
2	2.96	0.28	0.62	3.07	0.38	0.47
3	3.78	0.42	1.01	3.58	0.52	0.69
4	4.54	0.56	1.53	4.66	0.75	1.57
	Total Energy Dissipated		3.37	Total Energy Dissipated		2.90

*1 in = 25.4 mm
†1 kip = 4.448 kN
‡ 1 kip-in = 0.113 kN-m
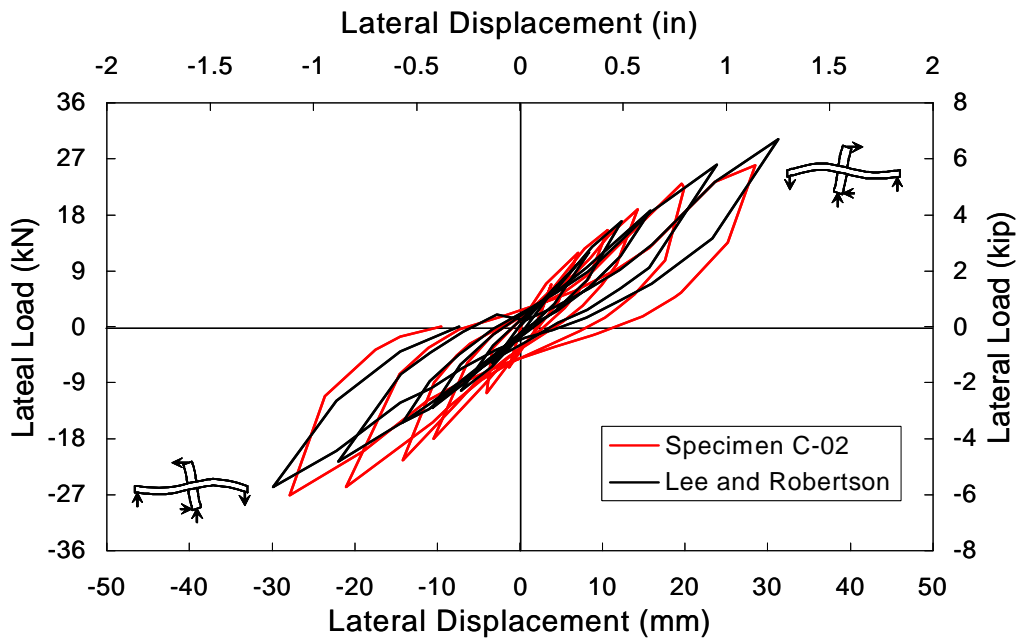
Figure 2.10 Reversed-Cyclic Load-Displacement Comparison, First Four Cycles

Analysis and test results presented above showed that the use of a steel column in flat-plate connection tests was acceptable. Previous tests showed that the lateral strength and stiffness of flat-plate slab-column assemblage was controlled by the behavior of the slab. The critical region of a flat-plate connection was also defined at a distance outside the slab-column interface. Therefore, if the concrete column mostly remains elastic during a flat-plate connection test, the use of a steel column should not significantly affect the behavior of the system.

31

2.4 CONNECTION UPGRADE DESIGN

The strength calculations shown in Appendix A.3 indicated that the interior connections of the prototype structure were punching critical under combined dead and earthquake loads. Therefore, secondary shear reinforcement was provided for test specimens A4-S and B4-S. Carbon fiber reinforced polymer (CFRP) stirrups were added around the column to increase the critical perimeter of the test specimen connections, and to provide secondary reinforcement. Stirrups were added in multiple perimeters, from the face of the column, until the concrete resistance exceeded the applied shear stress due to gravity and lateral loads. The required cross-sectional stirrup area was then determined based on the excess shear acting at the critical perimeter of the control test specimen.

2.4.1 Determining the Required Critical Perimeter

When subjected to combined gravity and lateral loads, the amount of unbalanced moment that acted on the connection controlled the punching shear capacity of the interior flat-plate assemblages. An upper bound connection shear stress could therefore be calculated based on the probable moment capacity of the slab. This capacity design philosophy was similar to that presented for moment frames in chapter 21 of ACI 318-02. In the chapter 21 provisions, beam ends are designed to yield and detailed to provide adequate rotational capacity for the development of plastic hinges. The connection regions of flat-plate structures are not meant to be a primary energy dissipating mechanism in the structure. However, if slab-column connections were designed such that the punching shear stress calculated from the unbalanced flexural capacity of the slab did not exceed the punching shear capacity at the critical perimeter, brittle connection failure could be avoided.

The lateral load capacity of the control test specimen connection was calculated based on flexural capacity and shear-flexure interaction. Detailed calculations are presented in Appendix A.4. Slab flexural and punching shear capacities were calculated by the provisions of ACI 318-02 and compared with the strength provisions of FEMA 356. Table 2.6 shows the lateral load capacities of the control test specimen based on these standards.

Flexural capacity of the slab was calculated based on the effective width of the column strip, and the probable yield strength of the longitudinal reinforcement. The effective width is defined in section 13.5.3.2 of ACI 318-02 as one and one-half times the slab thickness outside the face of the column, and in section 6.5.4.3 of FEMA as two and one-half times the slab thickness. This is shown in Figure 2.11. Two longitudinal bars were located at the extreme edges of the ACI effective width for both top and bottom mats of longitudinal reinforcement, but were included in the probable moment calculation. These bars were included in the calculation to have a conservative shear stress for the upgrade design. The lateral load capacity based on shear-flexure interaction is defined in both standards by equation (1.4). Gravity shear was calculated as 89.4 kN (20.1 kip) and the probable unbalanced moment was equal to 50 kN-m (450 kip-inches).

Table 2.6 Control Specimen Lateral Load Capacity

Strength Provision	Lateral Load Capacity	
	Probable Flexural Capacity (kips)*	Shear-Flexure Interaction (kips)
ACI 318-02	7.6[†]	6.4
FEMA 356	9.5	6.4

*1 kip =4.448 kN

[†] Calculation includes bars at the edge of the specifed effective width

(a)   (b)
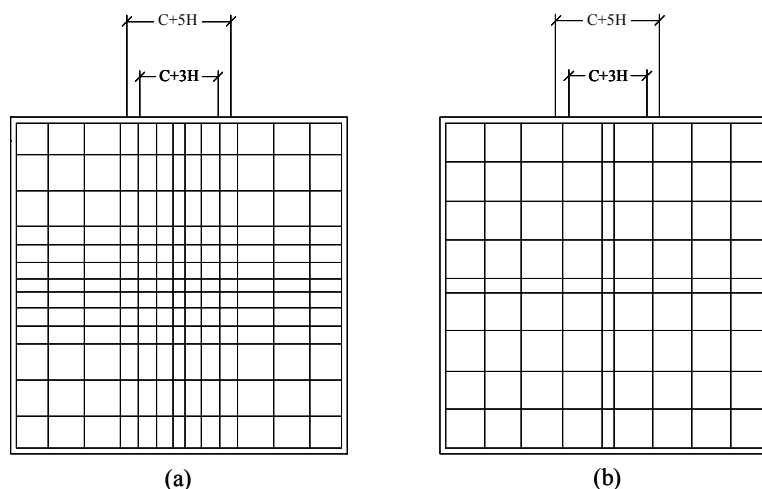
***Figure 2.11 ACI 318-02 and FEMA 356 Effective Width Zones: (a) Top Steel;
and, (b) Bottom Steel***

To upgrade the connection regions of the specimens A4-S and B4-S, CFRP shear stirrups were added in perimeters around the column. Binici and Bayrak [6] performed concentric flat-plate punching tests upgraded with CFRP stirrups, in multiple perimeters, around the slab-column interface. The first externally applied perimeter of CFRP shear stirrups was added to specimens at a distance of one-quarter of the specimen depth, *d/4*, and *d/2*, subsequently. In this study, CFRP stirrup were added in perimeters around the column (in the same

manner) and increased until concrete shear resistance at the critical section exceeded the shear stresses due to combined gravity shear and the probable unbalanced moment.

Shear resistance provided by upgraded connections was defined according to section 11.12.6 of ACI 318-02. The critical perimeter for an upgraded connection was calculated at a distance of *d/2* from the outer-most CFRP stirrup perimeter. Shear resistance provided by concrete was computed using a stress of $2\sqrt{f_c'}$. The shear stress that acted on the upgraded perimeter was calculated using the following equation:

$$v_n = \frac{V_g}{b_o \cdot d} + \frac{\gamma_v \cdot M_{probable} \cdot c}{J_c} \qquad (2.1)$$

The applied gravity shear and probable unbalanced moment were incorporated into equation (2.1), when the applied shear stress was calculated. The parameters J_c, c and b_o were calculated using the critical perimeter corresponding to the number of CFRP stirrup perimeters added to the connection. For upgrade specimens A4-S and B4-S, a total of four CFRP stirrup perimeters were calculated to be sufficient. Table 2.7 lists the shear stress associated with different numbers of externally applied CFRP stirrup perimeters. Calculations are presented in Appendix A.4.

Table 2.7 Shear Stress at Different Upgraded Connection Perimeters

No. of CFRP Stirrup Perimeters	Shear Stress at Upgraded Perimeter (psi)	Provided Shear Resistance (psi)
3	142	
4	116	126
5	98	

*1 psi = 6.894 kPa

2.4.2 CFRP Shear Stirrup Design

Once the number of stirrup perimeters has been defined, the total cross-sectional stirrup area was determined. Two alternate shear stirrup configurations were used to upgrade test specimens A4-S and B4-S. Figure 2.12 shows a sketch of the two upgrade configurations. The amount of required reinforcement was determined from equation (2.1), using the geometric properties of the control specimen, subtracting the concrete resistance.

Layout A4-S   Layout B4-S
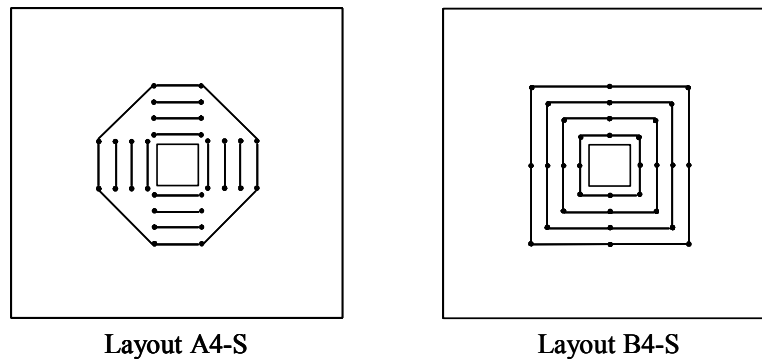
Figure 2.12 Connection Upgrade Configurations

Shear stirrup design calculations are provided in Appendix A.4. Material properties for CFRP shear stirrups can be found in section 2.6.3. An efficiency factor of one-third is applied to the ultimate CFRP strain, $\frac{1}{3} \cdot 0.012$, to be consistent with the previous research finding of Binici and Bayrak [6]. For

concentrically loaded specimens, their research showed CFRP stirrup strain levels should be limited to one-third of the rupture strain to control crack widths and have a reasonable strength contribution from the surrounding concrete. In both connection upgrade configurations, each perimeter contains eight holes through the slab. The thickness of the carbon fiber sheeting used to create the stirrups is 1 mm (0.039 in), which yielded a minimum required CFRP width of 36 mm (1.4 in) for each upgrade configuration.
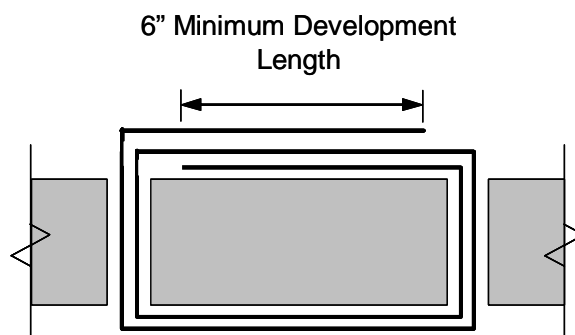
Figure 2.13 Connection Upgrade A4 CFRP Shear Stirrup Detail
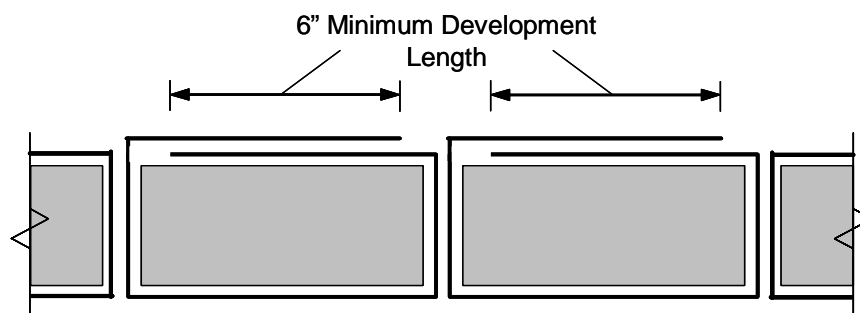
Figure 2.14 Connection Upgrade B4 CFRP Shear Stirrup Detail

19 mm (0.75 in) wide CFRP strips were used to create the stirrups for the upgraded specimen, which required two layers of CFRP per hole in the slab. Based on the geometry of the different connection upgrade layouts, different length CFRP strips must be provided. To create the stirrups for connection

37

upgrade A4-S, CFRP strips were "stitched" two times through each Hole through the slab. This is shown in Figure 2.13. CFRP strips were "stitched" though each Hole through the slab one time in connection upgrade B4-S, shown in Figure 2.14. Once again, this resulted in two CFRP layers per hole. To develop the strength of the CFRP strips, 152 mm (6 in) of additional CFRP material must be overlapped when constructing the stirrups. Table 2.8 lists the CFRP strip lengths for each perimeter of both upgrade layouts. The total amount of carbon fiber used in upgrade A4-S was 0.73 m^2 (0.87 yd^2) and 0.62 m^2 (0.74 yd^2) in upgrade B4-S. Upgrade specimen B4-S required 15% less carbon fiber to complete the connection upgrade. CFRP stirrup construction will be further discussed in section 3.4.1.2.

Table 2.8 Required CFRP Strip Lengths

Upgrade A4-S		Upgrade B4-S	
Perimeter (from column)	Length (in)*	Perimeter (from column)	Length (in)
		1	30
1 through 4	86	2	36
		3	40
Diagonal at 4	32	4	44

*1 in = 25.4 mm

2.5 SPECIMEN CONSTRUCTION

Test specimens were constructed and cast in two groups that consisted of specimens C-02, C63, A4-S and B4-S. As stated in section 2.3.1, each test specimen had the same amount and configuration of reinforcement, and anchorage details, except test specimen C-63. Specimen C-63 had discontinuous, bottom, longitudinal reinforcement, which made it compliant to the ACI 318-63 Code. Conversely, this specimen did not comply with the continuous bottom steel

requirement of section 21.12.6 of ACI 318-02. After formwork was constructed, reinforcing steel was placed and gaged; concrete was then poured.

Connection   Connection
Upgrade A4-S   Upgrade B4-S

Figure 2.15 Connection Upgrades A4-S and B4-S Prior to Casting Concrete

Formwork was built using 20 mm (0.75 in) thick plywood and 50 x 100 mm (2 x 4 in) stud grade wood, constructed to the dimensions specified in section 2.3.1. PVC pipes were positioned in the formwork, which created the appropriate openings in the slab for attaching the spreader beams, column sections and application of CFRP for test specimens A4-S and B4-S. 25.4 mm (1in) diameter PVC was used to create the connection holes for the spreader beams and column sections and 16 mm (0.625 in) PVC was used to create FRP holes. Figure 2.15 shows the connection regions of the upgraded test specimens, where upgrade patterns A4-S and B4-S can be observed. To secure the PVC piping, 50 mm (2 in) holes were drilled into the bottom of the formwork. PVC pipes were then glued into their respective holes using two-part epoxy. After all PVC was

positioned, gaps in the formwork were sealed with caulking and sprayed with form oil.

After the formwork was constructed, longitudinal reinforcing steel was installed. Longitudinal reinforcement was placed in two mats consisting of bars running north-south and east-west direction, tied together in a single mat. 19 mm (0.75 in) chairs were used to provide clear cover for the bottom mat of steel and 76 mm (3 in) plastic chairs were cut to 70 mm (2.75 in) to place the top mat of steel. When the longitudinal reinforcement was placed, four lifting inserts were positioned and strain gages were installed to each specimen. Strain gage placement will be discussed in section 3.3.6 . Figure 2.16 shows a picture of upgrade specimen B4-S, prior to concrete placement.

Figure 2.16 Upgrade Specimen B4-S, Prior to Casting Concrete

Ready-mixed concrete was used in the specimen construction. Upon arrival, slump was checked according to ASTM C143 procedures. Specific mix designs and material properties will be discussed in section 2.6. Concrete was placed using a bucket suspended by an overhead crane and compacted using electric hand vibrators. Slab surfaces were finished using hand and bull floats,

where burlap and plastic sheeting was placed over each specimen for 7 days to retain moisture while the specimens cured.

2.6   MATERIAL PROPERTIES

The materials used in the study are concrete, steel, carbon fiber reinforced polymers (CFRPs) and grout. The following section discusses the properties of each material.

2.6.1   Concrete

Table 2.9 Specified Mix Properties

Capitol Aggregates Mix Specifications				
Mix Design No.	Strength Range (psi)*	Aggregate Size (in)†	Slump (in)	Quantity (yd^3)
227	4000 - 6000	0.75	6	5

*1 psi = 6.89 kPa
† 1 in = 25.4 mm

The concrete mix was designed by Capitol Aggregates of Austin, Texas. A concrete compressive strength of 27.6 MPa (4,000 psi) was used in the prototype and test specimen design. Table 2.9 lists the specified properties given to Capitol Aggregates for the concrete mix.

Sixteen standard 150 mm by 305 mm (6 by 12 inch) test cylinders were made for each specimen in both casting groups. Compression tests conforming to ASTM C39 specifications and split cylinder tests conforming to ASTM C496 were performed to determine the compressive and tensile strength of each cast. The modulus of elasticity was calculated using the definition provided by section 8.5.1 of ACI 318-02. Material test results are shown in Table 2.10.

Table 2.10 Concrete Material Properties

Specimens A4-S and B4-S		Specimens C-02 and C-63	
Property	Mean	Property	Mean
f_c' (psi)*	4482	f'c (psi)	4016
f_t' (psi)	498	ft (psi)	438
E_{ACI} (ksi)†	3816	E_{ACI} (ksi)	3612

*1 psi = 6.89 kPa

† $E_{ACI} = 57\sqrt{f_c'}$

2.6.2 Longitudinal Reinforcement

Longitudinal reinforcing bars for all test specimens had a specified yield strength of 413 MPa (60 ksi) steel and were purchased in a single group, milled from the same heat. Tensile tests were performed according to ASTM A370 to determine tensile properties of the No. 4 reinforcing bars specified in the design. Figure 2.17 shows the stress versus strain relationship for the steel reinforcing bars used in the study and Table 2.11 lists the average material properties.

Table 2.11 Reinforcing Steel Material Properties

Property	Average
f_y (ksi)	65.8
f_u (ksi)	87.6
E (ksi)	29.1
Ultimate Strain (in/in)	0.152

*1 ksi = 6.89 MPa
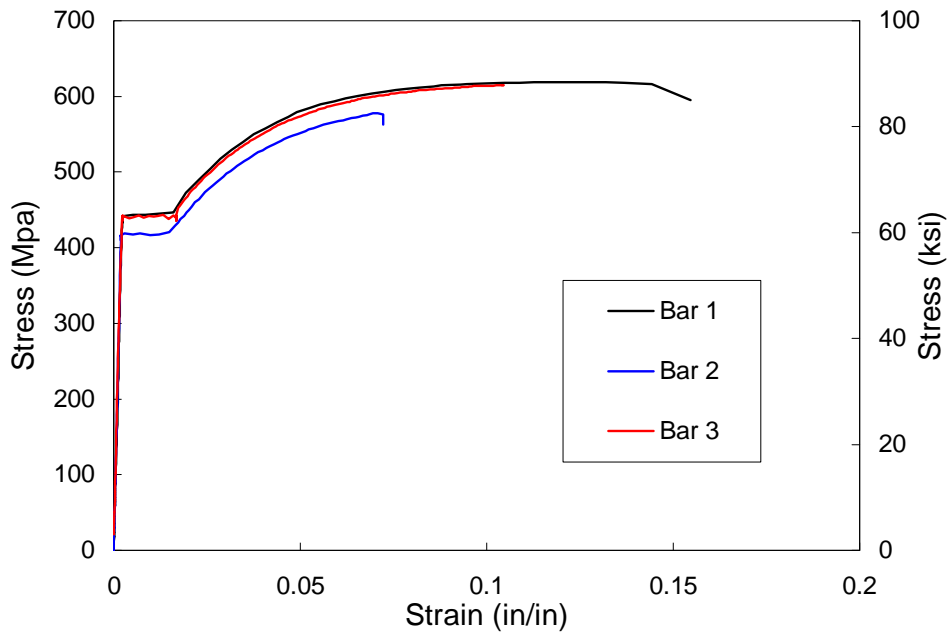
Figure 2.17 Stress versus Strain for Steel Reinforcing Bar Tests

2.6.3 CFRP Shear Reinforcement

The shear reinforcement used in the connection upgrades are a composite consisting of dry carbon fiber fabric and two-part epoxy. The CFRP system was the FYFE Co, Tyfo SCH-41S Composite, which used Tyfo S Epoxy. CFRP strips were constructed and tested in tension according to ASTM D3039. Tested material properties as well as reported material properties are listed in Table 2.12.

Table 2.12 Tested and Reported CFRP Material Properties

Tested Values		Reported Values		
Property	Average	Property	Best	Design
fu (ksi)	116	fu (ksi)	127	108
E (ksi)	10348	E (ksi)	10500	8900
Rupture Strain (in/in)	0.012	Rupture Strain (in/in)	0.012	0.012

*1 ksi = 6.89 MPa

43

2.6.4 Grout

SikaTop 111 Plus grout was used to fill low spots on top of the slab, at the connection region of each test specimen. The compressive properties of the grout were not tested, but reported values are listed in Table 2.13. The grout was chosen because it was stronger than the concrete and therefore would not crush during testing.

Table 2.13 Grout Compressive Properties

SikaTop 111 Plus	
Cure Time (day)	f_c' (ksi)
1	2.5
7	5.5
28	7

*1 ksi = 6.89 MPa

CHAPTER 3
Test Procedure

3.1 GENERAL

In the previous chapters, the motivation for the current research, the design and construction procedures of the specimens used in this study were presented. From the literature survey, the need to develop a simple method that upgrades flat-plate connections was established. It was shown that the strength and toughness of the connection could be improved, while the lateral stiffness of the original connection was not increased. Test specimens were designed from a prototype flat-plate structure that had connections with insufficient punching shear capacity when subjected to simulated seismic load conditions. Two different configurations of CFRP stirrups were designed to increase shear capacity of the slab-column connection.

This chapter presents the testing procedures used in the study. The simulated seismic tests were conducted in conjunction with a gravity shear stress of $0.133\sqrt{f_c^{'}}$ MPa ($1.6\sqrt{f_c^{'}}$ psi) acting on the critical perimeter of each test specimen. Reversed-cycled, quasi-static lateral displacements were applied to the top of each specimen's column to replicate earthquake effects. Each specimen was tested until a punching type failure occurred or the maximum stroke of the lateral MTS actuator was reached. At the conclusion of the simulated seismic tests, a vertical, monotonically increased concentric load was applied to each specimen to investigate residual gravity load capacity. The test setup, specimen instrumentation and testing protocol are discussed in the following sections.

3.2   TEST SETUP

A schematic of the test setup is shown in Figure 3.1. Detailed drawings can be found in Appendix B. The test setup was designed such that constant axial load can be applied to columns of each specimen while lateral displacements are imposed at the tip of the top column section. This allowed each specimen to be tested under combined gravity and lateral load conditions, which simulated movements due to strong ground motion.
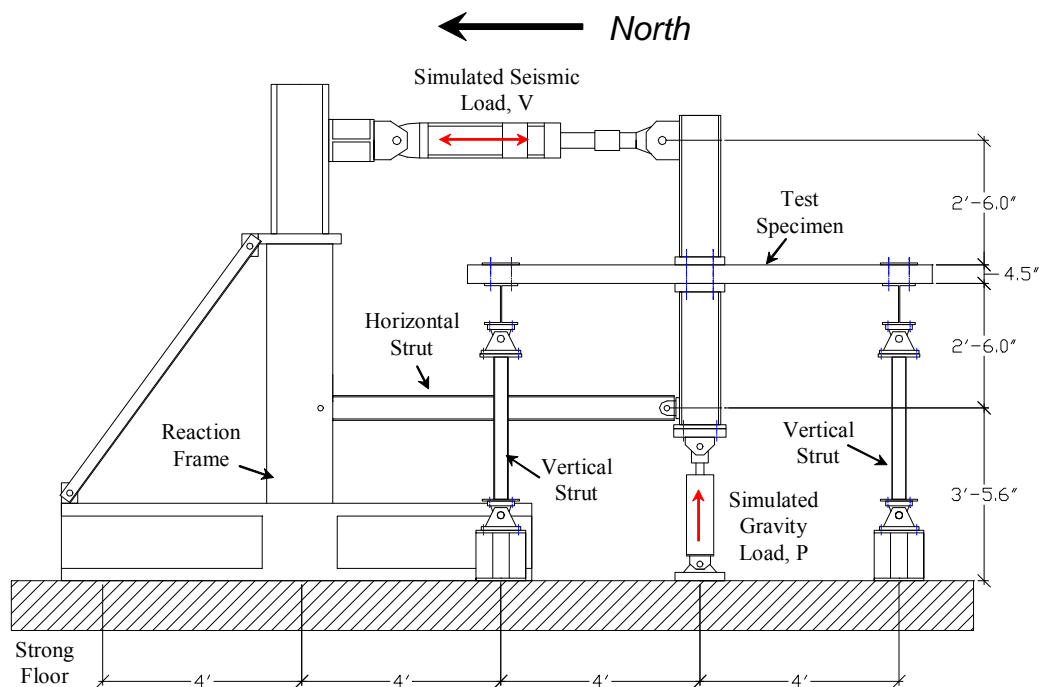
Figure 3.1 Test Setup Elevation

Gravity loads were applied using a hydraulic jack and resisted using vertical struts fixed to the laboratory strong floor. Lateral loads were applied

46

using a horizontal hydraulic actuator and resisted using a lateral strut attached to a steel reaction frame. A picture of the test setup is shown in Figure 3.2.
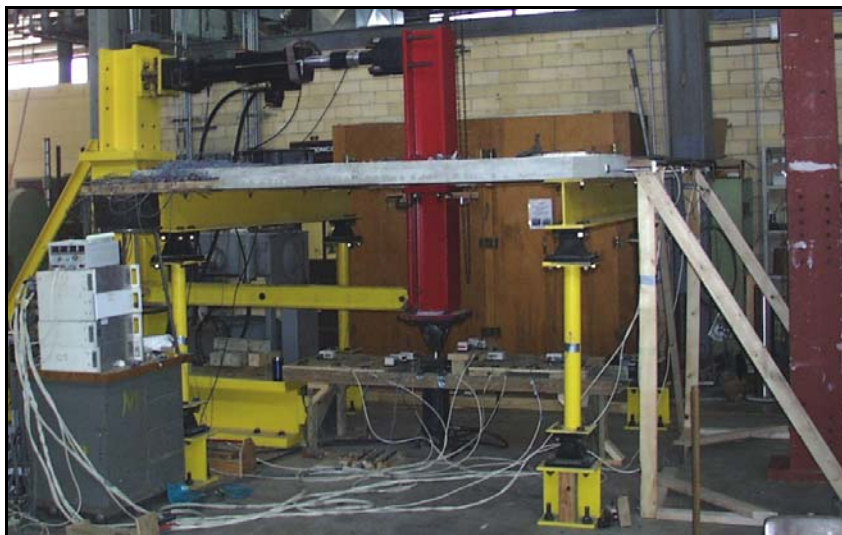
Figure 3.2 Test Setup

3.2.1   Vertical Loads

As stated in section 2.2.3, a shear stress under gravity load of $0.133\sqrt{f_c'}$ MPa ($1.6\sqrt{f_c'}$ psi) (acting on the critical perimeter) was desired. To produce this shear stress an axial load of 95 kN (21.3 kips) was applied to the bottom column section using a hydraulic jack and a load maintainer. The jack had a cross-sectional area of 12,626 mm^2 (19.57 in^2) and was bolted to the bottom column of a test specimen using a clevis connection and bolted to the laboratory strong floor, as shown in Figure 3.1. A load maintainer was to keep constant load on the column. The load maintainer functioned by balancing a counterweight that regulated the flow of hydraulic oil in the system. The counterweight was specifically calibrated such that the force developed by the hydraulic oil pressure

in the jack was equal to the shear stress at the critical perimeter and fluctuations in the column load were minimized. Figure 3.3 is a schematic of the hydraulic line setup. During the post-failure tests, the hydraulic jack was disconnected from the load maintainer and connected to a pneumatic oil pump to apply column loads.
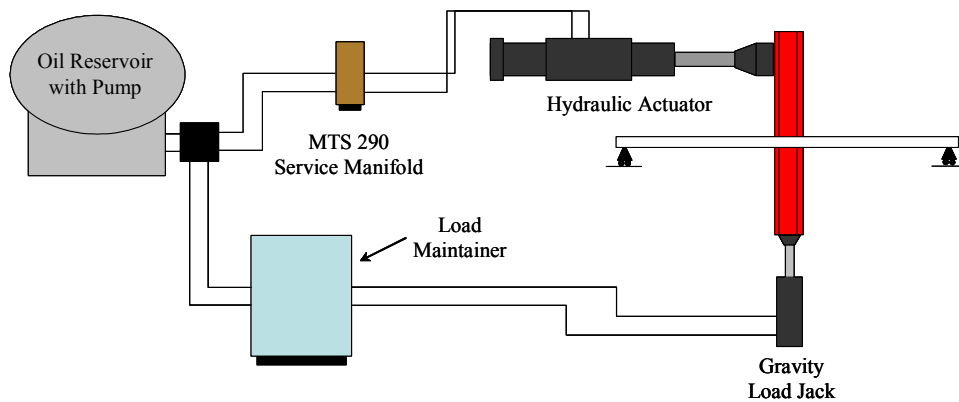
Figure 3.3 Hydraulic Lines Schematic

To resist vertical loads, each specimen was supported at opposite slab edges by two spreader beams, positioned transverse to the direction of lateral loading. Figure 3.4(a) shows a picture of the spreader beam connection. Spreader beams were fixed to the test specimen by bolting through the slab thickness to bear on 254 by 254 mm (10 by 10 in) steel plates, positioned on the top face of the slab. The slab was bolted to the spreader beam at four equally spaced locations. The bottom of each spreader beam was bolted to two vertical struts that were hinged at each end by clevis brackets. The ends of each strut were then bolted to a section of wide flange and fixed to the laboratory strong floor.

<div align="center">(a)   (b)</div>
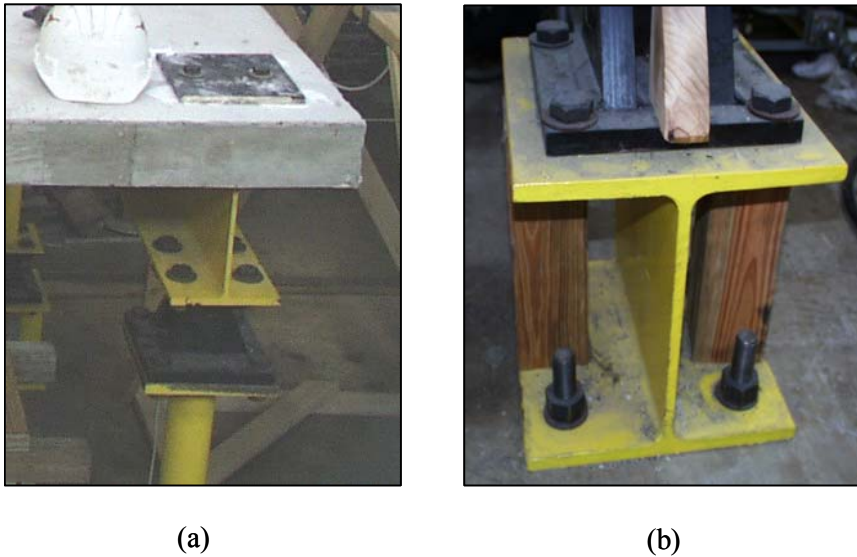
Figure 3.4 Vertical Strut Detail

It should be noted that the vertical load resisting system was geometrically unstable in the direction of lateral loading and vulnerable to sway buckling prior to being tested. The lateral reaction strut provided geometric stability to the system and was connected at all times while the specimen was in the test frame. The stability of the system was checked prior to the application of simulated gravity load. Lateral stiffness was provided by the horizontal reaction strut and each clevis was found to prevent sway buckling. Figure 3.4(b) shows the connection of the vertical strut to the strong floor.

3.2.2 Lateral Loads

During the tests, reversed-cyclic, lateral displacements were applied using an hydraulic actuator, to simulate seismic load conditions. To accomplish this, a MTS 407 controller was used in conjunction with the MTS 290 service manifold to operate the hydraulic actuator under displacement control.

Figure 3.5 Lateral-Strut Connection

A steel reaction frame was used to position the lateral actuator and to transfer lateral load back to the laboratory strong floor (Figure 3.1). The reaction frame was fabricated from heavy wide flange sections (W14x257 and W14x426) and supported by a diagonal strut. A three foot W12x152 extension was welded vertically to the top of the frame so the lateral actuator could be positioned at the correct height. Calculations showed the lateral displacement of the wide flange extension was negligible at the load levels expected during the tests. As mentioned in the previous section, a lateral strut consisting of two C6x13 American Standard Channels were bolted to the steel frame and the test specimen. Figure 3.5 shows a picture of the lateral strut connection. In addition to lateral stability, the lateral strut provided a horizontal reaction for the lateral actuator. The net horizontal force that acted at the base of the frame was zero, leaving a vertical force couple to be equilibrated by the laboratory strong floor.

3.2.3 Boundary Conditions

The boundary conditions of the test setup simulate a load case considering lateral load. As in previous tests ([5], [8], [10], [15], [17], [20], [21], and [23]), points of inflection corresponding to zero moment were assumed to be located at mid-span of the slabs and mid-height of the columns of the prototype structure. It would have been difficult to accurately simulate the exact boundary conditions of a structure subjected to gravity and lateral loads in a single bay slab-column connection test. The location of inflection points in structures deviates from mid-slab-span and mid-column height during earthquakes as the direction of lateral load changes and moment and shear redistributes. For all practical purposes, and to be consistent with previously tested interior slab-column connections, points of inflection in the slabs and columns were assumed to be located at mid-points.

The spreader beam clevises allowed each test specimen to rotate in the direction of lateral loading, while the remaining degrees of freedom were locally restrained. This created points of zero moment at the centerline of the spreader-beams, and generated mid-span points of inflection for the lateral load moment diagram.

3.3 INSTRUMENTATION AND DATA RECORDING

Each test specimen was extensively instrumented and lateral and gravity loads, column and slab displacements, connection and column rotations, longitudinal, CFRP and vertical strut strains were measured and recorded. All instrumentation was connected into a scanner and data was recorded using Ferguson Structural Engineering Laboratory's data acquisition software, DAQ. Instrumentation was grouped as follows:

3.3.1 Lateral Loads

Lateral loads were measured by a load cell integrated into the MTS hydraulic actuator. Voltage from the load cell was read by the MTS 407 Controller on a 10 volt scale and transferred to the DAQ. Figure 3.6 shows the position of the load cell. The load cell in the actuator was calibrated by MTS, having a load limit of 250 kN (55 kips).

3.3.2 Gravity Loads

During the lateral load tests, the gravity load is held constant using a load maintainer. A pressure gage on the load maintainer displayed the pressure in the hydraulic line attached to the vertical ram. In this way, the column load was monitored and kept constant throughout the test. For the residual gravity load tests, a pressure transducer was attached into the hydraulic line and read by the DAQ.
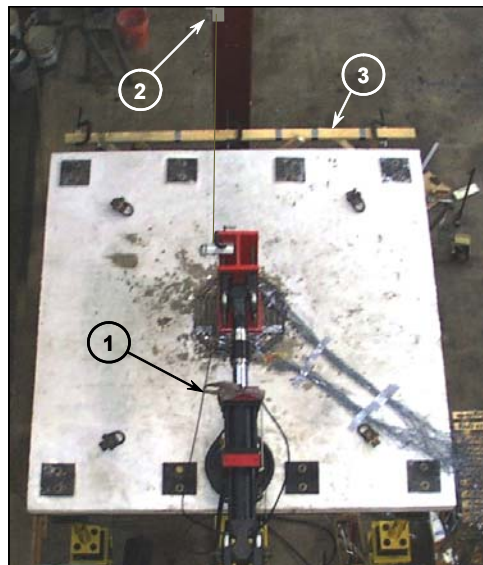
1 MTS hydraulic actuator, which contained a load cell and LVDT that measured lateral load and displacement.

2 Horizontal string potentiometer used to measure column displacement at the position of applied lateral load.

3 Horizontal linear potentiometers used to measure slab displacement

Figure 3.6 Lateral Instrumentation

3.3.3 Column Lateral Displacement

An internal displacement transducer (LVDT), within the hydraulic actuator, measured ram stroke. Voltage from the LVDT was output to the MTS 407 controller on a ten volt scale and transferred to the DAQ. Column displacement was also measured by a string potentiometer at the point of lateral load application, shown in Figure 3.6. The additional string potentiometer was used as a back up and checked error in the measurements made by the LVDT. Some error is introduced into the readings made by the LVDT due to deformations experienced by the horizontal actuator's components and minor movements of the reaction frame, while being tested.

3.3.4 Slab Displacement

Horizontal slab displacements were measured using three linear potentiometers. The linear potentiometers were equally spaced, placed at the slab edges and centerline (Figure 3.6). Aluminum plates were epoxied to edge of each specimen to provide a smooth contact surface for the linear potentiometers. A detailed picture of the horizontal liner potentiometers is shown in Figure 3.7. Data from these displacement transducers was used to measure any twisting of the slab during the tests.
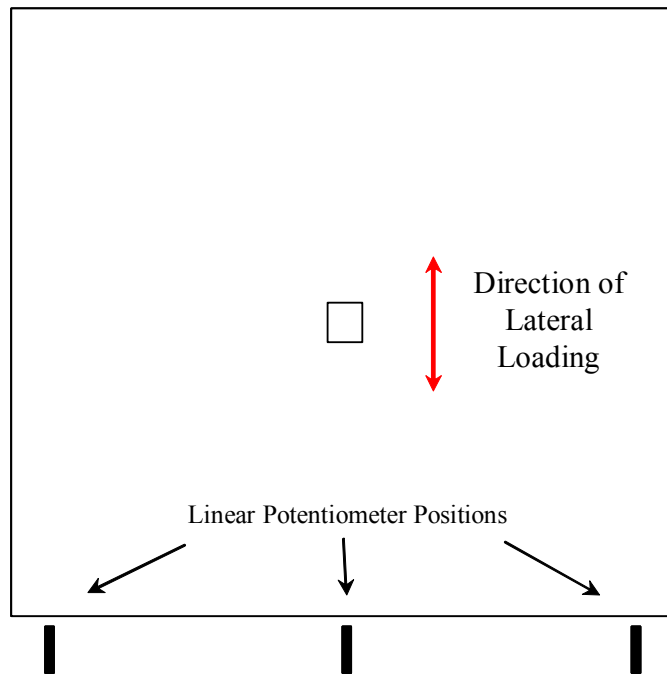
Figure 3.7 Lateral Instrumentation

3.3.5 Connection Rotation

Four string pots were positioned near the column and fixed to the slab to measure vertical displacements (Figure 3.8). The strings extensions had lengths of 1905 mm and 2160 mm (75 and 85 in) and were made from steel fishing leaders. Wooden blocks with brass hooks were epoxied to the bottom face of the slab to attach the string extensions. Slab rotations were calculated using average values of the north and south string pots. In addition, rotational transducers were also used to measure rotation of the specimen near the connection. Figure 3.8 also shows one of two rotation transducers that were bolted to the bottom column, just below the slab-column connection.
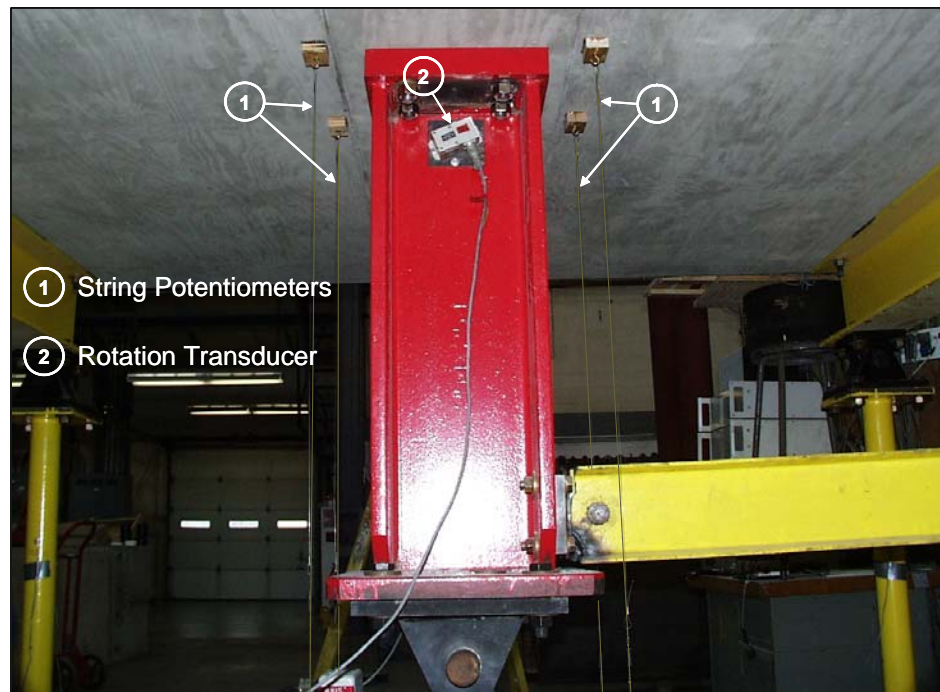
Figure 3.8 Rotation Instrumentation

3.3.6   Strain Gages

Strain gages manufactured by the Tokyo Sokki Kenkyujo Company were attached to steel longitudinal reinforcing bars prior to concrete placement. FLA-5-11-3LT strain gages were used to measure strains in the steel reinforcing bars of this study. A mechanical grinder was used to remove the deformations on the steel reinforcing bars at the corresponding strain gage positions.   The steel surfaces were then cleaned and strain gages were attached to the reinforcing bars using CN adhesive. Figure 3.9 and Figure 3.10 show the strain gage positions on the bottom and tops layers of steel within the slab.
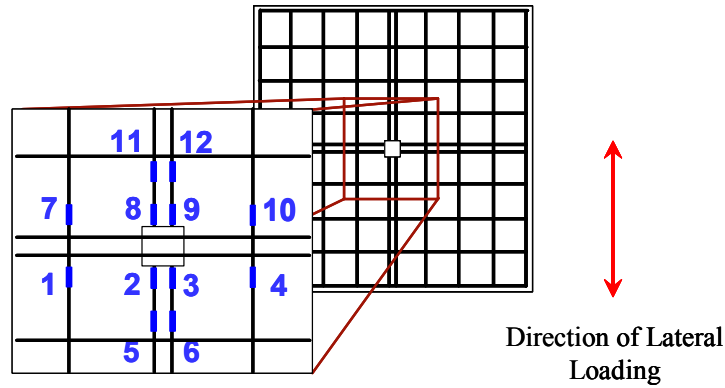
Figure 3.9 Bottom Steel Strain Gage Positioning
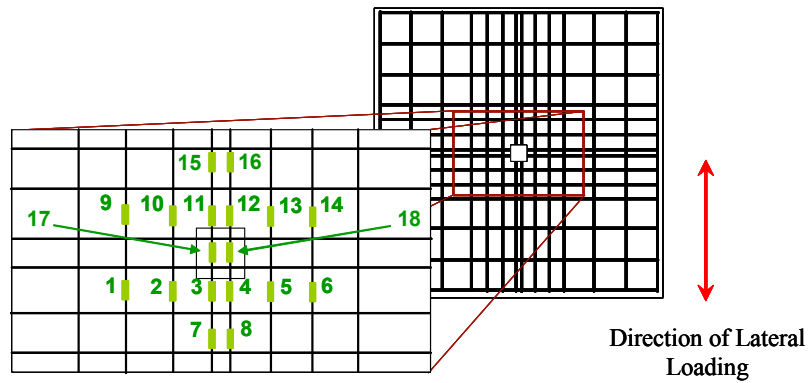
Figure 3.10 Top Steel Strain Gage Positioning

Before filling the holes through the slab with epoxy, BFLA-5-11-3LT strain gages were attached vertically to the CFRP stirrups. These gages were manufactured by the same company, and were rated for much greater strain levels that the "FLA" type strain gages used for steel reinforcing bars. This is mainly due to a more flexible backing material used to attach the foil gage by the manufacturer. The CFRP surfaces were prepped using PS-2 resin and the strain

gages were glued using CNY adhesive. Figure 3.11 and Figure 3.12 show the gage layout and strain gage numbers for upgrade patterns A4 and B4.
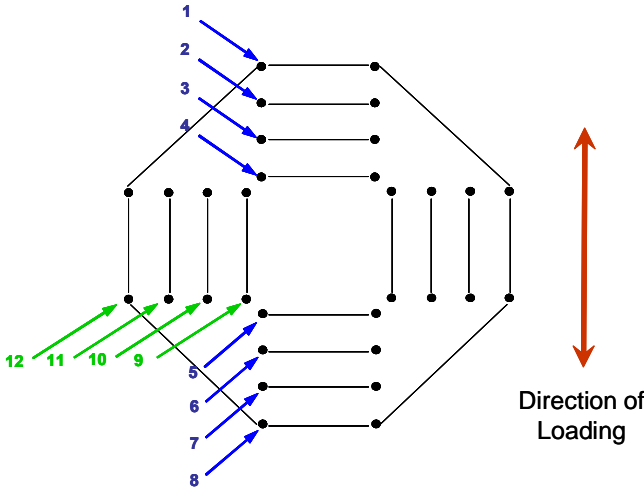
Figure 3.11 Upgrade A4-S CFRP Strain Gage Positioning
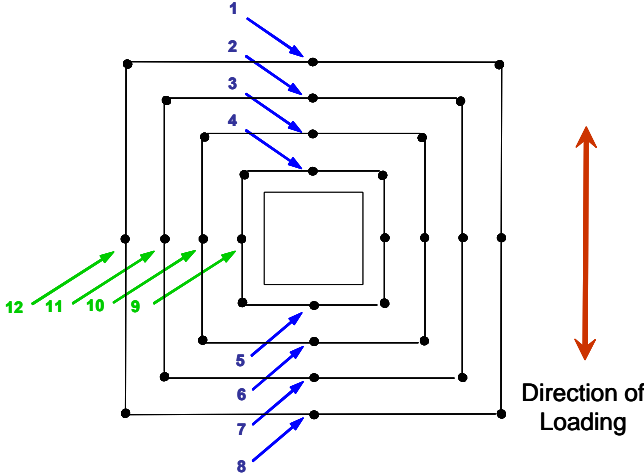
Figure 3.12 Upgrade B4 CFRP Strain Gage Positioning

3.4   TEST PROTOCOL

The test procedure is outlined in the following section. Each specimen was setup and tested using the established protocol.

3.4.1   Assembling the Specimens

Each slab specimen was removed from formwork after curing using lifting inserts that were placed in the reinforcing bar cages, before concrete was cast. Specimens were moved to an assembly area using an overhead crane, where the spreader beams and column sections were fastened to the test specimen (Figure 3.13).

Figure 3.13 Specimen Assembly Area

For ease of construction, the spreader beams were placed on four large concrete blocks before the slab was moved into position (Figure 3.13). As mentioned in section 3.2, bolted connections were used to attach each spreader beam to the test specimens through holes in the slab thickness. 19 mm (0.75 in) diameter bolts were used to attach the spreader beam to the slab. After the bolt

holes were aligned with spreader beam, hydro-stone was mixed and spread around on the top face of the slab to create a level surface. 254 x 254 mm (10 x 10 in) steel plates were then positioned and the bolts were tightened by hand.

Figure 3.14 Specimen A4-S Slab-Column Connection

In the final step of test specimen assembly, column sections were fixed to the test slabs. Because the specimen was elevated on concrete blocks, the bottom section of the column could be positioned directly under the column holes in the slab. The overhead crane was then used to move and position the top column section. Grout was placed in low spots at the slab-column connections, which created a uniform surface.

3.4.1.1 Column fastening

Two methods were used to fasten the columns to the slabs in the study. In the first method, the top column section of specimen A4-S was placed directly onto the top face of the slab where eight 22 mm (0.875 in) diameter bolts were fastened using wrenches (Figure 3.14). Wrenches were used because the base plate detail did not permit the use of pneumatic lug-wrenches. In the second method, a post-tensioning method was developed to fasten the bolts. Figure 3.15

shows a picture of the post-tensioning system. To assure uniform stress in each bolt, two 107 kN (12 ton) hydraulic rams were placed in the center of each bolt group, on the column base plate. A 25.4 mm (1 in) thick steel plate was constructed and fit over the rams. Eight 19 mm (0.75 in) ASTM Grade 8 threaded rods were then fitted through the bolt holes and fastened to the steel plate and bottom column section.
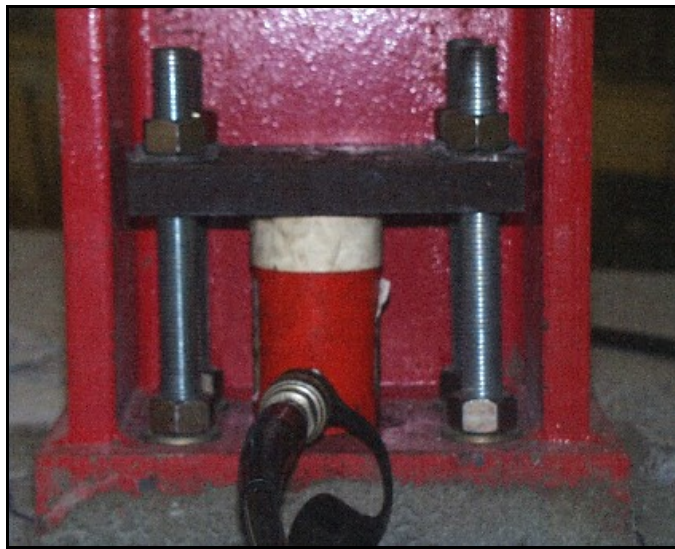
Figure 3.15 Post-Tensioning Method of Tightening Column Bolts

Each bolt was post-tensioned to 12.5 kN (2.8 kips). This post-tensioning force was determined to be appropriate because it provided a slab-column connection without any gaps and the bolts could be removed using a wrench. Being able to remove the bolts by hand indicated that the applied post-tensioning force was not too large as to alter the behavior of the connection. Test results for specimens B4-S, C-02 and C-63 were therefore consistent with specimen A4-S, but easier to assemble.

3.4.1.2 Specimen Upgrade

After the column sections were fixed to the slab, CFRP stirrups were installed to strengthen the connection regions of specimens A4-S and B4-S. Pressurized air was used to clean out debris accrued from slab movement and the column being fixed. Fiber strips were then cut to length and width, as specified in section 2.4, from a stock roll of carbon fiber fabric. Two part epoxy was proportioned and mixed in a 19 L (5 gal) bucket and the strips were stitched into the slab, forming closed-stirrups. Stitching the carbon fiber stirrups required two people: one person soaked the fiber strands and wove strips through the top of the slab; the second person wove strips from the bottom slab face, through the holes in the slab, back to the top face of the slab. Weaving began from the inner-most perimeter of the holes in the slab, and moved out until each side of the column had been stitched. Finally, plywood, wrapped in plastic, was pushed against on each side of the slab, to remove air pockets so the fibers bonded to form a continuous stirrup. The CFRP stirrups were allowed to cure at least three days prior to testing.

Figure 3.16 Upgrade B4 Slab-Column Connection

After the stirrups had cured, the layer of plywood on top of the slab was removed. Strain gages were then attached to the CFRP stirrups as described in section 3.3. Once the gages were attached, hydra-stone was placed on the bottom face of the slab, to plug the holes through the slab. Two part epoxy was poured into the voids that remained in the holes in the slab, and allowed to cure.

3.4.1.3 Comments on Externally Applied CFRP Stirrups

Care should be taken when upgrading flat-plate connections with externally bonded CFRP stirrups. Persons applying the stirrups need full body cover-alls to protect against uncured epoxy when handling the wetted carbon fiber strips. Eye protection is necessary when working overhead, because uncured epoxy will drip. The persons applying the stirrups will not be able to see each other (one person is located on top of the slab and one person below), so a method of communication should be established prior to starting the procedure. Over the period of the study, temperatures ranged from 0 degrees to 38 degrees Celsius (32° – 100^oF). Temperature is a concern because it can affect the curing rate of the epoxy, but adversely affects working conditions when the temperature is high.

Of the two connection upgrades, configuration B4-S was not as difficult to construct as configuration A4-S. The total amount of carbon fiber used in configuration B4-S was 15% less than upgrade A4-S. Also, because the strips were shorter, less uncured epoxy dripped from the CFRP strip during the construction of a single stirrup. However, the construction time of both connection upgrades was about equal. Upgrade B4-S had a smaller amount of material, but there was not as much movement when applying A4-S.

3.4.2 Specimen Placement in the Test Frame

Each test specimen was moved from the assembly area to the test frame using the overhead crane. Before the specimens were moved to the test frame, the

horizontal and vertical struts were locked into place using wooden blocks. The overhead crane lifted and positioned each test specimen so the vertical and lateral struts could be appropriately bolted. The vertical ram was extended into position using a hand pump and fastened to the bottom column (Figure 3.2). The horizontal ram was moved into position prior to testing.

3.4.3 Instrumentation

All instruments were positioned, wired and checked as described in section 3.3. The data acquisition system was then setup and checked prior to loading.

3.4.4 Lateral Load Test

All blocks restraining the horizontal and vertical struts were removed and the DAQ was switched on. The MTS actuator was then lowered into place and bolted to the top of the column section. All instrumentation was rechecked and zeroed. The DAQ was then set to record data and the load maintainer was set to apply a constant pressure of 7.5 MPa (1090 psi), corresponding to a vertical axial load of 21.3 kips (94.7 kN). Finally, the reversed-cyclic lateral displacement protocol was applied.
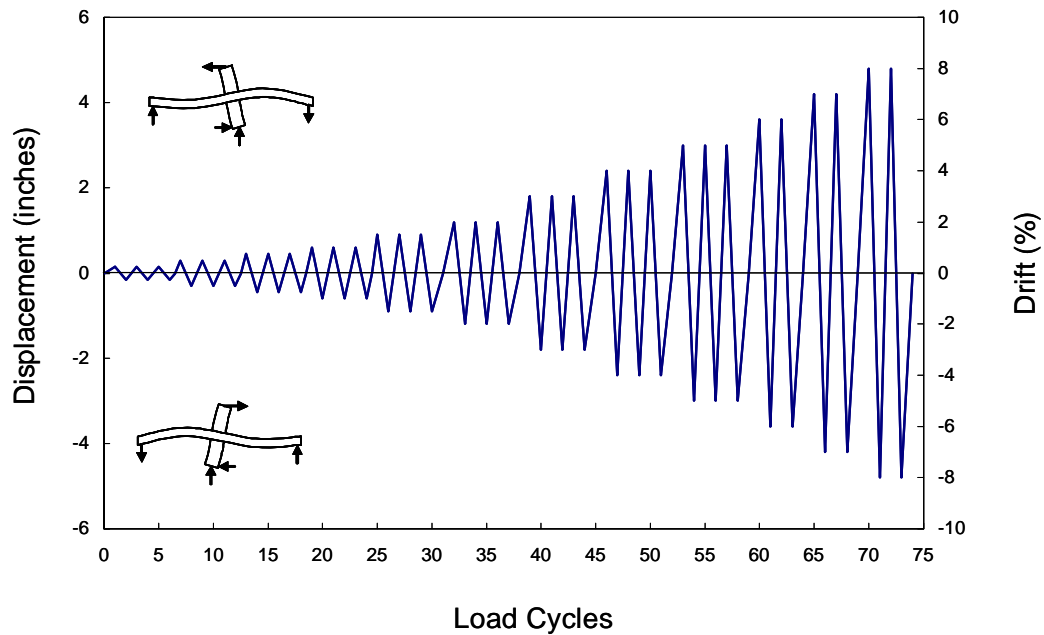
Figure 3.17 Lateral Displacement Protocol

The lateral displacement protocol was adopted from ACI ITG/T1.1-99, *Acceptance Criteria for Moment Frames Based on Structural Testing.* Figure 3.17 is a plot showing the displacement history followed during testing. FEMA 356 [12] states:

> *"The strength and deformation capacities of concrete members shall correspond to values resulting from earthquake loadings involving three fully reversed cycles to the design deformation level, unless a larger or smaller number of deformation cycles is determined considering earthquake duration and the dynamic properties of the structure" (p. 6-14).*

Three fully reversed cycles were applied to each specimen from drift ratios of 0.25% to 6%. After a drift ratio of 6%, two fully reversed cycles were applied to each test specimen. 6% drift was assumed to be a large drift-ratio (this drift-ratio

64

is unrealistic for existing flat-plate structures. However, if the test specimens can resist combined gravity and lateral loads to such drift-levels, the performance flat-plate structures under more reasonable load levels should be adequate). Test specimens exhibited a very stable response when three repeated cycles were applied at each drift level. Hence, two repetitions within an applied drift-cycle after 6% inter-story drift was achieved. The first three drift increments (0.25%, 0.5% and 0.75%) were chosen so data in the linear elastic range could be recorded. Drift increments were increased until the specimen lost the ability to carry a significant portion of applied lateral load, or the hydraulic actuator reached its limit of 254 mm (10 in) of total stroke.

3.4.5 Residual Gravity Load Capacity Tests

To determine the residual gravity load capacity of each specimen, the lateral actuator was disconnected from the top of the column and moved using a stationary crane. The load maintainer was disconnected from the vertical jack and a pneumatic pump was attached. A pressure transducer was installed and attached to the DAQ. Vertical load was applied until a punching failure occurred.

CHAPTER 4

Presentation and Discussion of Experimental Results

4.1 INTRODUCTION

Experimental results of control specimens C-02, C-63, upgraded specimens A4-S and B4-S are presented and discussed in this chapter. All specimens were prepared and tested as described in chapters 2 and 3. General test observations, presentation and evaluation criteria, lateral load versus drift response, unbalanced moment versus rotation behavior and backbone curves are presented and discussed. Then crack patterns, steel and CFRP strains, strength and stiffness degradation of each test specimen and ductility parameters are also examined. Finally, the results from the residual gravity load carrying capacity tests are critically analyzed.

4.2 GENERAL TEST OBSERVATIONS

Each test specimen was subjected to the following loading sequence as part of the test protocol:

(i) Simulated Seismic Tests

- Initial gravity loading;
- Combined gravity and lateral loading.

(ii) Post-Earthquake Tests

- Residual gravity load carrying capacity.

Each specimen in the study displayed similar observable characteristics until the 2.5% applied drift-cycle, during the first phase of testing. At this drift-

ratio, a punching shear failure initiated in test specimens C-02 and C-63. Upgraded specimens A4-S and B4-S resisted gradually increasing lateral displacement cycles through a lateral drift-ratio of 8.3% (the maximum stroke of the horizontal ram). Both of the upgraded specimens also resisted greater lateral loads than each control specimen, but the change in lateral stiffness was insignificant. The final failure mechanism of each upgraded specimen was a punching shear failure that occurred during the residual gravity load capacity tests.

4.3 PERFORMANCE EVALUATION CRITERIA

The overall performance of the test specimens in this study varied when subjected to combined gravity loads and reversed-cyclic lateral displacements. Each specimen did not deform or fail symmetrically during the tests. In order to evaluate seismic performance of the control and upgraded test specimens, a consistent basis for quantifying specimen behavior must be established. In this section, the sign conventions, terminology related to reversed-cyclic load-deformation relations and the ductility parameters used to present and evaluate the test results are defined

4.3.1 Sign Convention

Figure 4.1 shows a schematic of the positive sign conventions associated with the test. Lateral loads were applied to the test specimen in the North and South directions. Positive lateral loads are associated with the horizontal ram displacing the top column section towards the south. Vertically applied load on each test specimen, and corresponding displacements of test specimens are considered positive. Positive unbalanced moments are those that rotate the connection region of each specimen clockwise, facing east, as shown in Figure 4.1. Reinforcement tensile strains are indicated as positive.
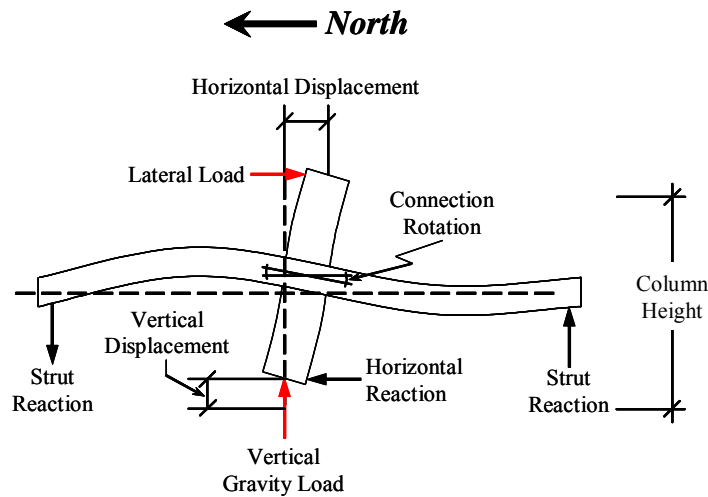
Figure 4.1 Positive Sign Conventions

4.3.2   Reversed-Cyclic Load-Deformation Terminology

A specimen's maximum lateral load, displacement and stiffness for a given lateral drift-cycle are shown in Figure 4.2. The maximum lateral load and displacement peak for a specific drift-cycle are listed in both "push" and "pull" directions for the given drift-cycle.   The maximum displacement of both the "push" and "pull" phases of an applied drift-cycle (and corresponding lateral loads) are used to define lateral stiffness. Because each test specimens does not deform symmetrically, two stiffnesses are calculated for a given drift-cycle (K_i^+ and K_i^-).   Lateral load-displacement backbone curves are developed using the lateral load peaks and corresponding displacements.
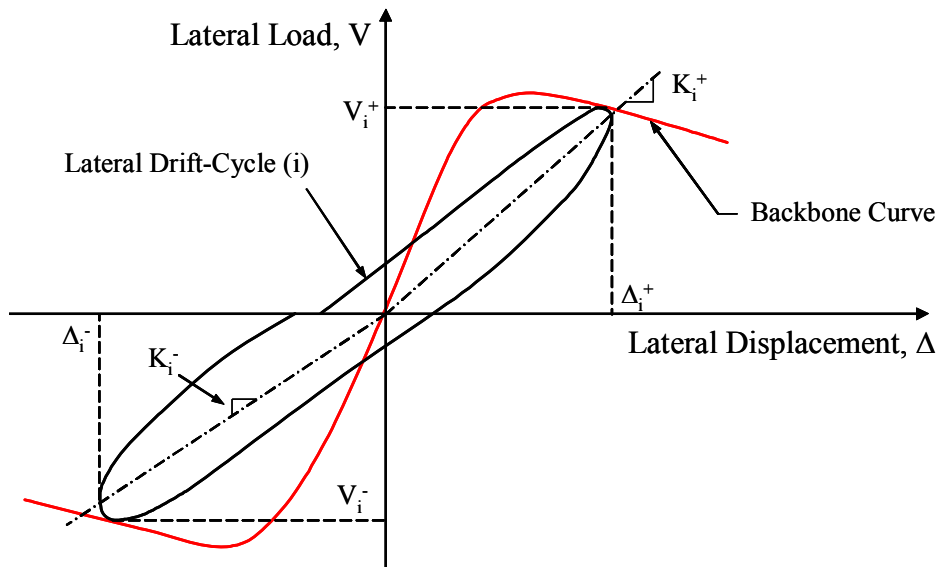
Figure 4.2 Lateral Load, Displacement and Stiffness of the ith Lateral

Drift-Cycle

Lateral displacements of test specimens can be expressed in terms of inter-story drift ratios. Drift ratio is defined by dividing the lateral displacement of the column tip by the test specimen story height. In this study, an applied drift-cycle is defined by the lateral-deformation protocol, established in section 3.4.5. Although the prescribed displacement protocol for each test specimen were symmetrical "push" and "pull" cycles, minor differences occurred during testing that resulted in some asymmetrical response. In addition, punching shear failure initiated in the control specimens at a given "push" or "pull" cycle, after which asymmetrical behavior followed. Therefore, the lateral drift-ratio at which punching initiated and completed is presented. Specimen drift capacity will be defined as the drift where punching shear failure initiated.

Unbalanced moment, connection rotation and rotational stiffness for a given lateral drift-ratio are defined in Figure 4.3. The methods for defining each

parameter are similar to those used to define the load-deformation relations. Rotational stiffness of a given drift-ratio is defined using the maximum connection rotation for both the "push" and "pull" phases of a given drift-cycle. Unbalanced moment versus connection rotation backbone curve is defined using the peak unbalanced moment and corresponding rotations of each drift-cycle in a given test. Ultimate connection rotation capacity will also be defined as the rotation at which a punching shear failure initiated.
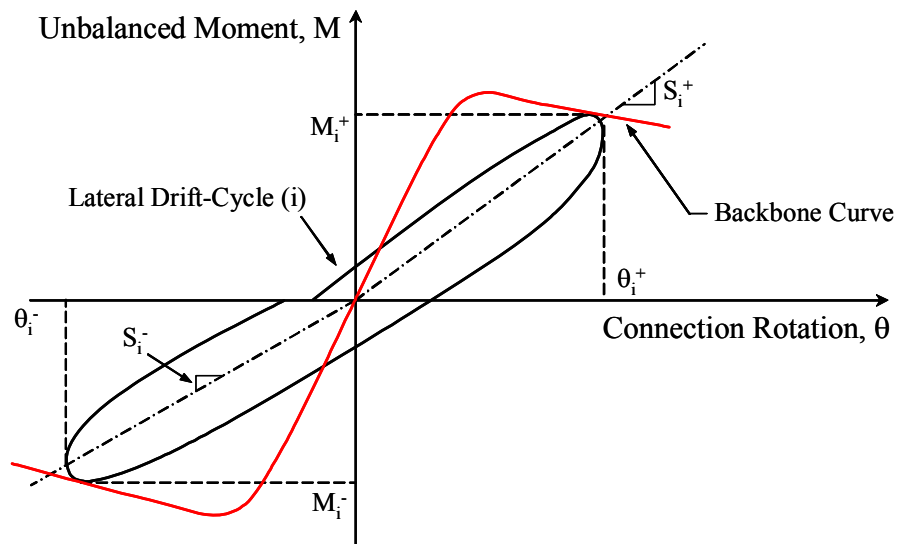
Figure 4.3 Unbalanced Moment, Connection Rotation and Stiffness of the ith Lateral Drift-Cycle

4.4 LATERAL LOAD VERSUS DRIFT

Lateral load versus drift relationship for test specimens C-02, C-63, A4-S and B4-S are shown in Figure 4.4 to Figure 4.7. The bottom horizontal axis of these plots shows lateral inter-story drift, defined as the horizontal displacement of the top column relative to the bottom column, divided by the height of the

column. The top horizontal axis shows the horizontal displacement of the top of the upper column section relative to the bottom of the lower column section. The left vertical axis is the applied lateral load and the right vertical axis is the corresponding unbalanced moment. Plots showing the equivalent U.S. customary units can be found in Appendix C.

Control specimens C-02 and C-63 exhibited punching shear failures that resulted in a significant drop in lateral load. As previously mentioned, the application of the gravity load cracked the top face of each specimen. At a drift ratio of 2%, cracks began to open and considerable pinching occurred in the lateral load-deformation plots. Concrete began to crush and spall around each specimens' column base plate, on the bottom slab face, prior to punching shear failure.

Punching initiated on the north side of the column of specimen C-63 at a drift ratio of 2.26% and punched on the south side at an applied drift ratio of 1.38%. At this point the punching cone fully formed. At a drift-ratio of 1.7%, yielding spread across the gaged bars. This covered a width of c+3.5h, transverse to the direction of loading. Specific reinforcing steel strain profiles will be further discussed in section 4.6. In specimen C-02, punching initiated on the north side of the column at a drift-ratio of 2.44% and completed when a drift-ratio of 2.4% was applied on the following, southern drift excursion.

When upgraded with CFRP shear reinforcement, specimens A4-S and B4-S had significant increases in ductility and energy dissipation capacities when compared with control specimens. The upgraded test specimens displayed similar behavior to the control specimens through 2.5% inter-story drift, but specimens A4-S and B4-S did not experience a punching shear failure while subjected to combined gravity and lateral loads. Both upgraded specimens sustained substantial reinforcing bar yielding. Flexural cracks on the top slab face of

71

specimens A4-S and B4-S opened wider as drift excursions increased. Crack widths increased, as inelastic deformations increased, which augmented pinching in the load-displacement hysteresis loops at larger drift-ratios. Test specimens A4-S and B4-S displayed superior seismic behavior in comparison with control specimens C-02 and C-63 (Figure 4.4 through Figure 4.7). This is shown by the preponderant hysteretic response, which will be further discussed in section 4.11.

Both upgraded test specimens also had increases in lateral load capacity. The maximum lateral load resisted by specimen A4-S was 41.2 kN (9.3 kips), which is a 50% increase in strength over specimen C-02. None of the CFRP stirrups in connection upgrade A4-S sustained any damage due to combined gravity and lateral load testing. Specimen B4-S withstood a maximum lateral load of 48 kN (10.8 kips); an increase of 74% over control specimen C-02. At a drift-ratio of 8.3% (applied in the northern direction), an exterior perimeter, north-south CFRP stirrup positioned at the southwest corner of the connection upgrade ruptured. The CFRP strand rupture resulted in a 30% loss in lateral load capacity.
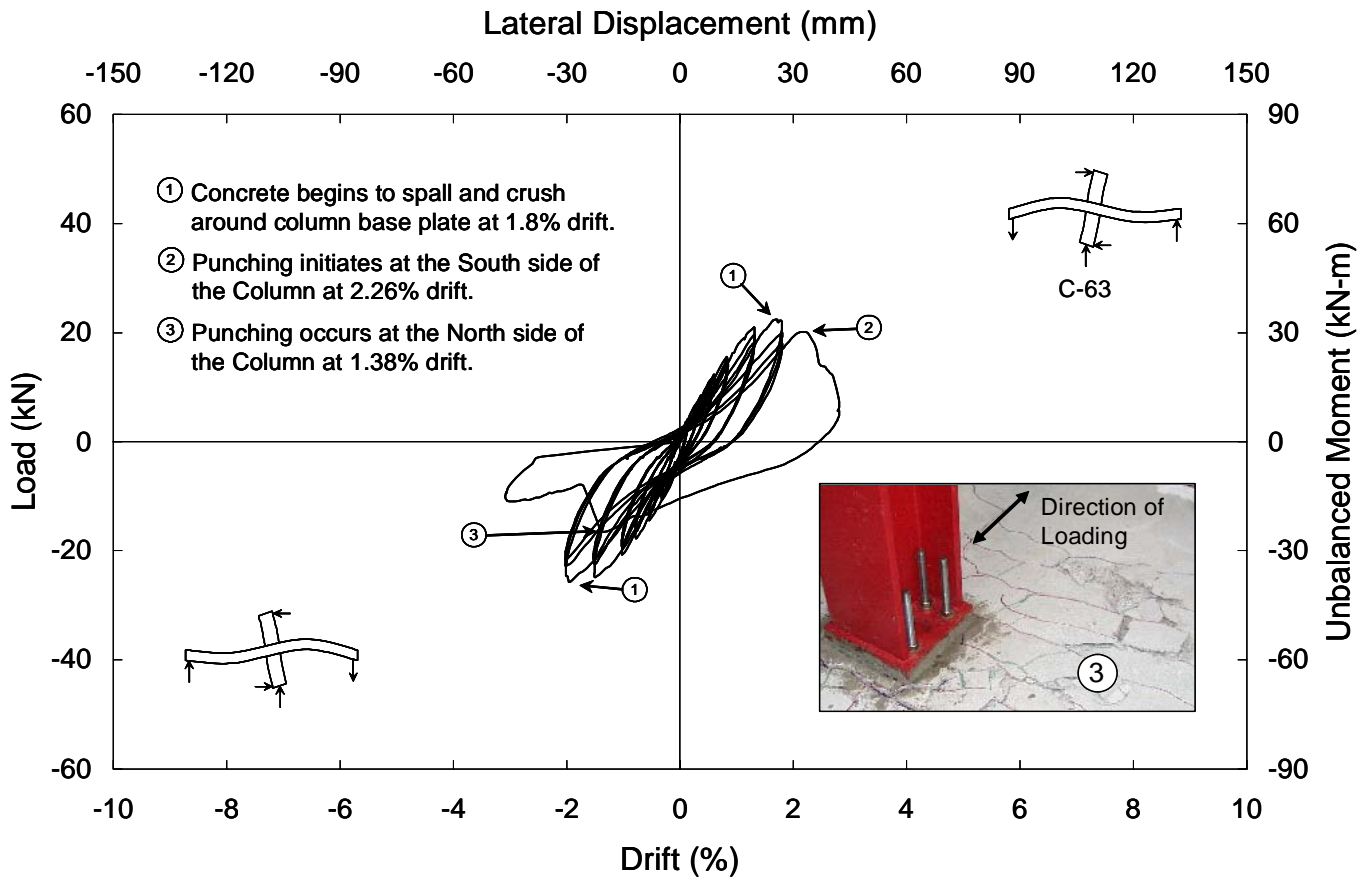
Figure 4.4 Specimen C-63 Load versus Drift

The figure shows a graph with axes:
- Top axis: Lateral Displacement (mm), ranging from -150 to 150
- Bottom axis: Drift (%), ranging from -10 to 10
- Left axis: Load (kN), ranging from -60 to 60
- Right axis: Unbalanced Moment (kN-m), ranging from -90 to 90

Legend:
① Concrete begins to spall and crush around column base plate at 1.8% drift.
② Punching initiates at the South side of the Column at 2.26% drift.
③ Punching occurs at the North side of the Column at 1.38% drift.

C-63

Direction of Loading

Figure 4.5 Specimen C-02 Load versus Drift

The figure shows a plot with axes:
- Top axis: Lateral Displacement (mm), ranging from -150 to 150
- Left axis: Load (kN), ranging from -60 to 60
- Right axis: Unbalanced Moment (kN-m), ranging from -90 to 90
- Bottom axis: Drift (%), ranging from -10 to 10

Annotations on the plot:

① Top steel strain at 1% drift: $\varepsilon_s = 2.0\varepsilon_y$.

② At 1.7% drift, top steel strain > $2\varepsilon_y$ across c+3.5h, transverse to direction of lateral load.

③ Cracks form around the column base plate on the bottom face of slab at 3% drift.

④ Punching initiates at the South side of the Column at 2.44% drift.

⑤ Punching occurs at the North side of the Column at 2.4% drift.

C-02

Direction of Loading

Figure 4.6 Specimen A4-S Load versus Drift
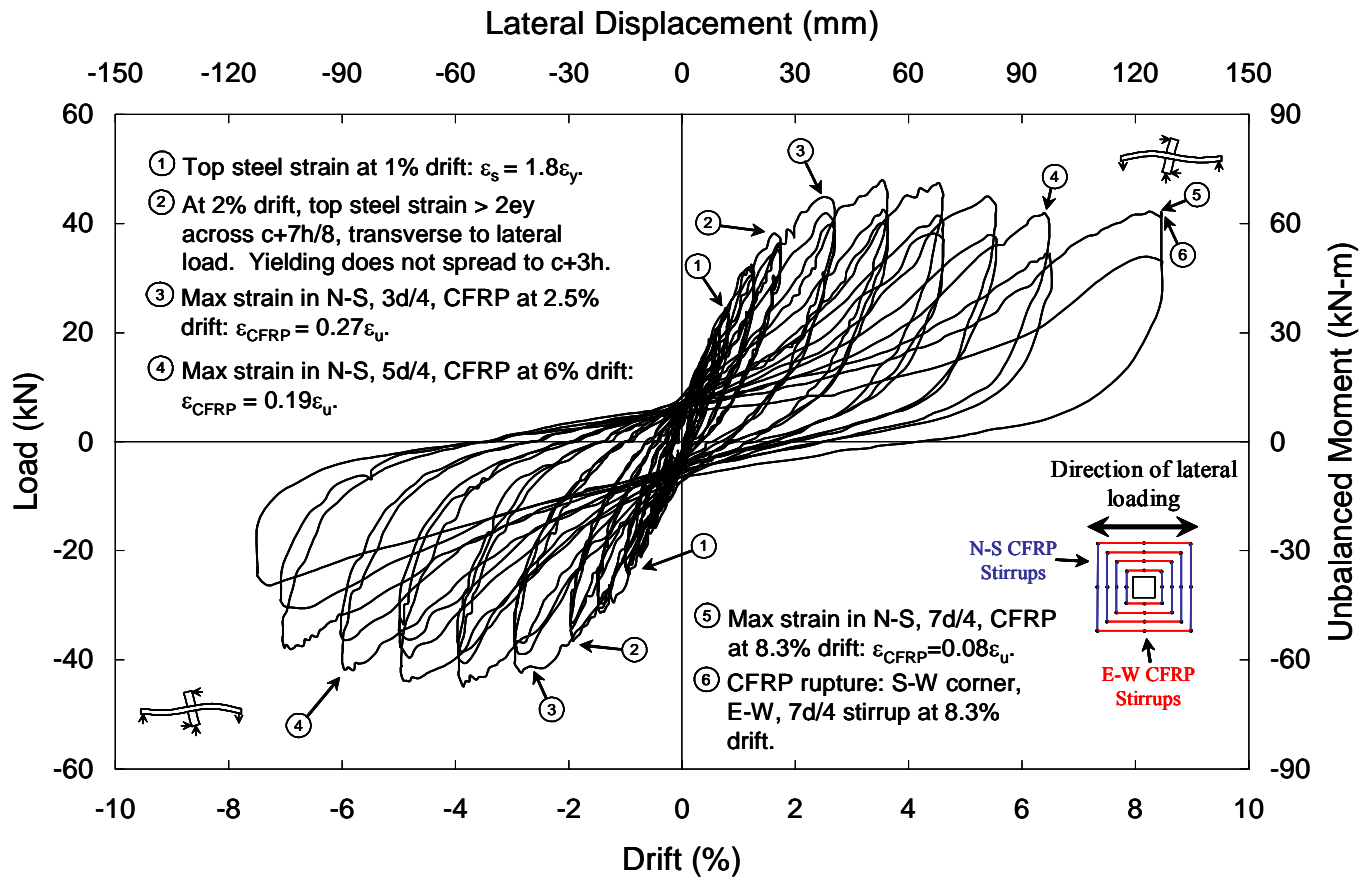
Figure 4.7 Specimen B4-S Load versus Drift

4.5 **UNBALANCED MOMENT VERSUS SLAB CONNECTION ROTATION**

Figure 4.8 through Figure 4.11 are plots showing applied unbalanced moment versus connection rotation behavior of the test specimens. Connection rotations were measured as described in section 3.3.5. The horizontal axes of Figures 4.19 through 4.22 show connection rotations measured in radians and degrees. The total unbalanced moment is equal to the summation of the positive and negative moments acting across the slab section at the column face. Unbalanced moment is calculated by multiplying the applied lateral load by the column height.

As stated in the previous section, control specimens C-63 and C-02 experienced punching shear failures. Both control specimens first exhibited signs of punching shear failure on the north side of the column face, and then punching shear failure was observed on the south column face at the completion of the drift-cycle. Punching shear failure initiated at a joint rotation of 0.019 radians and completed at 0.011 radians for specimen C-63. This corresponded to unbalanced moments of 30.4 kN-m (269 kip-in) and 25.2 kN-m (223 kip-in), respectively. In specimen C-02, punching shear failure initiated at 0.023 radians and completed at 0.017 radians, which corresponded to applied moments of 23.9 kN-m (212 kip-in) and 24.4 kN-m (216 kip-in).

Upgraded specimens A4-S and B4-S attained greater rotational capacities without failing in two-way shear because of the additional CFRP shear reinforcement. The maximum recorded connection rotation for specimen A4-S was 0.06 radians. No data could be recorded after this rotation because readings from the instruments were saturated. After instrument saturation occurred three more drift-cycles were applied during the test. Specimen B4-S had a maximum

77

connection rotation of 0.067 radians before a CFRP strand rupture occurred. The increased joint rotational capacity permitted the longitudinal reinforcing steel to deform well into the inelastic range, which allowed further energy dissipation.

The maximum unbalanced moments resisted by specimens A4-S and B4-S are 63 kN-m and 73 kN-m (558 kip-in and 647 kip-in). This was a 50% increase in unbalanced moment capacity for specimen A4-S and 74% increase for specimen B4-S over control specimen C-02. Yielding occurred across the effective width of the top mat of longitudinal reinforcement during the test of control specimen C-02. Therefore, the increase in the upgraded specimens' unbalanced moment capacity was attributed to strain hardening and the horizontal components of the CFRP stirrups, positioned in the direction of lateral loading. Contributions of CFRP stirrups to flexural strength will be further discussed in section 4.8.3.2.

The strength increase provided by the CFRP stirrups was accompanied by a very small (3%) increase in lateral stiffness for specimen B4-S. If the lateral stiffness of the specimen significantly increased this could increase natural frequency of the structure, which may also lead to increased inertial forces during an earthquake. However, a 3% increase in lateral stiffness would have had an insignificant effect on the natural frequency of a structure similar to the test specimens because negligible mass was added by upgrading the test specimens. Test specimen stiffness will be discussed in section 4.9.

Rotation (degrees)

① Concrete begins to spall and crush around column base plate at 0.016 radians.

② Punching initiates at the South side of the Column at 0.019 radians.

③ Punching occurs at the North side of the Column at 0.011 radians.

C-63

Direction of Loading

③

Unbalanced Moment (kN-m)

Unbalanced Moment (kip-inch)

Rotation (radians)
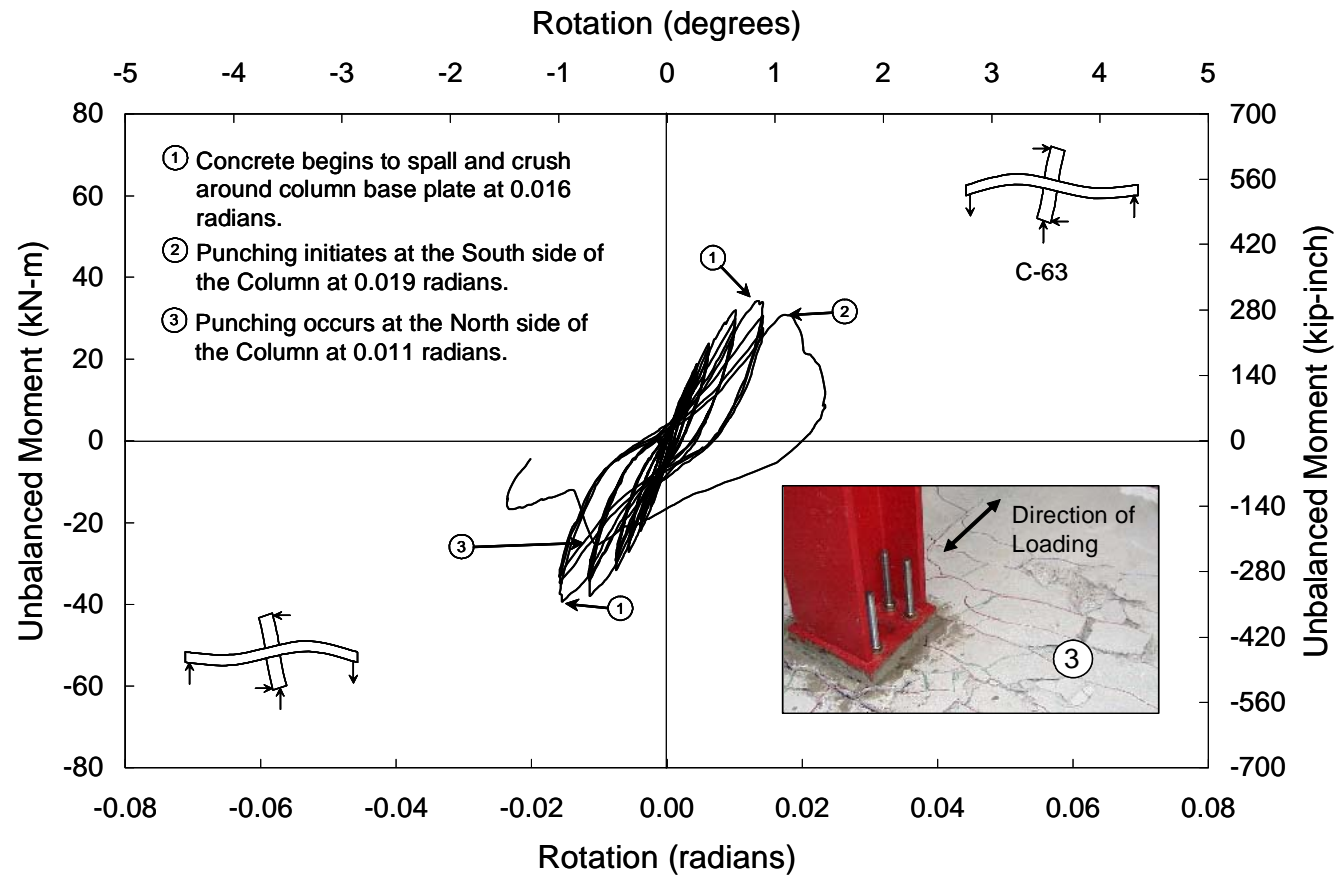
Figure 4.8 Control Specimen C-63 Unbalanced Moment versus Connection Rotation

Rotation (degrees)

① Top steel strain at 0.007 radians $\varepsilon_s = 2.0\varepsilon_y$.

② At 0.015 radians, top steel strain > $2\varepsilon_y$ across c+3.5h, transverse to direction of lateral load.

③ Cracks form around the column base plate on the bottom face of slab at 0.022 radians.

④ Punching initiates at the South side of the Column at 0.023 radians.

C-02

Direction of Loading

⑤ Punching occurs at the North side of the Column at 0.017 radians.

Rotation (radians)

Figure 4.9 Control Specimen C-02 Unbalanced Moment versus Connection Rotation

∞

The chart axes and labels:

Lateral Displacement (mm) — top axis: -150, -120, -90, -60, -30, 0, 30, 60, 90, 120, 150

Load (kN) — left axis: -60, -40, -20, 0, 20, 40, 60

Unbalanced Moment (kN-m) — right axis: -90, -60, -30, 0, 30, 60, 90

Drift (%) — bottom axis: -10, -8, -6, -4, -2, 0, 2, 4, 6, 8, 10

A4-S

① Top steel strain at 1% drift: $\varepsilon_s = 2.7\varepsilon_y$.

② Max strain in N-S, d/4, CFRP at 1.5% drift: $\varepsilon_{CFRP} = 0.08\varepsilon_u$.

③ At 2% drift, top steel strain > $2\varepsilon_y$ across c+3.5h, transverse to direction of lateral load.

④ Max E-W, d/4, CFRP strain at 3.5% drift: $\varepsilon_{CFRP} = 0.13\varepsilon_u$.

⑤ Max E-W, 3d/4, CFRP strain at 8% drift: $\varepsilon_{CFRP} = 0.1\varepsilon_u$.

Direction of lateral loading

N-S CFRP Stirrups

E-W CFRP Stirrups

∞

Figure 4.10 Upgrade Specimen A4-S Unbalanced Moment versus Connection Rotation
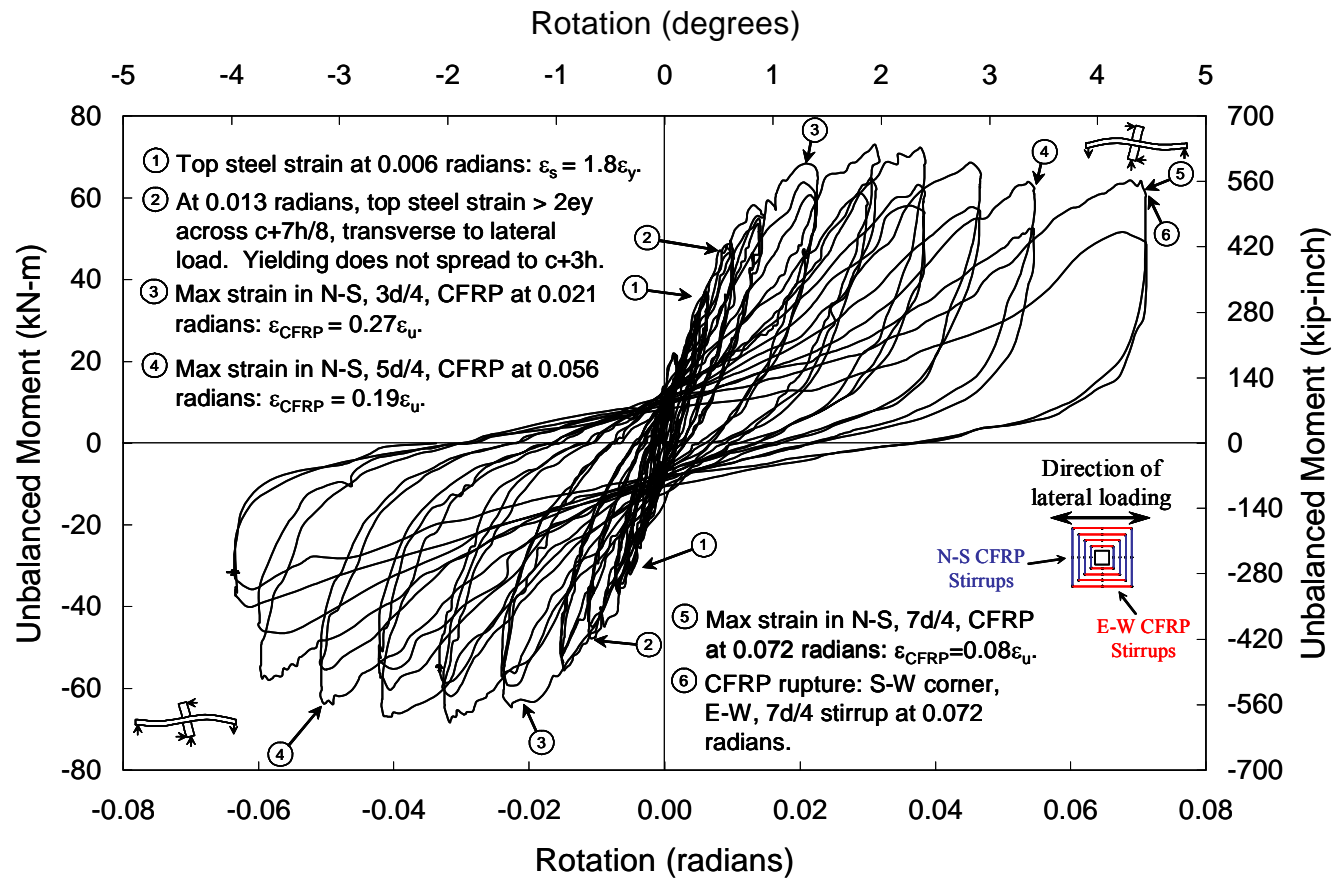
Figure 4.11 Upgrade Specimen B4-S Unbalanced Moment versus Connection Rotation

4.6   BACKBONE CURVES

This section discussed the lateral load-drift and unbalanced moment-connection rotation backbone curves. Peak lateral loads and unbalanced moments at applied drift-cycles are defined in section 4.3.2.

4.6.1   Lateral Load-Drift Backbone Curve

During the combined gravity and lateral load tests, both control specimens did not exhibit ductile behavior. The lateral load-drift backbone curves for each specimen are plotted in Figure 4.12. Test specimen C-63 attained a maximum lateral load of 24.5 kN (5.5 kips) and punching shear failure initiated at a drift ratio of 2.26%. Control specimen C-02 sustained a maximum lateral load of 27.1 kN (6 kips) for two applied drift-cycles. However, specimen C-02 experienced a punching shear failure on the subsequent drift-cycle.

The poor inelastic behavior displayed by specimens C-63 and C-02 was eliminated in upgraded specimens A4-S and B4-S. After achieving a maximum lateral load of 41.5 kN (9.3 kips), specimen A4-S retained 80% of the maximum resisted lateral load up to an inter-story drift of 8.3%. Following the initial strength degradation, the lateral load carrying capacity increased after an applied drift of 7%, most likely due to the onset of strain hardening in the reinforcing steel. The maximum lateral load resisted by specimen B4-S was 48 kN (10.8 kips). After reaching the peak lateral load peak, specimen B4-S demonstrated a strength decay of 12.5% until CFRP stirrup rupture occurred at 8.3% inter-story drift. This resulted in a 41% decrease in lateral load resistance on the completion of the applied drift-cycle.
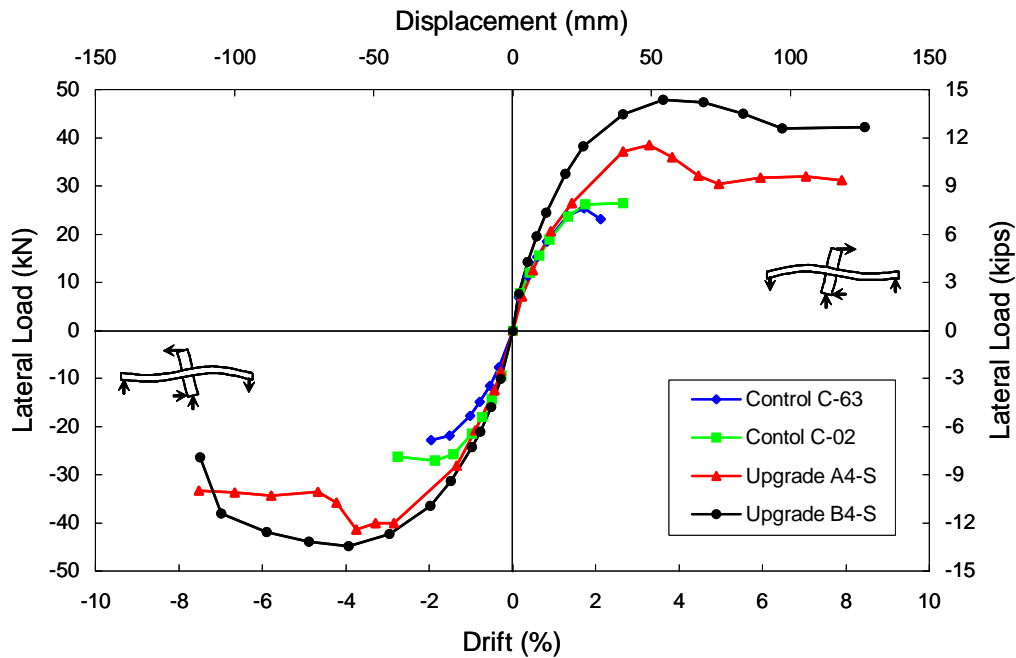
Figure 4.12 Lateral Load versus Drift Backbone Curves

4.6.2   Unbalanced Moment-Connection Rotation Backbone Curve

The unbalanced moment-rotation backbone curves of each test specimen followed the general behavioral trends exhibited by the lateral load-displacement backbone curves, shown in Figure 4.13.   The maximum moment resisted by specimens C-63 and C-02 was 37.3 kN-m (330 kip-in) and 41 kN-m (360 kip-in). For both control specimens, punching shear failure initiated on the south column face at rotations of 0.019 and 0.023 radians, respectively.   As previously stated, the connection rotations of upgrade specimen A4-S could not be recorded past 0.057 radians because the readings from the instrument readings are saturated. Both upgraded specimens displayed ductile behavior throughout the test, as evidenced by the stable hysteretic response observed during the test (Figure 4.10

and Figure 4.11). Specimen A4-S withstood a maximum moment of 63 kN-m (557 kip-in). A 20% drop in unbalanced moment capacity occurred at a rotation of 0.042 radians, yet specimen A4-S maintained its unbalanced moment capacity for the remaining lateral drift-excursions. Specimen B4-S withstood the largest unbalanced moment in the study, equal to 73 kN-m (647 kip-in), which decreased by 42% after CFRP stirrup rupture occurred.
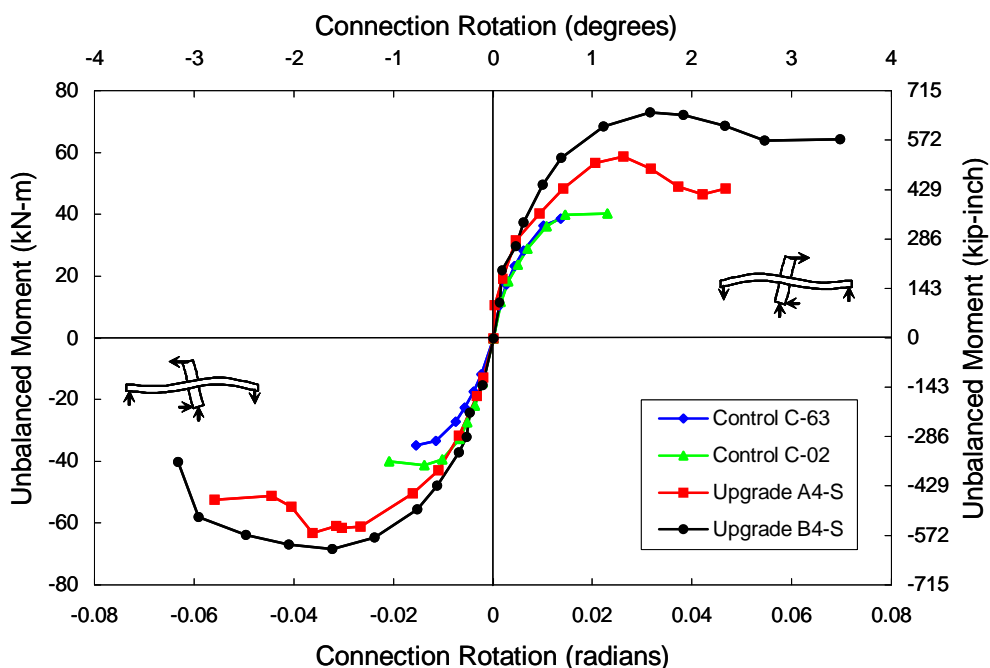
Figure 4.13 Unbalanced Moment versus Rotation Backbone Curves

4.7 CRACK PATTERNS

Crack patterns were visible on the tension face of each test specimen during all phases of the tests conducted in this study. In the first phases of testing, flexural cracks formed on the top face of each test specimen, primarily transverse

to the direction of loading, when the gravity load was applied. Figure 4.14 shows the formation of typical crack patterns on specimen A4-S, after the application of gravity load. All visible cracks were marked with colored pens during the test.
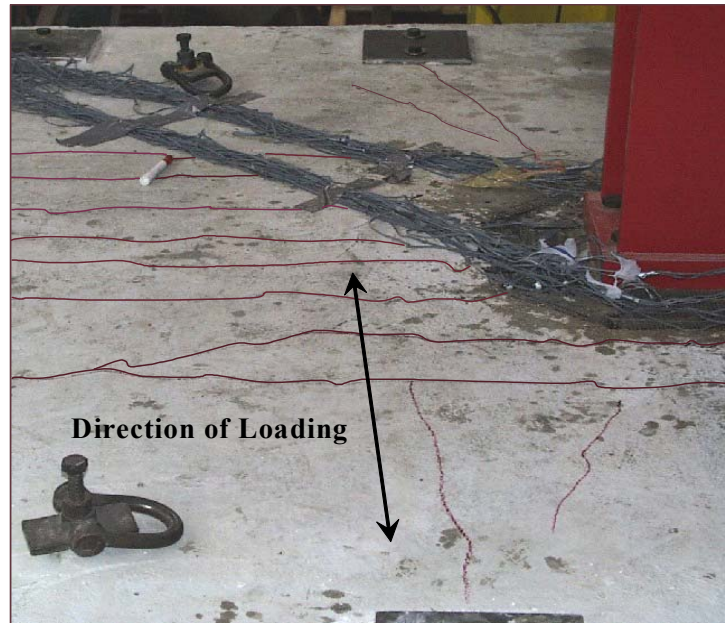
Figure 4.14 Gravity Load Cracking of Upgrade Specimen A4-S

Flexural cracks spread across the top face of each slab after the lateral loads were applied. The number of new cracks and the width of existing cracks increased with increased lateral displacements. Qualitative evaluation of cracks was performed by visual inspection; however, exact measurements of crack widths were not carried out during testing. Additional flexural cracks were marked at drift intervals of 1% and 2% inter-story drift for all test specimens. Figure 4.15 (a) and (b) and Figure 4.16 (a) and (b) show the location of cracks at the top face of the slabs at 1% and 2% drift intervals for test specimens A4-S and B4-S.

Deterioration of concrete on the compression face of the slab indicated the onset of a punching shear failure. Concrete began to crush and spall around the

column base plate of control specimens C-02 and C-63, Figure 4.17(a) and (b), and outside the connection upgrade region of upgrade specimens A4-S and B4-S, Figure 4.18(a) and (b). The top-face of test specimens C-63, C-02, A4-S and B4-S after the occurrence of punching shear failures are shown in Figure 4.19 through Figure 4.22.
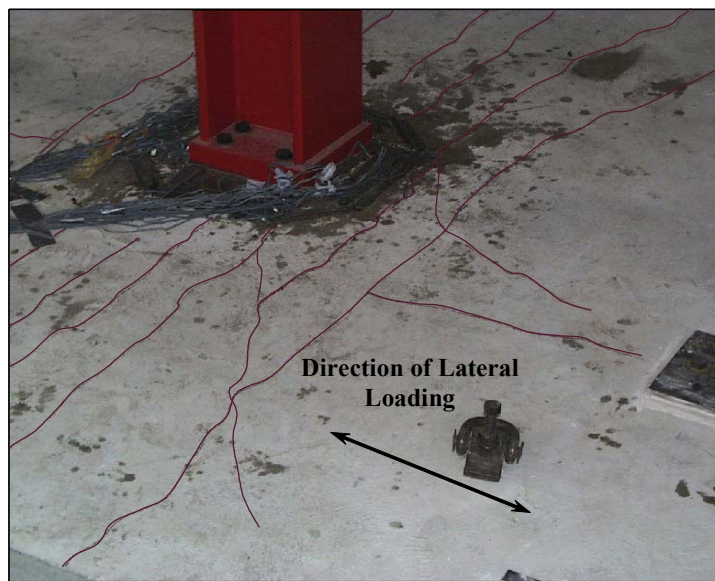
(a)
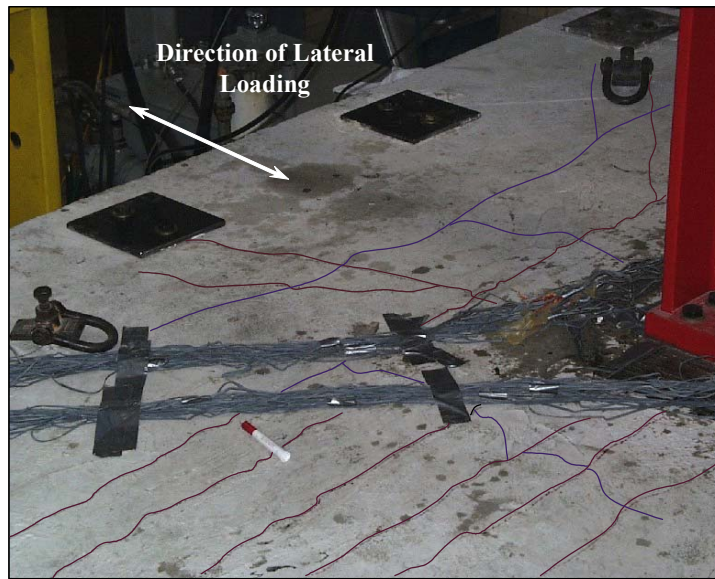
(b)

Figure 4.15 Flexural Cracking in Specimen A4-S after (a) 1% Lateral Drift;
and, (b) 2% Lateral Drift
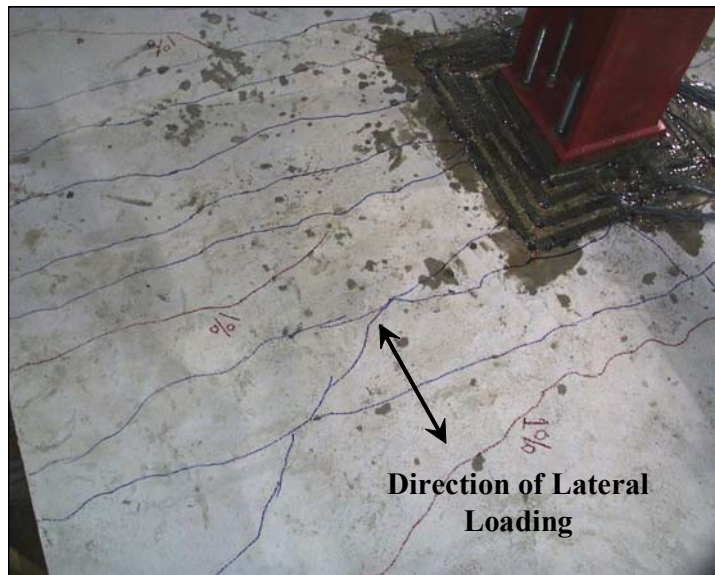
(a)

(b)

Figure 4.16 Flexural Cracking in Specimen B4-S after (a) 1% Lateral Drift; and, (b) 2% Lateral Drift

(a)   (b)

Figure 4.17 Initiation of Punching Shear Failure for (a) Control Specimen C-02; and, (b) Control Specimen C-63

(a)   (b)
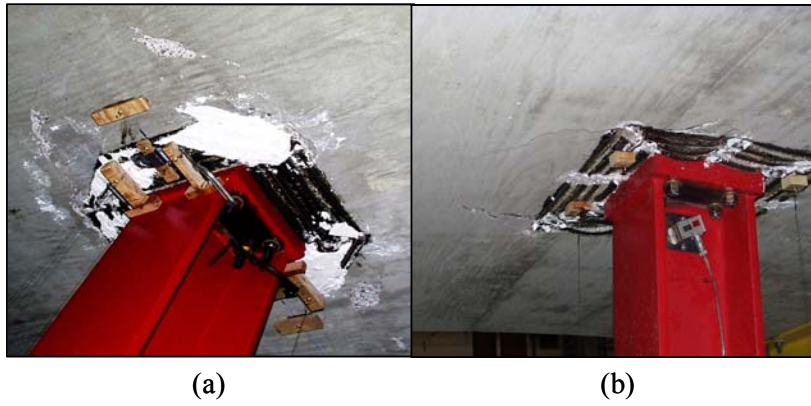
Figure 4.18 (a) Crushing and Spalling of Upgrade Specimen A4-S; (b)
Initiation of punching shear failure in Upgrade Specimen B4-S
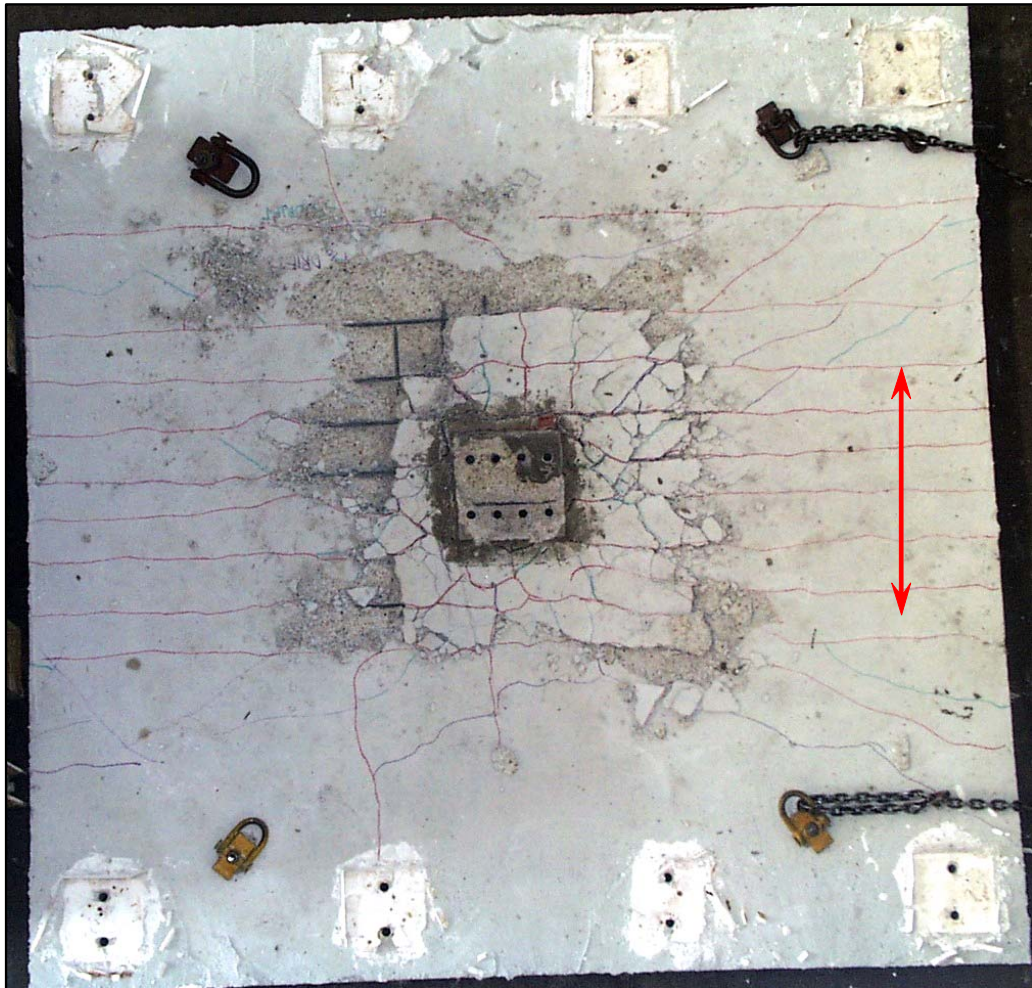
Direction of Lateral Loading denoted with: ⟵⟶

Figure 4.19 Control Specimen C-63: Tension Face Punching Shear Failure Crack Profile
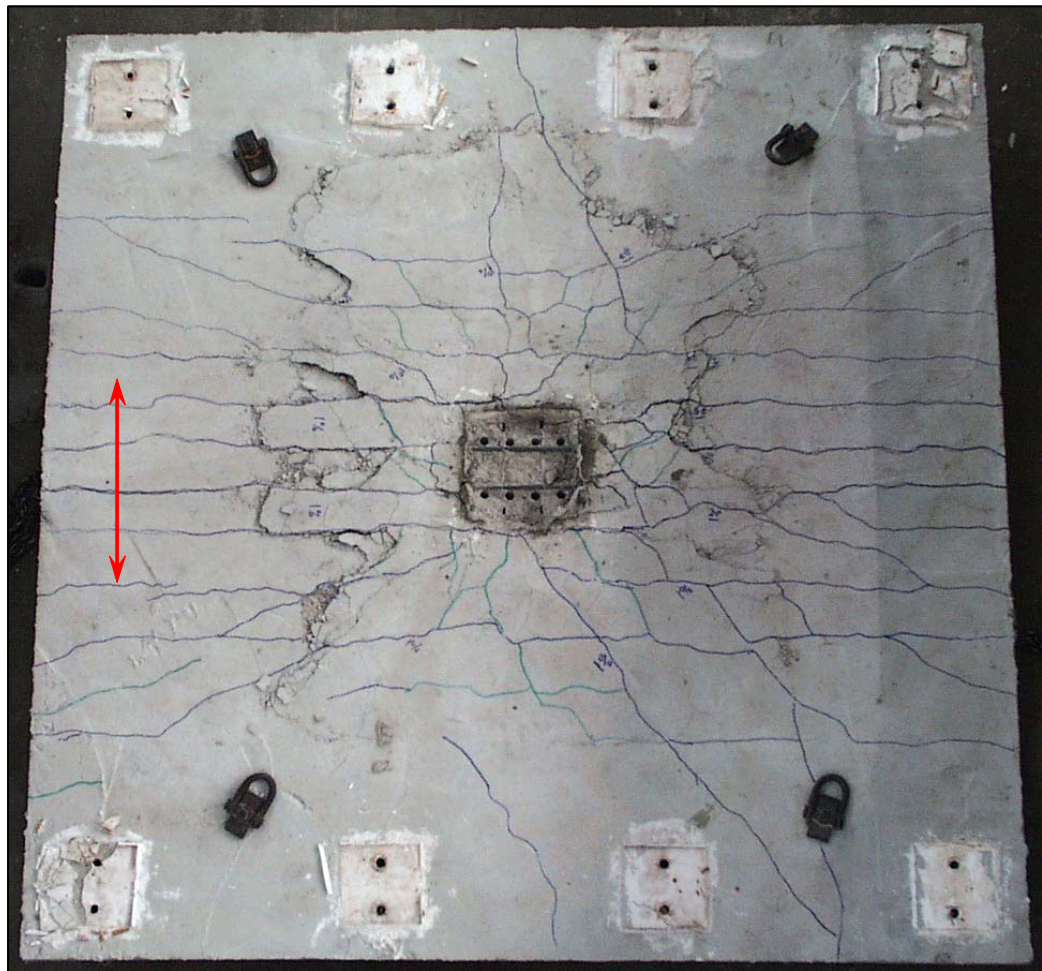
Direction of Lateral Loading denoted with: ⟷

Figure 4.20 Control Specimen C-02 Tension Face Punching Shear Failure
Crack Profile

Direction of Lateral Loading denoted with: ⟷

Figure 4.21 Specimen A4-S Tension Face Punching Shear Failure Crack Profile
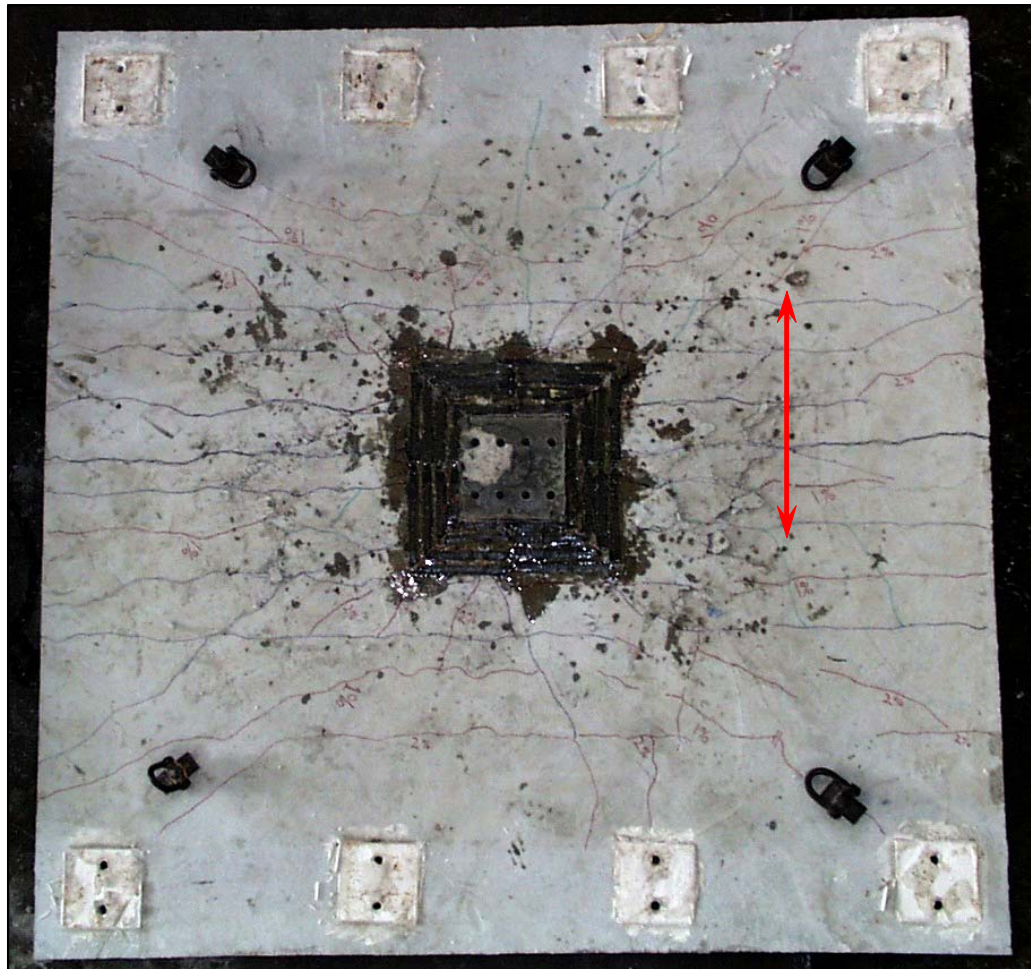
Direction of Lateral Loading denoted with:

Figure 4.22 Specimen B4-S Tension Face Punching Shear Failure Crack Profile

4.8 REINFORCEMENT STRAINS

Steel and CFRP reinforcement strains measured during the simulated seismic tests are discussed in this section. Strain gage data was also analyzed for the initial gravity load test phase. Reinforcing bar strain data was arranged in each load phase to create strain profiles transverse to and in the direction of

loading, for the longitudinal bars positioned parallel to the applied lateral load. Transverse strain profiles list the strain values of the steel reinforcing bars within the ACI 318-02 effective width. Strain profiles in the direction of loading list the strain values of the two centerline steel bars. Figure 4.23 shows the strain gages used in these strain profiles. CFRP stirrup strain profiles were also analyzed in both the transverse and direction of loading. CFRP strain profiles for specimen A4-S are shown in Figure 4.24 and for specimen B4-S are shown in Figure 4.25. Maximum strain values of all available data will be presented for each perimeter of CFRP stirrups.

Direction of Lateral
Loading

(a)

(b)
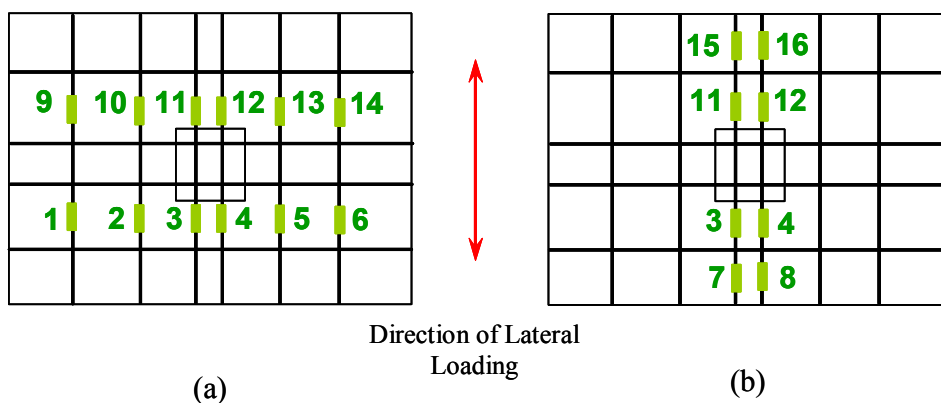
Figure 4.23 Gages used to Define Top Reinforcing Steel Strain Profiles: (a) Transverse to the Direction of Loading; (b) In the Direction of Loading
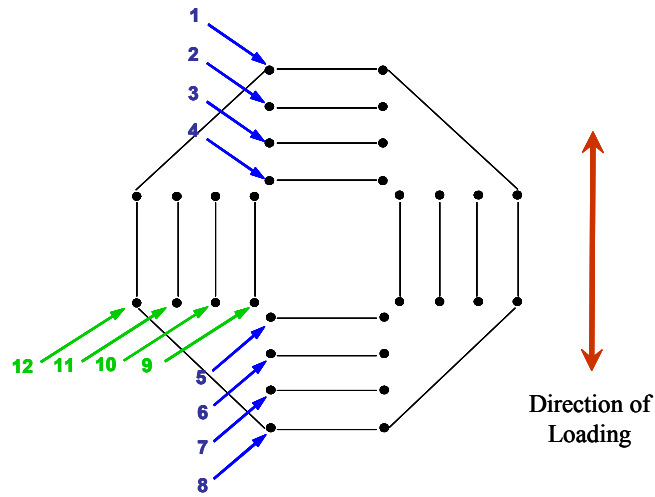
Gages used to establish the strain profiles in the
direction of loading shown in blue.

Gages used to establish the strain profiles transverse
to the direction of loading shown in red.

Figure 4.24 Specimen A4-S CFRP Strain Gage Profiles
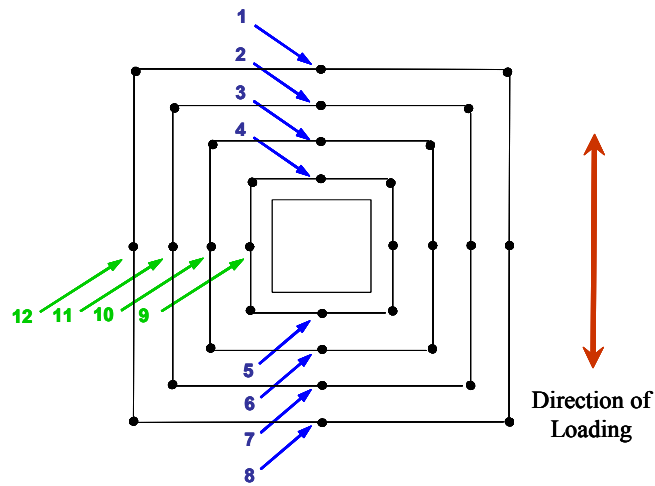
Gages used to establish the strain profiles in the
direction of loading shown in blue.

Gages used to establish the strain profiles transverse
to the direction of loading shown in red.

Figure 4.25 Specimen B4-S CFRP Strain Gage Profiles

96

4.8.1   Longitudinal Reinforcing Steel Strains under the Initial Gravity Load

Table 4.1 and Table 4.2 list each test specimen's top mat, reinforcing steel strain values transverse to and in the direction of loading, for the bars positioned parallel to the applied lateral load. The application of the gravity load caused the top mat of steel reinforcement to yield around the columns of each test specimen, except B4-S. For the strain profile established transverse to the direction to loading, yielding was limited to the two centerline bars of the control specimens. For specimen A4-S, yielding spread throughout all of the gaged bars in the top mat of steel in the transverse direction to lateral loading and along all the gages in the direction of lateral loading. The steel reinforcement of specimen B4-S did not yield under gravity load due to the influence of the CFRP strands of the connection upgrade, serving as flexural reinforcement.

Table 4.1 Top Reinforcing Bar Strains at the Total Applied Gravity Load
Transverse to the Direction of Lateral Loading

Test Specimen	Reinforcing Bar Strain Transverse to the Direction of Lateral Loading (micro strain)					
	−356 (mm)*	−203 (mm)	−51 (mm)	51 (mm)	203 (mm)	356 (mm)
A4-S	2500	2350	2250	2400	2700	2100
B4-S	1300	1550	1000	2250	1600	550
C-02	2000	–	2600	2200	–	2100
C-63	–	–	–	–	–	–

*Distance from test specimen centerline

Yielding of flexural reinforcement upon the application of large gravity loads is consistent with the findings of Pan and Moehle [23]. The test specimens in Pan and Moehle's study had reinforcement ratios of 0.76% (at the column face within the ACI effective width, C+3H) and a slab thickness of 123 mm (4.25 in). Longitudinal reinforcing steel strains were shown to be at around the tested yield

strain after the application of gravity load (pp. 158-165, [23]). It was also reported that there was an increase in the presence of flexural cracks on the top slab face with an applied gravity load of $0.35V_o$ (pp. 30, [23]). These findings lead to the V_g/V_o ratio limitation of 0.4 for flat-plate structures subjected to seismic loads (ACI 318 section 21.12.6.8). Therefore, if flat-plate slab-column connections can be shown to behave satisfactorily at high levels of gravity shear, these connections should perform well at lower, and possibly more realistic, gravity load levels.

Table 4.2 Top Reinforcing Bar Strains at the Total Applied Gravity Load in the Direction of Lateral Loading

Test Specimen	Reinforcing Bar Strain in the Direction of Lateral Loading (microstrain)			
	- 305 (mm)*	- 152.5 (mm)	152.5 (mm)	305 (mm)
A4-S	2600	2300	2400	2600
B4-S	1250	1100	2250	950
C-02	2050	2600	2200	1700
C-63	–	–	–	–

*Distance from test specimen centerline

For each specimen in the study, all gaged bottom mat, steel reinforcement did not yield upon the application of gravity load. Initially, all gaged bottom steel reinforcement was in compression. As the gravity load increased, however, the neutral axis passed below the bottom steel reinforcement, which caused the longitudinal bars to go into tension.

4.8.2 CFRP Stirrup Strains under the Initial Gravity Load

Table 4.3 lists the CFRP strains for specimens A4-S and B4-S. For each upgraded specimen, CFRP strains decreased with distance from the face of the column. After the installation of CFRP reinforcement, The holes through the

slabs were filled with epoxy. As a result, the strains measured at the vertical components of the CFRP stirrups were initially compatible with the relevant strains in the concrete slab, until cracking occurred. Therefore, the vertical strain should decrease with distance (measured from the face of the column) since the applied shear stress decreased with distance from the column face. Prior to the application of lateral loads, the recorded CFRP stirrup strains in specimen A4-S were measured to be less than 3% of the rupture strain and less than 10% of the CFRP rupture strain in specimen B4-S. These strain values are low because no inclined cracks have formed in the upgraded regions.

Table 4.3 CFRP Strains upon Application of the Gravity Load

Gravity Load CFRP Strain								
Test Specimen	Distanace From Column Face in the Direction of Loading							
	d/4	Percent of ε_{ult}	3d/4	Percent of ε_{ult}	5d/4	Percent of ε_{ult}	7d/4	Percent of ε_{ult}
A4-S	300	2.6	100	0.8	–	–	50	0.6
B4-S	–	–	1000	8.0	450	3.7	350	2.8

Differences in measured CFRP strain between specimens A4-S and B4-S can be attributed to CFRP stirrup configurations. The use of CFRP stirrups for the slab-column connection upgrade was solely intended to provide shear reinforcement. However, the vertical legs of the CFRP stirrups also provided anchorage for the horizontal lengths of each stirrup, which then worked as flexural reinforcement. The CFRP reinforcement configuration of connection upgrade B4-S provided greater flexural reinforcement than specimen A4-S during the lateral load tests due to a larger amount of horizontal CFRP that ran in the direction of lateral loading. This was shown by the reduced longitudinal reinforcement strains in specimen B4-S in comparison to specimen A4-S. CFRP flexural resistance contributions will be further discussed in section 4.8.3.2.

4.8.3 Reinforcing Bar Strain Profiles during Simulated Seismic Tests

Strain data for the simulated seismic tests was analyzed to find maximum strain values for each test specimen at given lateral drift cycles. Maximum strain values for the top mats of steel reinforcement will be presented for test specimens C-02, A4-S and B4-S in the direction of lateral loading and transverse to the direction of lateral loading. The top layer of steel of specimen C-63 was not gaged. Available CFRP strain gage data will be presented transverse to and in the direction of lateral loading for both upgraded specimens (Figure 4.24 and Figure 4.25). All CFRP strain gages are mounted vertically on the CFRP stirrups, within the holes through the slab, in the upgrade region.

4.8.3.1 Steel Reinforcing Bar Strains

Table 4.4 lists the reinforcing steel strains of specimen C-02 in the direction of lateral loading. This data indicated that considerable yielding occurred along the length of the top mat, centerline reinforcement, at the face of the column, before the specimen punched. This behavior was expected because of the high level of gravity shear applied in combination with lateral loads. Table 4.5 shows the reinforcing steel strains of specimen C-02 transverse to the direction of lateral loading. During the 2% applied drift-cycle, yielding spread across the gaged bars, which had a width of c+3.5h. This data suggests the effective width of c+3h, defined in ACI 318-02, accurately represents the portion of the slab contributing to the resistance of unbalanced moments. Longitudinal steel was not sufficiently gaged (transverse to the direction of loading) to determine if the effective width defined in FEMA 356 (c+5h) was accurate. However, it is plausible that bars in this region actively participated in unbalanced moment resistance due to the amount of yielding that was measured.

Table 4.4 Specimen C-02 Maximum Top Mat Rebar Strains per Drift-Cycle in the Direction of Lateral Loading

Drift (%)	Specimen C-02							
	Rebar Strain (microstrain) Meassured From Specimen Centerline Positioned in the Direction of Lateral Loading							
	−305 (mm)*		−152.5 (mm)		152.5 (mm)		305 (mm)	
	8[#]	$\varepsilon/\varepsilon_y$	3	$\varepsilon/\varepsilon_y$	12	$\varepsilon/\varepsilon_y$	15	$\varepsilon/\varepsilon_y$
$	1900	0.8	2700	1.2	2200	1.0	1700	0.7
0.25	2300	1.0	3300	1.5	2400	1.1	1900	0.8
0.5	2500	1.1	3850	1.7	2700	1.2	2150	0.9
1	2650	1.2	4550	2.0	2950	1.3	2250	1.0
1.5	2750	1.2	6200	2.7	3250	1.4	2350	1.0
2	2900	1.3	7400	3.3	9400	4.2	2400	1.1
2.5	2850	1.3	Gage Failed		14100	6.2	2450	1.1
3	2600	1.1			Gage Failed		2300	1.0
3.5	2900	1.3					2300	1.0

* Distance from the centerline of the test specimen
[#] Strain gage number, see Figure 4.22
$ Strain under gravity load

Table 4.5 Specimen C-02 Maximum Top Mat Rebar Strains per Drift-cycle Transverse to the Direction of Lateral Loading

	Specimen C-02										
Drift (%)	Rebar Strain (microstrain) Meassured From Specimen Centerline Positioned Transverse to the Direction of Lateral Loading (mm)										
	−356 (mm)*		−203 (mm)		−51 (mm)		51 (mm)		203 (mm)		356 (mm)	
	$1^{\#}$	$\varepsilon/\varepsilon_y$			11	$\varepsilon/\varepsilon_y$	4	$\varepsilon/\varepsilon_y$			6	$\varepsilon/\varepsilon_y$
$	2000	0.9	N.A.		2600	1.2	2200	1.1	N.A.		1700	0.9
0.25	2400	1.0			3300	1.5	2900	1.3			2400	1.0
0.5	2650	1.2			3900	1.7	3100	1.4			2600	1.2
1	2900	1.3			4600	2.0	4200	1.9			2800	1.3
1.5	3500	1.6			6300	2.7	9650	4.3			3600	1.6
2	13800	6.1			7400	3.3	16600	7.4			14400	6.4
2.5	13900	6.1			19500	8.6	17300	7.6			16000	7.1
3	14000	6.2			Gage Failed		17600	7.8			Gage Failed	
3.5	Gage Failed						Gage Failed					

* Distance from the centerline of the test specimen

$^{\#}$ Strain gage number, see Figure 4.22

$ Strain under gravity load

The top mat reinforcing steel strain profiles parallel to the direction of loading are shown in Table 4.6 and Table 4.7. Specimen A4-S had similar strain profiles to specimen C-02 at the early stages of loading. However, test specimen A4-S survived an applied drift-ratio of 8.3%. Yielding spread along the total gaged length of the top layer of steel reinforcement at an applied drift-cycle of 2%. All the top-steel strain-gages of specimen A4-S failed after the 3% applied drift-cycle. It is therefore plausible that strain-hardening occurred during the final drift excursions. The strain profile transverse to the direction of loading showed that yielding across the gaged bars was greater than $2\varepsilon_y$ at the 2% applied drift-cycle. This also indicates the effective width defined by ACI 318-02 is appropriate.

Table 4.6 Specimen A4-S Top Steel Maximum Top Mat Rebar Strains per Drift-Cycle in the Direction of Lateral Loading

Drift (%)	Specimen A4-S
	Rebar Strain (microstrain) Meassured From Specimen Centerline Positioned in the Direction of Lateral Loading
	−305 (mm)*		−152.5 (mm)		152.5 (mm)		305 (mm)	
	$8^{\#}$	$\varepsilon/\varepsilon_y$	4	$\varepsilon/\varepsilon_y$	11	$\varepsilon/\varepsilon_y$	15	$\varepsilon/\varepsilon_y$
$	1550	0.7	2600	1.1	2350	1.0	2600	1.1
0.25	1700	0.8	2900	1.3	2850	1.3	2900	1.3
0.5	1850	0.8	3200	1.4	3100	1.4	3200	1.4
1	2200	1.0	6000	2.7	4700	2.1	6000	2.7
1.5	2350	1.0	16600	7.3	17600	7.8	16600	7.3
2	2400	1.1			21200	9.4		
2.5	2400	1.1						
3	18300	8.1						
3.5								
4								
4.5			Gage Failure		Gage Failed		Gage Failed	
5	Gage Failed							
6								
7								
8								
8.3								

* Distance from the centerline of the test specimen
\# Strain gage number, see Figure 4.22
$ Strain under gravity load

Table 4.7 Specimen A4-S Maximum Top Mat Rebar Strains per Drift-cycle Transverse to the Direction of Lateral Loading

Specimen A4-S												
Drift (%)	Rebar Strain (microstrain) Meassured From Specimen Centerline Positioned Transverse to the Direction of Lateral Loading											
	−356 (mm)*		−203 (mm)		−51 (mm)		51 (mm)		203 (mm)		356 (mm)	
	1[#]	$\varepsilon/\varepsilon_y$	2	$\varepsilon/\varepsilon_y$	3	$\varepsilon/\varepsilon_y$	4	$\varepsilon/\varepsilon_y$	5	$\varepsilon/\varepsilon_y$	6	$\varepsilon/\varepsilon_y$
$	2500	1.1	2350	1.0	2250	1.0	2400	1.1	2700	1.2	2100	0.9
0.25	2800	1.2	200	0.1	2650	1.2	2900	1.3	3200	1.4	2300	1.0
0.5	3000	1.3	3200	1.4	2900	1.3	3200	1.4	3900	1.7	2500	1.1
1	3400	1.5	6300	2.8	4000	1.8	6000	2.7	8900	3.9	3000	1.3
1.5	2500	1.1	12000	5.3	7800	3.4	16600	7.3	14300	6.3	3000	1.3
2	8900	3.9	13600	6.0	10500	4.6			16000	7.1	3000	1.3
2.5			15600	6.9	14600	6.5			18300	8.1	6800	3.0
3			15200	6.7								
3.5	Gage Failure		13200	5.8								
4			18700	8.3			Gage Failure					
4.5					Gage Failure				Gage Failure		Gage Failure	
5			Gage Failure									
6												
7												
8												
8.3												

* Distance from the centerline of the test specimen
[#] Strain gage number, see Figure 4.22
$ Strain under gravity load

Specimen B4-S top and bottom steel reinforcing strains are shown in Table 4.8 and Table 4.9. The top steel reinforcement strain profiles followed the general trends of the strains measured in specimen A4-S. Significant yielding did not spread across the gaged bars, transverse to the direction of loading, throughout the test. The fraction of longitudinal steel that actively participated in the unbalanced moment resistance was located within a width of c+7h/8. For this specimen, the ACI 318-02 effective width would therefore be conservative. However, the reduction of longitudinal bars that actively resisted unbalanced moment could be attributed to the CFRP reinforcement contributing to the flexural strength of the specimen.

104

Table 4.8 Specimen B4-S Top Steel Maximum Top Mat Rebar Strains per Drift-Cycle in the Direction of Lateral Loading

Specimen B4-S								
Drift (%)	Rebar Strain (microstrain) Meassured From Specimen Centerline Positioned in the Direction of Lateral Loading							
	−305 (mm)*		−152.5 (mm)		152.5 (mm)		305 (mm)	
	7[#]	$\varepsilon/\varepsilon_y$	4	$\varepsilon/\varepsilon_y$	11	$\varepsilon/\varepsilon_y$	15	$\varepsilon/\varepsilon_y$
$	1300	0.6	2600	0.9	2200	0.9	1700	0.4
0.25	1600	0.7	2400	1.0	2400	1.0	1800	0.5
0.5	2000	0.9	2500	1.1	3000	1.3	1750	0.6
1	2100	1.0	3700	1.6	4000	1.8	1800	0.7
1.5	2400	1.1	4900	2.2	7100	3.2	1850	0.8
2	2900	1.3			15000	6.6	2000	0.9
2.5	3100	1.4					2100	0.9
3	7900	3.5					2200	1.0
4	10800	4.8	Gage Failed		Gage Failed			
5	Gage Failed						Gage Failed	
6								
7								
8.3								

* Distance from the centerline of the test specimen

[#] Strain gage number, see Figure 4.22

$ Strain under gravity load

105

Table 4.9 Specimen B4-S Maximum Top Mat Rebar Strains per Drift-cycle Transverse to the Direction of Lateral Loading

Drift (%)	Specimen B4-S											
	Rebar Strain (microstrain) Meassured From Specimen Centerline Positioned Transverse to the Direction of Lateral Loading											
	−356 (mm)*		−203 (mm)		−51 (mm)		51 (mm)		203 (mm)		356 (mm)	
	$1^{\#}$	$\varepsilon/\varepsilon_y$	2	$\varepsilon/\varepsilon_y$	11	$\varepsilon/\varepsilon_y$	4	$\varepsilon/\varepsilon_y$	5	$\varepsilon/\varepsilon_y$	6	$\varepsilon/\varepsilon_y$
\$	1300	0.6	1500	0.8	1000	0.9	2200	0.9	1600	0.6	2100	0.5
0.25	1600	0.7	2300	1.0	2400	1.0	2400	1.0	1750	0.8	1400	0.6
0.5	1900	0.8	2700	1.2	2900	1.3	2500	1.1	2200	1.0	1700	0.7
1	2100	0.9	3900	1.7	4000	1.8	3700	1.6	2600	1.1	1900	0.8
1.5	2400	1.1	11700	5.2	7200	3.2	4900	2.2	3000	1.4	2000	0.9
2	2800	1.2	15000	6.6	15000	6.6	Gage Failed		12100	5.4	2100	0.9
2.5	3000	1.4			20000	8.8			15200	6.7	2100	0.9
3	3000	1.3			Gage Failed				15300	7.0	2000	0.9
4	3100	1.3	Gage Failed						16800	7.4	2000	0.9
5	3000	1.3			Gage Failed						1900	0.8
6	3100	1.3							Gage Failed		1700	0.8
7	3600	1.6									1700	0.7
8.3	5200	2.3									1400	0.6

* Distance from the centerline of the test specimen

\# Strain gage number, see Figure 4.22

\$ Strain under gravity load

4.8.3.2   CFRP Strains

Table 4.10 and Table 4.11 list the maximum CFRP strain values for upgraded specimens A4-S and B4-S. The available maximum values of strain at each drift-cycle are listed. Strain gages were difficult to place within the holes through the slab of specimen B4-S due to the CFRP stirrup configuration of the upgrade (Figure 2.12). Because of this, strain gages could not be installed in some specified locations, and some of the installed gages failed at the early stages of testing. Strain gage failure is marked in Table 4.10 and Table 4.11.

Table 4.10 shows that for comparable cases (i.e. same distance away from the column's face and at the same drift level), the strains in the CFRP stirrups

positioned in the north-south direction (direction of lateral loading) are less than those in the east-west direction. This was mainly due to the fact that all of the gages placed in the E-W direction were very close to or exactly at maximum moment sections. Considering moment-shear interaction, it could be proved that sections adjacent to the column face (transverse to the direction of lateral loading) would be most critical. The maximum stirrup strain value in the north-south direction occurred at the first CFRP stirrup perimeter (located d/4 from the column face) at a lateral drift of 1.5%, followed by a decrease in strain. This reduction in strain can be attributed to the formation of flexural cracks at the slab-column interface and shear cracking adjacent to it (Figure 4.26). As inclined cracking progressed, load redistributed throughout the CFRP stirrups of the connection upgrade. Load redistribution commenced at 2.5% and 3% inter-story drift, which coincided with punching shear failure drift-levels of the control specimens.

CFRP stirrups positioned in the east-west direction experienced a significant increase in strain within the 3% drift-cycle. As previously mentioned, this was caused by the formation of inclined cracks through the connection upgrade. Increased strain at this drift-cycle also corresponded with yielding of the bottom mat of longitudinal steel reinforcement. This indicated that dowel action may be triggered as shear cracks form around the connection.

Table 4.10 Specimen A4-S Maximum CFRP Strains Per Drift-Cycle

Drift (%)	CFRP Strains (microstrain)							
	N-S CFRP Perimeter Stirrups				E-W CFRP Perimeter Stirrups			
	d/4	3d/4	5d/4	7d/4	d/4	3d/4	5d/4	7d/4
$	300	100		100	900	0	200	
0.25	400	100		100	900	100	200	
0.5	600	200		200	800	100	200	
1	900	200		300	700	100	300	
1.5	1000	200		500	300	300	400	
2	900	300		600	100	400	400	
2.5	600	400		700	600	500	500	
3	500	300	Gages Failed	700	1300	700	600	Gages Failed
3.5	200	300		500	1500	800	400	
4	500	400		500	1500	1200	800	
4.5	400	500		400	1400	1100	800	
5	300	600		400	1200	1100	700	
6	400	600		400	1100	1300	700	
7	400	500		400	900	1400	800	
8	500	600		400	1700	1500	800	
8.3	500	600		400	1700	1400	800	

$ Strain under gravity load

Upgraded specimen A4-S had an increased unbalanced moment capacity of 49% over control specimen C-02. This can be attributed to strain hardening of the longitudinal steel and contributions of the E-W CFRP reinforcement to the flexural capacity of the slab. However, longitudinal steel gages failed after an applied drift-ratio of 4%, and the CFRP reinforcement was not sufficiently gaged to determine the strains within the CFRP stirrups. During the simulated seismic tests, CFRP stirrups were influenced by shear forces, flexural forces and strand development. The mechanics are complicated and further research is needed to determine the contributions of CFRP reinforcement and longitudinal steel to the flexural strength increases.
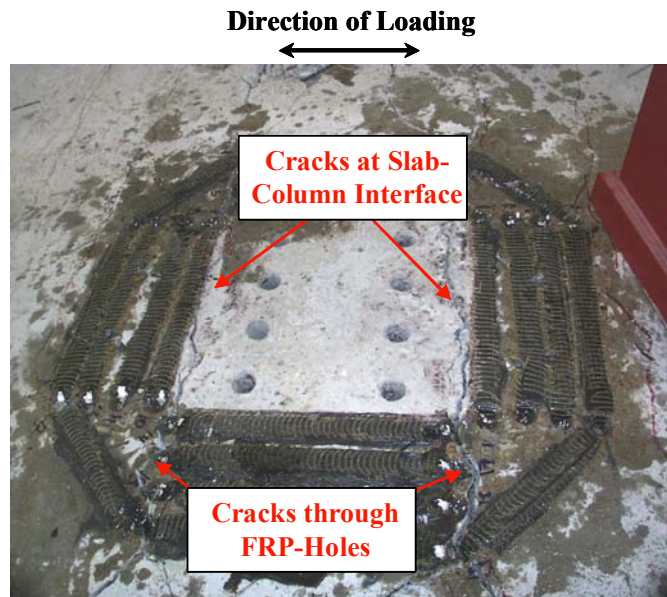
Figure 4.26 Cracks through Specimen A4-S Connection Region

The CFRP strains measured in specimen B4-S are listed in Table 4.11. The strain profile of specimen B4-S displayed similar characteristics to specimen A4-S. Strain data for the E-W stirrups was not obtained because the gages could not be placed in the corresponding holes through the slab. Strain redistribution initiated at 2.5% to 3% inter-story drift, which corresponded to inclined cracking within the connection upgrade region. As mentioned in section 4.8.3.2, the measured strains in the CFRP stirrups of specimen B4-S were larger than those in specimen A4-S. However, the total unbalanced moment resisted by test specimen B4-S was greater than test specimen A4-S due to CFRP configurations. As stated earlier, greater CFRP strains measured in the vertical holes through the slab in specimen B4-S may be partially due to the fact that the vertical legs of the CFRP strips acted as anchorage when the horizontal lengths flexurally strengthened the test specimen. However, the horizontal lengths of the closed stirrups also served as anchorage for the vertical legs that provided shear reinforcement. The exact

mechanics of this interaction cannot be explained with the limited data, and number of specimens, collected during this study.

Table 4.11 Specimen B4-S Maximum CFRP Strains Per Drift Cycle

Drift (%)	CFRP Strains (microstrain)			
	N-S Perimeter Stirrups			
	d/4	3d/4	5d/4	7d/4
$	Gages Failed	1000	400	300
0.25		1100	500	400
0.5		1800	900	400
1		2200	1000	400
1.5		2500	1200	400
2		3000	1300	500
2.5		3200	1900	600
3		1300	2000	600
4		1300	1900	700
5		1400	2100	800
6		1300	2200	900
7		1200	2000	900
8.3		1200	2000	1000

$ Strain under gravity load

At a drift ratio of 8.3%, the exterior CFRP strand located at the southwest corner of connection upgrade B4 ruptured at the top corner of the hole through the slab. This is shown in Figure 4.27. Once again, the exact mechanics are not known, but the stirrup most likely ruptured due to a stress concentration caused by shear and flexural interaction, and the 90 degree stirrup-bend located at the point of rupture. To account for stress concentrations at CFRP stirrup bends and fiber irregularity, Binici and Bayrak [6] recommend the use of an efficiency factor of 1/3 the CFRP rupture strain for stirrup design.
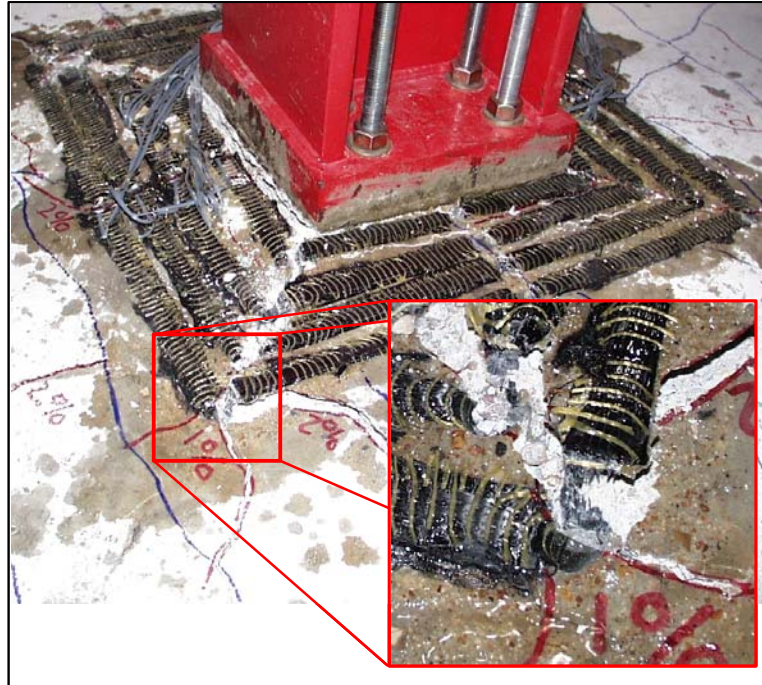
Figure 4.27 Upgrade Specimen B4-S CFRP Stirrup Rupture

4.9 STIFFNESS DEGRADATION

The lateral stiffness degradation of the slab-column sub-assemblages and rotational stiffness degradation of the connection regions are discussed in this section. The stiffness of each drift-cycle is defined as described in section 4.3.2. The initial stiffness of each test specimen was obtained using the backbone curves. The stiffness degradation of each test specimen with increased drift-cycles and degradation experienced during repeated drift levels are discussed.

4.9.1 Lateral Stiffness Degradation

Figure 4.28 shows the lateral stiffness degradation experienced by all test specimens. The stiffness values shown in this figure correspond to the maximum

lateral stiffness measured at each applied drift-cycle. Logarithmic trend lines were fit to all sets of data. The trend lines used in Figure 4.28 are not intended to generate universal equations; rather, they can be used to compare the general lateral stiffness degradation trends of the test specimens.

The initial lateral stiffness of each specimen shown in Figure 4.28 was somewhat different. Both upgraded test specimens should have had slightly higher initial stiffness values due to the flexural contribution of CFRP reinforcement to the lateral strength of these specimens. However, specimen A4-S exhibited a 22% lower initial lateral stiffness than control specimen C-02 and 6% lower initial stiffness than specimen C-63. These stiffness differences can be attributed to the variability of crack formations during the application of gravity load. The initial lateral stiffness of test specimen B4-S was found to be 3% greater than control specimen C-02. Therefore, the additional CFRP stirrups had insignificant affects on the initial lateral stiffness of the test specimens in this study.
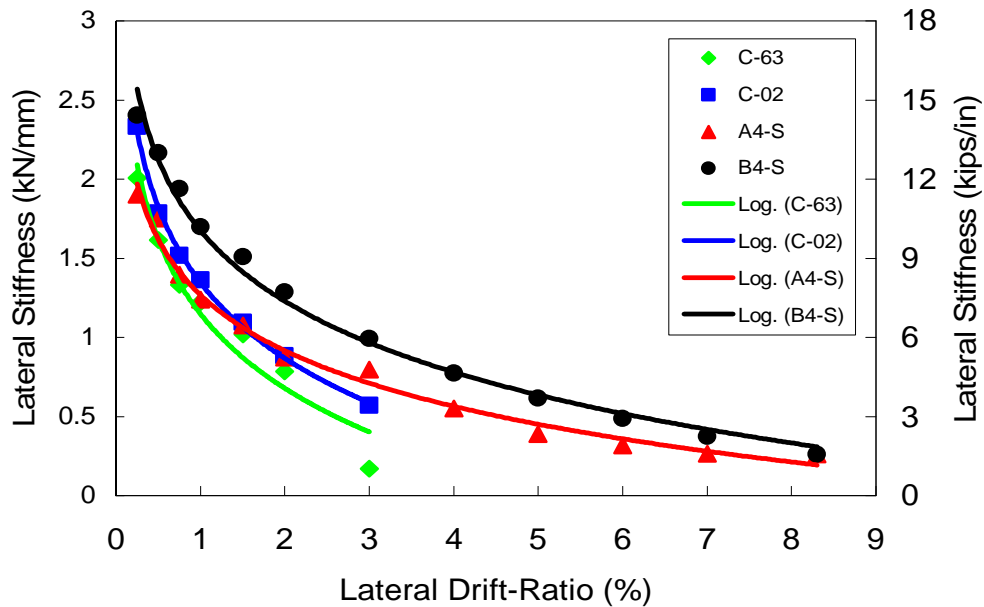
Figure 4.28 Peak Lateral Stiffness versus Applied Drift-Ratio

With gradually increased inelastic deformation cycles, the upgraded test specimens exhibited greater lateral stiffness values in comparison to the control specimens. The lateral stiffness of control specimen C-02 and C-63 rapidly degraded at each applied drift-cycle until punching shear failures occurred. Despite having the lowest initial stiffness, the lateral stiffness decay of specimen A4-S decreased compared with each control specimen at an applied drift-ratio of 1.5%. Specimen A4-S displayed stable hysteretic response with gradual stiffness degradation at large inelastic deformation cycles. The stiffness decay of specimen B4-S paralleled specimen A4-S, but specimen B4-S had somewhat greater stiffness through the test.

The lateral stiffness degradation of each specimen was correlated to the amount of damage incurred at the connection region. Lateral stiffness of specimens A4-S and B4-S did not degrade as rapidly as the control specimens

because the CFRP stirrups prevented the formation of large cracks and associated damage in the joint region. Figure 4.29(a) and (b) show connection region cracking of specimens A4-S and B4-S. Cracking occurred in the connection region of the upgraded specimens, however, cracks propagated through the holes in the slabs along the face of the column base plate, transverse to the direction of loading. Cracks propagation in control specimen C-02 and C-63 are shown in Figure 4.30(a) and (b). This figure shows that cracks spread throughout the connection region, which ultimately resulted in punching shear failure. Of the upgraded specimens, A4-S showed the least amount of damage in the connection region (Figure 4.29).

Direction of lateral loading denoted by: ⟷

(a)   (b)

Figure 4.29 Connection Region Cracks: (a) Specimen B4-S; (b) Specimen A4-S

Direction of lateral loading denoted by: ⟷

(a)   (b)

Figure 4.30 Connection Region Cracks: (a) Specimen C-02; (b) Specimen C-63

Figure 4.31 shows the lateral stiffness degradation for the initial and final cycle repetitions of each specimen in the study. As previously stated, each applied drift-cycle was repeated three times up to an inter-story drift of 6%, after which two drift-cycle repetitions were carried out. Examination of Figure 4.31 indicates that stiffness degradation took place when the specimen was subjected to repeated lateral displacement excursions at each drift level. However, the magnitude of stiffness degradation within repeated drift-cycles was reasonably small. Therefore, damage incurred by the application of lateral displacements happened during the first cycle of an applied drift-series. Upon repetition, lateral stiffness was negligibly altered.
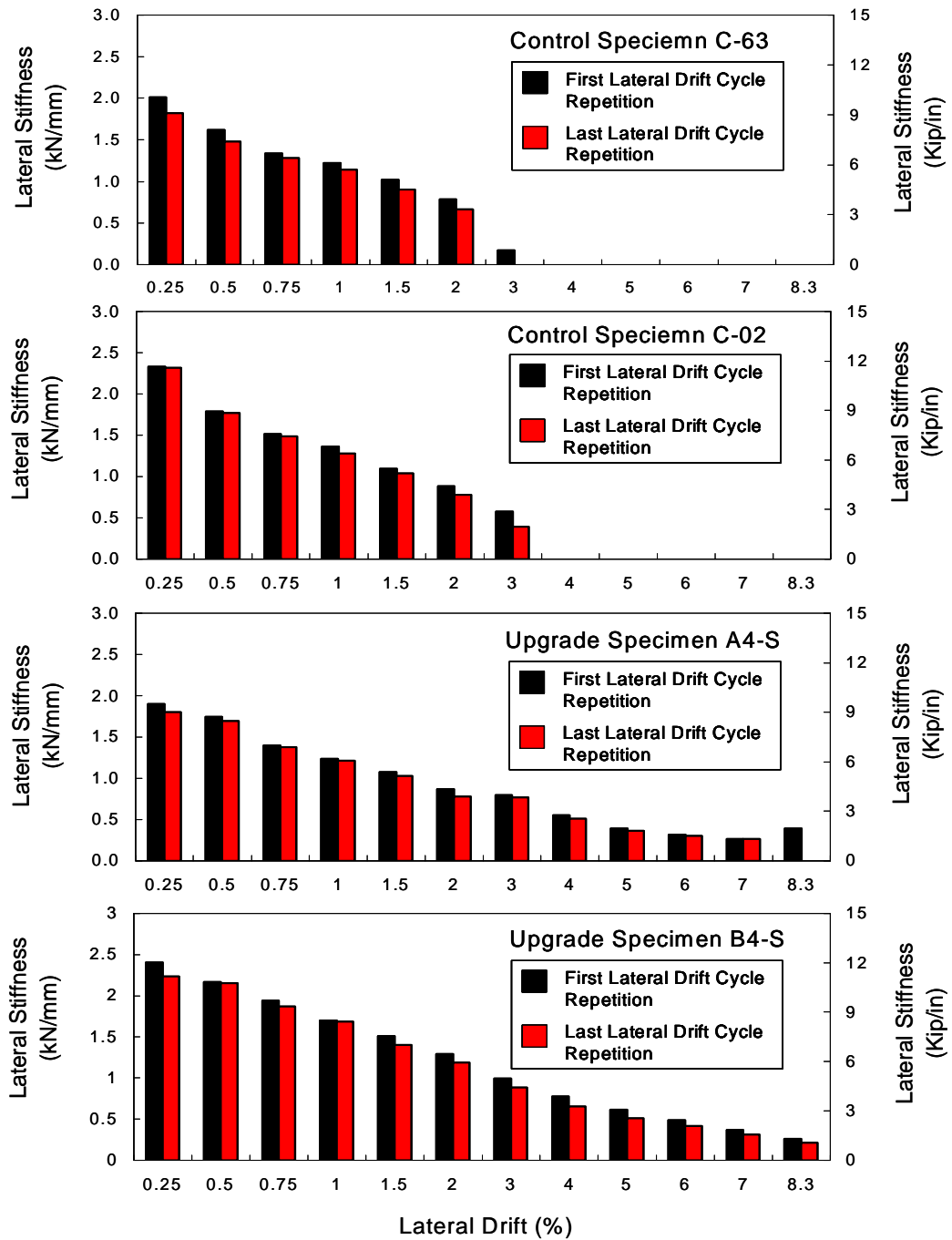
Figure 4.31 Lateral Stiffness Degradation per Drift-Cycle

4.9.2   Rotational Stiffness Degradation

Figure 4.32 shows a plot of rotational stiffness versus applied drift cycle for each test specimen.   The initial rotational stiffness of the upgraded test specimens was noticeably higher than that of the control specimens.   This could be attributed to the contribution of the CRFP reinforcement to the increased flexural strength of specimens A4-S and B4-S.   The initial rotational stiffness of specimens A4-S and B4-S was found to be 32% and 37% higher than specimen C-02, respectively.   Specimen C-63 displayed a 13% lower initial rotational stiffness than specimen C-02.

Rotational stiffness degradation of each test specimen followed similar trends when compared to the lateral stiffness degradation of the test specimens. Both control specimens displayed expeditious rotational stiffness degradation until punching shear failures occurred (Figure 4.33).   Specimen A4-S experienced somewhat higher initial rotational stiffness degradation than the control specimens; however the behavior stabilized at an applied drift of 2%.   After this drift-cycle, specimen A4-S displayed stable hysteretic behavior and gradually decreased rotational stiffness through the 6% applied drift-ratio.   Specimen B4-S had the greatest overall stiffness.   The rotational stiffness degradation trends of specimen B4-S appeared to be similar to those of A4-S.

Figure 4.33 shows the rotational stiffness degradation for the initial and final cycle repetitions for each applied drift-cycle.   Parallel to what was demonstrated in the previous section; the rotational stiffness degradation within an applied drift-level is minimal.   Therefore, most of the damage was accumulated by the application of the first rotation cycle of an applied drift-cycle.
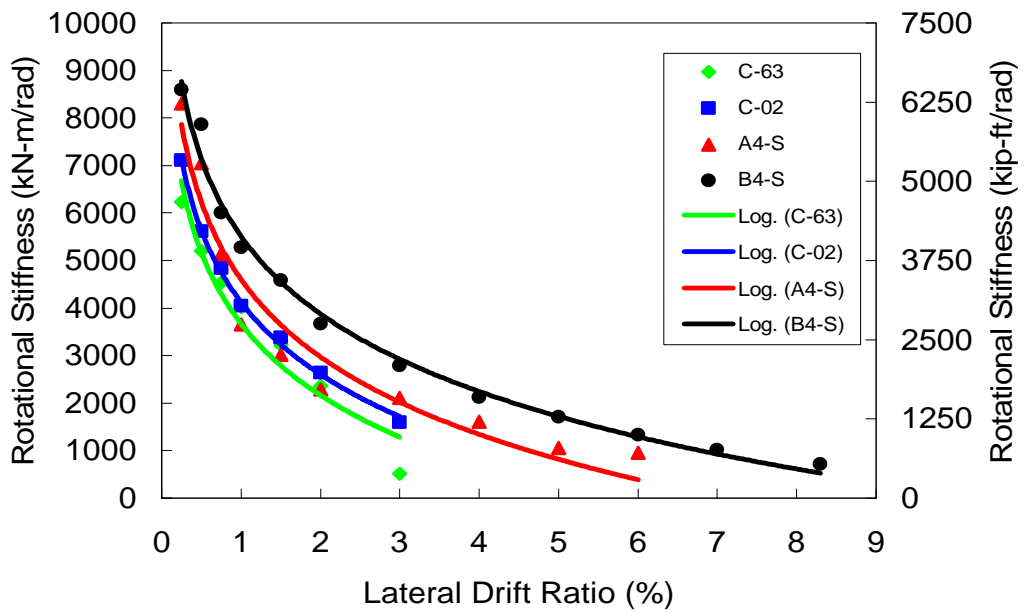
Figure 4.32 Rotational Stiffness Degradation per Drift-Cycle
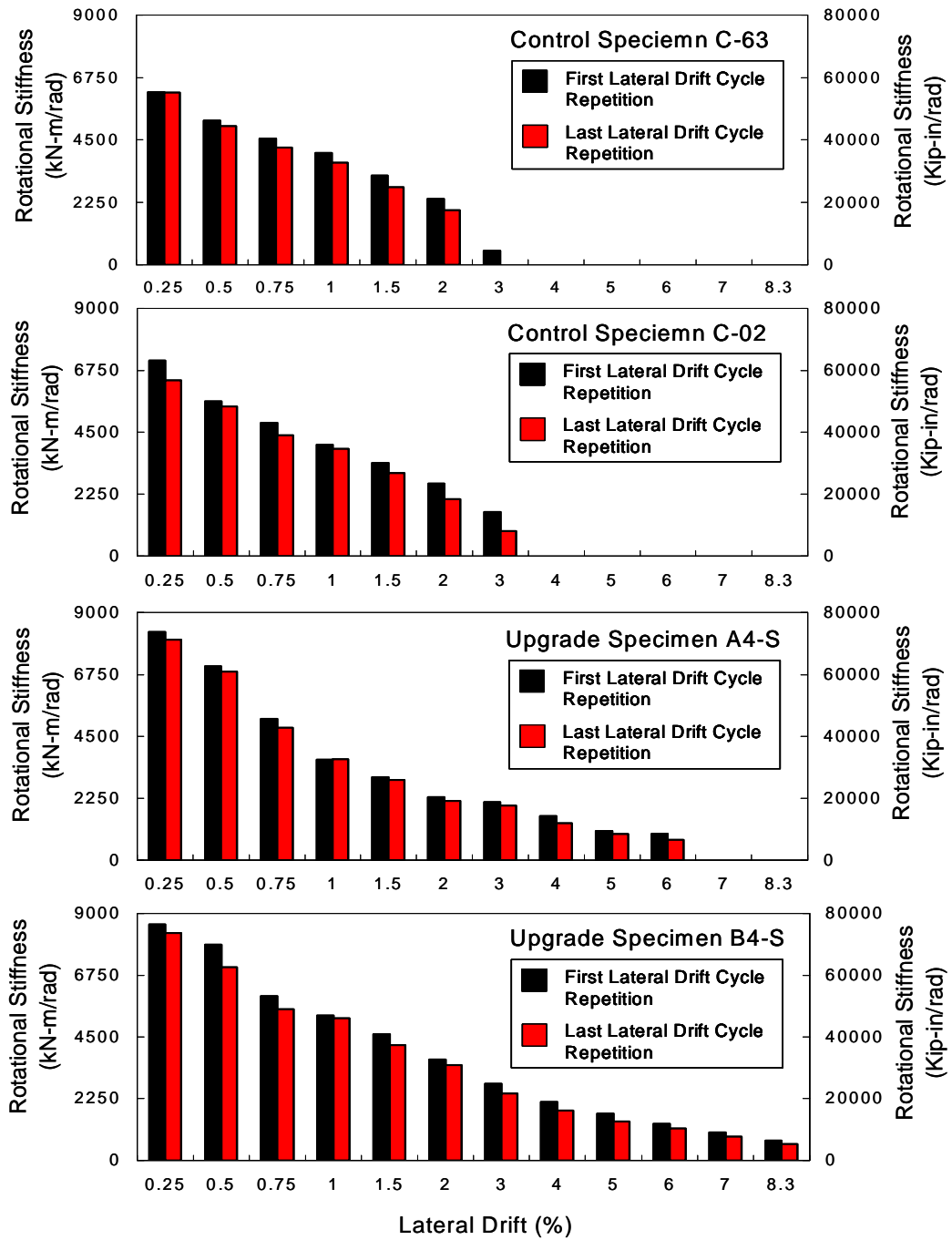
Figure 4.33 Rotational Stiffness Degradation per Drift-Cycle

4.10 STRENGTH DEGRADATION

Strength degradation of the test specimens is discussed in this section. Peak lateral loads and unbalanced moments at applied drift-cycles are defined in section 4.3.2. Strength degradation trends between individual repetitions within a given drift-cycle are discussed.

4.10.1 Lateral Load Degradation

Figure 4.34 shows a comparison of the average lateral load degradation within each drift-cycle group, for each specimen in the study. Both control specimens exhibited little strength decrease, within a given applied drift-cycle group, until the maximum lateral load was resisted. After this point, specimen C-02 experienced a punching shear failure. However, specimen C-02 showed signs of a strength decrease during the final drift-cycle. This proved that after the initiation of punching shear failure, specimen C-02 showed some ability to carry gravity loads and reduced levels of lateral loads. Continuous bottom layer steel therefore helped prevent sudden failure and possible progressive collapse associated with the punching shear mechanism. Whereas, specimen C-63 experienced brittle failure and was not able to maintain its lateral load carrying capacity after punching shear failure initiated. The gravity load carrying capacity was subsequently lost.
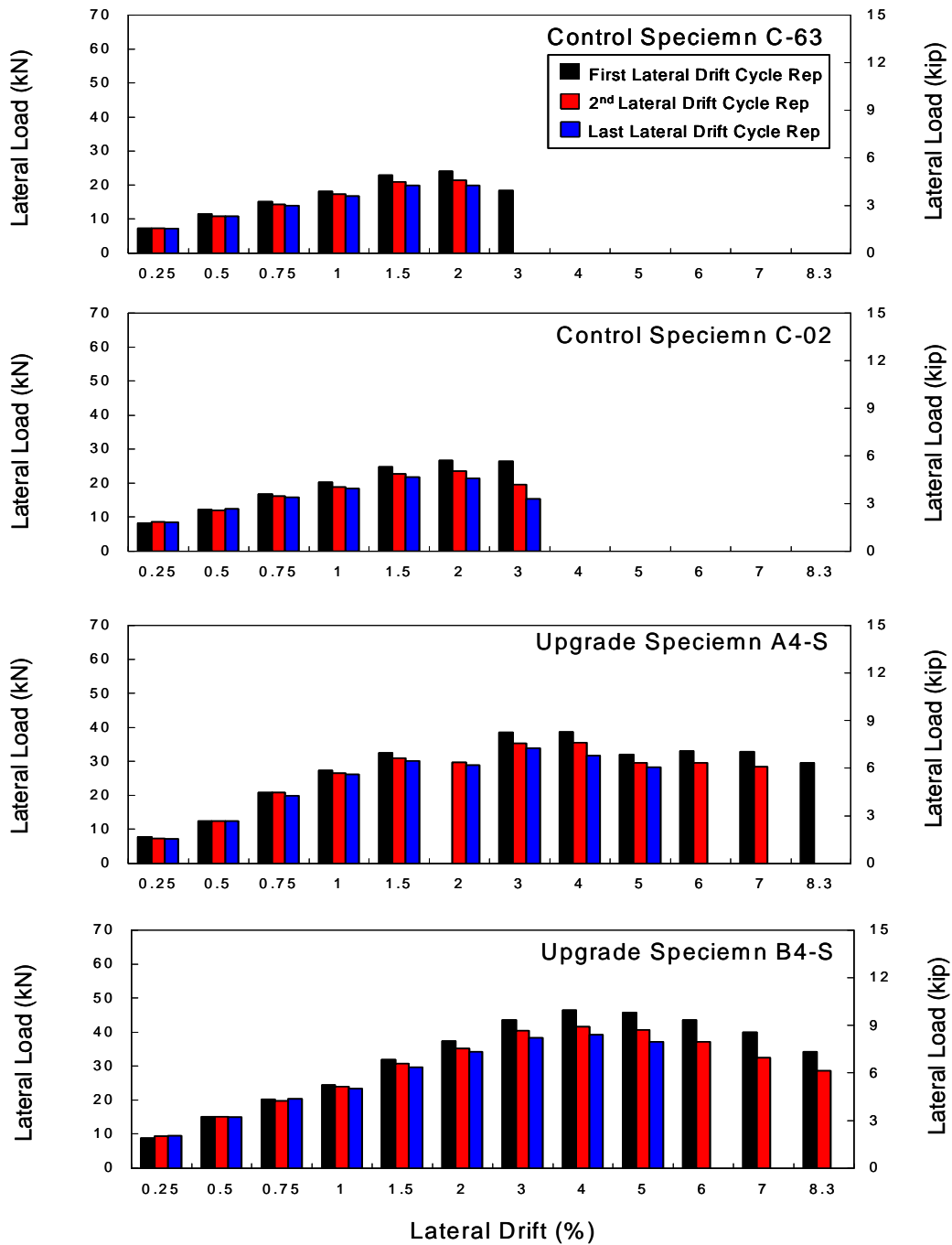
Figure 4.34 Strength Degradation per Lateral Drift-Cycle

121

Specimens A4-S and B4-S experienced similar strength degradation trends within each applied drift-cycle-group of the simulated seismic tests. As exhibited by the control specimens, both specimens showed little strength degradation within a drift-cycle-group through an applied drift-ratio of 2%. As the longitudinal reinforcement yielded and flexural cracks opened, strength degradation within a drift-cycle-group increased. However, after the maximum lateral load was resisted by the upgraded specimens, strength degradation between drift-cycled repetitions two and three was small when compared with drift-cycle repetitions one and two. This indicated that the most damage occurred during the initial drift excursion of each drift-cycle-group. Therefore, the overall behavior of the upgraded test specimens was not significantly changed when the drift protocol was switched from three-repetitions to two-repetitions after an inter-story drift ratio of 6%.

4.10.2 Unbalanced Moment Degradation

Figure 4.35 shows the average unbalanced moment degradation within each drift-cycle for each test specimen. Unbalanced moment degradation also followed the general trends displayed in the lateral strength decay. Minimal unbalanced moment degradation occurred within a given drift-cycle-group for the control specimens, until the initiation of punching shear failures. As longitudinal reinforcing steel yielding spread (after the 3% applied drift-cycle), unbalanced moment degradation increased within a drift-cycle-group. Once again, the greatest degradation occurred between cycle repetitions one and two after the maximum average unbalanced moment was achieved.
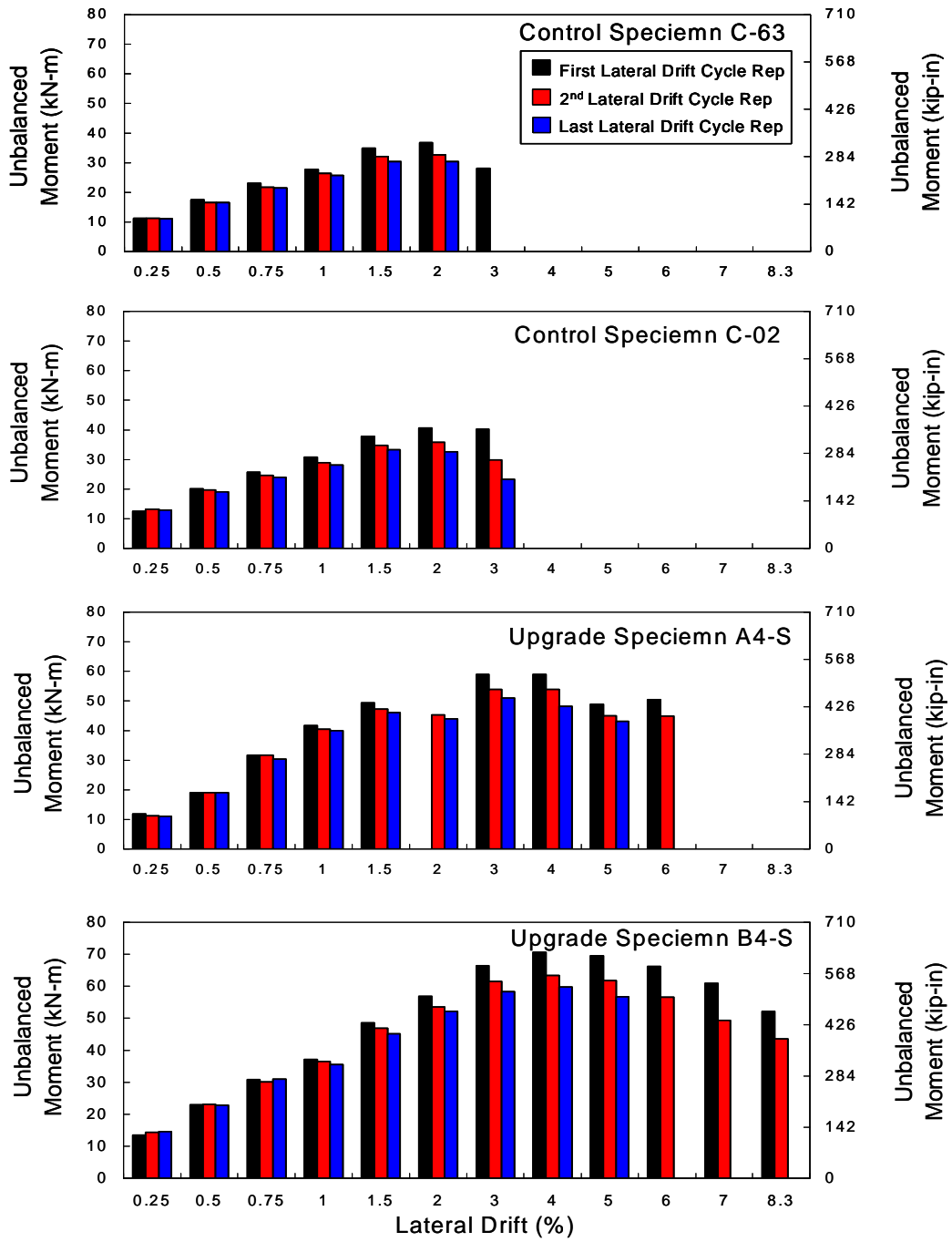
Figure 4.35 Unbalanced Moment Degradation per Lateral Drift Cycle

123

4.11 DUCTILITY PARAMETERS

The load-displacement and unbalanced moment-rotation ductility parameters are discussed in the following sections. All ductility parameters were calculated from the data recorded in the testing phase of the study. A computer program was written using C++ code to determine the necessary load, unbalanced moment, displacement, rotation, stiffness and hysteresis data defined in section 4.3.2. The program used numerical integration to calculate the area enclosed by the hysteresis curves. MathCad 2002 spreadsheets were then created to calculate the specific ductility parameters defined in the following sections. Detailed calculations and C++ code are presented in Appendix D.

Figure 4.36 defines the ductility parameters used to evaluate the post-elastic behavior of the test specimens in the study. All ductility parameters definitions used in this study were defined by Ehsani and Wight [9]. These criteria are displacement and rotational ductility factors (μ_Δ, μ_θ), cumulative ductility ratios (N_Δ, N_θ) and work and energy-damage indicators (W, E).

4.11.1 Ductility Factors

Displacement and rotational ductility factors (μ_Δ, μ_θ) are calculated from the backbone curves defined in section 4.3.2. Δ_1 and θ_1 are the yield displacement and rotation defined in Figure 4.36. Δ_2 and θ_2 are the displacement and rotation corresponding to a 20% reduction in lateral load and unbalanced moment capacity on the descending branch of the each backbone curve. The ductility parameters used in this study are defined as the ratio of Δ_2 to Δ_1 and θ_2 to θ_1, and will be presented for both the directions of lateral loading

124
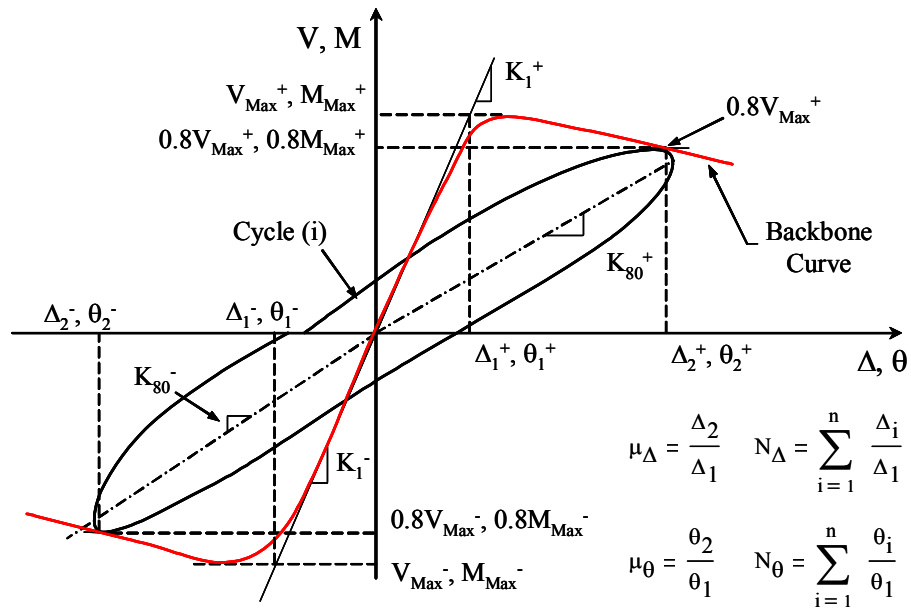
Figure 4.36 Displacement and Rotation Ductility Factors and Cumulative Ductility Ratios

4.11.1.1 Ductility Ratios

The displacement and rotation ductility ratios (N_Δ, N_θ) are defined in Figure 4.36. These parameters are also determined using the backbone curves from section 4.3.2. N_Δ and N_θ are the cumulative ratios of the peak displacement or rotation at the ith drift-cycle (Δ_i and θ_i) normalized to the yield displacement or rotation (Δ_1 and θ_1). Two ductility ratios are presented for both lateral load-displacement and unbalanced moment-rotation data. $N_{\Delta 80}$ and $N_{\theta 80}$ are the cumulative ductility ratios corresponding to the drift-cycle where a 20% reduction in lateral load, or unbalanced moment, occurs on the descending branch of a given backbone curve. The total displacement and rotation ductility ratios, $N_{\Delta t}$ and $N_{\theta t}$, are the collective summation of the ductility ratios from the entire test.

4.11.1.2 Work and Energy Indicators

In this study, two indexes are used to quantify the amount of energy dissipated within each specimen's slab-column connection during each drift-cycle: the work indicator, W, and the energy indicator, E (pp.760 [9]). The work indicator, represents the work done on a test specimen by the applied lateral load. Equation (4.1) defines the work-damage indicator.

$$W = \frac{1}{V_{Max} \cdot \Delta_1} \cdot \sum_{i=1}^{n} w_i \cdot \left(\frac{K_i}{K_1} \right) \cdot \left(\frac{\Delta_i}{\Delta_1} \right)^2 \qquad (4.1)$$

Where,

V_{Max} = the average of V_{Max}^+ and V_{Max}^-, shown in Figure 4.36;

w_i = the energy dissipated in the ith drift-cycle, calculated from the area of the ith load-displacement loop;

Δ_1 = the average of Δ_1^+ and Δ_1^-, shown in Figure 4.36;

Δ_i = the average of Δ_i^+ and Δ_i^-, shown in Figure 4.36;

K_1 = the average of K_1^+ and K_1^-, shown in Figure 4.36;

K_i = the average of K_i^+ and K_i^-, shown in Figure 4.36.

Work-damage is calculated for the cumulative drift-cycles until a 20% loss of the maximum lateral load (W_{80}) and for the total number of drift-cycles in a test (W_t).

Energy dissipated in the slab-column connection by unbalanced moment is represented by the energy-damage indicator, E, defined in equation (4.2).

126

$$E = \frac{1}{M_{Max} \cdot \theta_1} \cdot \sum_{i=1}^{n} e_i \cdot \left(\frac{b_o}{d}\right)\left(\frac{S_i}{S_1}\right) \cdot \left(\frac{\theta_i}{\theta_1}\right)^2 \qquad\qquad (4.2)$$

Where,

M_{Max} = the average of M_{Max}^+ and M_{Max}^-, shown in Figure 4.36;

e_i = the energy dissipated within the slab-column connection in the ith drift-cycle, calculated from the area of the ith load-displacement loop;

θ_1 = the average of θ_1^+ and θ_1^-, shown in Figure 4.36;

θ_i = the average of θ_i^+ and θ_i^-, shown in Figure 4.36;

S_1 = the average of S_1^+ and S_1^-, shown in Figure 4.36;

S_i = the average of S_i^+ and S_i^-, shown in Figure 4.36;

b_o = ACI 318-02 critical perimeter;

d = slab depth.

Again, the energy-damage indicator is calculated for the collective drift-cycles corresponding to a 20% decrease in lateral load (E_{80}) and the total cycles (E_t) in accrued during the test.

4.11.2 Lateral Load-Displacement Ductility Parameters

The post-elastic, lateral load deformation behavior of the tested slab-column connections significantly improved when upgraded using CFRP stirrups. This is evidenced by the lateral load-deformation ductility parameters listed in Table 4.12. The lateral displacement ductility factor of both of the upgraded specimens was two times that of control specimen C-02, when "pushed" in the south direction. When the specimen was "pulled" in the north direction, the ductility factor of specimen B4-S dropped to 1.75 times C-02 because the CFRP strand ruptured. However, these ductility measurements indicated that both the

upgraded specimens had stable descending branches and that they can undergo significant inelastic deformations without losing strength.

Table 4.12 Lateral Load-Displacement Ductility Parameters

Specimen	f'c (ksi)	Ductility Factor		Cumulative Ductility Ratios		Work Indicators	
		$\mu_{\Delta80}$ (+)	$\mu_{\Delta80}$ (−)	$N_{\Delta80}$	$N_{\Delta t}$	W_{80}	W_t
A4-S	4.5	6.9	5.9	86	86	119	119
B4-S	4.5	6.9	4.9	67	73	108	118
C-02	4	3.1	2.8	30	30	33	33
C-63	4	2.4	2.3	23	23	27	27

A similar pattern was found in the cumulative ductility ratio parameters. Specimens A4-S and B4-S both had ductility ratios, $N_{\Delta80}$ and $N_{\Delta t}$, more than two times greater than control specimen C-02. A4-S had equivalent $N_{\Delta80}$ and $N_{\Delta t}$ ratios because the lateral load did not drop below 80% of maximum value over the duration of the test. The ductility ratios $N_{\Delta80}$ to $N_{\Delta t}$ of specimen A4-S were also 30% and 18% greater than those of specimen B4-S.

The work-damage indicators, W_{80} to W_t, more than tripled for test specimens A4-S and B4-S over control specimen C-02. This indicates the energy dissipation characteristics of test specimens A4-S and B4-S were much greater than the control specimens. The addition of CFRP shear stirrups increased the punching shear strength of specimens A4-S and B4-S. This allowed the upgraded specimens to undergo significant inelastic lateral deformations. Larger load-deformation hysteresis loops were therefore generated because more energy was absorbed from the lateral loads acting upon the upgrade specimens. Specimens A4-S and B4-S dissipated almost the same amount of total energy during the lateral load tests. However, the energy dissipation characteristics of specimen A4-S are somewhat better because connection upgrade A4-S maintained 80% of the lateral load capacity over the duration of the test.

128

4.11.3 Unbalanced Moment-Rotation Ductility parameters

The unbalanced moment-rotation ductility parameters listed in Table 4.13 show upgrading flat-plate slab-column connections using CFRP stirrups greatly increased the inelastic rotation capacity of the slab-column connection. The rotation ductility factors presented in Table 4.13 indicated that both upgraded specimens have over two times the inelastic rotational capacity of the control specimens. Specimen A4-S would have had a greater ductility factor because the load-deformation backbone curve did not drop below 80% of the maximum resisted lateral load for the duration of the test. The ductility factor calculated from the "pulled" direction was again lower for specimen B4-S due to CFRP strand rupture. However, the difference was not significant because strand rupture did not occur until the final applied drift-cycle.

Table 4.13 Unbalanced Moment-Rotation Ductility Parameters

Specimen	f'c (ksi)	Ductility Factor		Cumulative Ductility Ratios		Energy Indicators	
		$\mu_{\theta 80}$ (+)	$\mu_{\theta 80}$ (−)	$N_{\theta 80}$	$N_{\theta t}$	E_{80}	E_t
A4-S*	4.5	6.9	7.2	98	98	5861	5861
B4-S	4.5	10.2	9.3	77	85	4505	4959
C-02	4	3.7	3.2	29	29	587	587
C-63	4	2.4	2.5	26	26	430	430

* Rotation data ends at 0.05 radians because instrumentation saturated.

The ductility ratios $N_{\theta 80}$ and $N_{\theta t}$ followed the same trend as the rotational ductility parameter, $\mu_{\theta 80}$. Specimen B4-S has a $N_{\theta 80}$ value 2.7 times larger than specimen C-02. Specimen A4-S exhibited the greatest quantified cumulative ductility ratio, where $N_{\theta 80}$ is 3.8 times that of control specimen C-02 and 27% greater than specimen B4-S. This shows that specimen A4-S had superior energy dissipation and deformation characteristics.

The total energy dissipated in the connection region of the upgraded test specimens was significantly greater than the control specimens. The calculated energy-damage parameter was over 8.5 times greater for specimen B4-S when compared with specimen C-02. For specimen A4-S this ratio increased to 10 times. The energy-damage parameter could therefore be an important ductility parameter that may be used to quantify the seismic performance of specimens A4-S and B4-S. This is because the energy dissipated in the connection region of the upgraded test specimens was 8-10 times greater than the energy dissipated by the control specimens. Conversely, the superior performance of upgraded joints could be defined by energy damage indicators that are an order of magnitude larger than those of the control specimens.

4.12 RESIDUAL GRAVITY LOAD CARRYING CAPACITY

After the conclusion of the lateral load tests, monotonically increased concentric axial load was applied to each test specimen's column, as described in section 3.4.6. Table 4.14 summarizes the results of these tests. Load-deformation curves obtained during these tests can be found in Appendix C.

Table 4.14 Test Specimen Post-Failure Concentric Axial Load Capacities

Test Specimen	Maximum Vertical Concentric load (kN)	Maximum Lateral Drift Ratio (%)	Percent of Applied ACI 11.12.2.1 Punching Shear Strength (%)
C-63	121	1.8	51
C-02	155	2.4	65
A4-S	228	8.1	96
B4-S	168	8.0	71

The ratio of the residual gravity load carrying capacities of each specimen to the concentric punching strength of specimen C-02 (based equation (11-35) in section 11.12.2.1 of ACI 318-02) are shown in Table 4.14. The residual gravity

load ratio was normalized to the concentric punching capacity, calculated using the critical perimeter of the control specimens. Upgrade specimen A4-S had the best post-seismic-event performance, retaining 96% of the concentric punching shear strength prior to seismic upgrade. Specimen B4-S retained 76% of the concentric punching shear strength. The residual shear resistance of control specimen C-02 was attributed to dowel action provided by the continuous bottom mat reinforcement placed through the connection region, as prescribed by Chapter 21 of ACI 318-02. Control specimen C-63 did not have continuous bottom mat reinforcement. Testing was stopped when the column began to punch through the centerline bars of steel in the top mat. Test observations indicated that without continuous bottom mat reinforcement passing through the connection region, specimen C-63 was highly susceptible to brittle failure that may have lead to progressive collapse in a typical structure.

The amount of damage incurred from simulated seismic tests played a key role in the post-earthquake gravity load carrying capacity of flat-plate slab-column connections. The connection upgrades in specimens A4-S and B4-S had equivalent amounts of vertical shear reinforcement. Hence, failure of both upgraded specimens A4-S and B4-S occurred outside the CFRP reinforced connection region. The shear resistance provided by damaged concrete in flat-plate slab-column connections due to seismic effects therefore requires further research. The results reported in this study are neither conclusive nor sufficient to make any recommendations that could later be codified. Instead, they were intended to provide preliminary information for researchers who may study the gravity load carrying capacity of earthquake damaged slab-column connections.

CHAPTER 5

Summary and Conclusions

5.1 SUMMARY

The main objective of the study was to investigate the behavior of interior reinforced concrete flat-plates subjected to gravity and simulated seismic loads. Test specimens in the study included two flat-plate slabs designed according to ACI 318-63 and ACI 318-02 requirements and two flat-plate connections upgraded with additional CFRP stirrups positioned radially around the slab-column interface. Upon completion of the simulated seismic tests, the residual gravity load carrying capacity of each slab-column connection was then investigated.

An experimental program was conducted to achieve the objectives of the study. Design and descriptions of the prototype structure, test specimens and connection upgrade design can be found in Chapter 2. Test procedures are discussed in Chapter 3. The test results are presented and discussed in Chapter 4.

5.1.1 Prototype Structure

The prototype structure selected for the study was a four-story reinforced concrete flat-plate structure with span lengths of 4.9 m (16 ft) in both directions. Features of the prototype structure include a 203 mm (8 in) slab, supported by 508 mm (20 in) square columns, without drop panels, column capitals or edge beams. The prototype structure had a story height of 3 m (10 ft).

5.1.2   Test Specimens

Four test specimens were nominally constructed half-scale of the prototype structure. The slab plan dimensions were 2.8 x 2.8m (9.3 x 9.3ft) and had a thickness of 114 mm (4.5 in). The columns consisted of two W10x88 steel sections, welded to 305 mm (12 in) square base plates. The column sections had nominal heights of 762 mm (30 in) and were bolted through holes in the test slabs. The specified compressive strength of the concrete was 28 MPa (4000 psi) and all longitudinal slab reinforcement were No. 4, 414 MPa (grade 60) steel reinforcing bars. Test specimen C-02 was detailed according to ACI 318-63 provisions and specimens C-02, A4-S and B4-S were detailed according to ACI 318-02 provisions. Test specimens A4-S and B4-S were reinforced using CFRP strips weaved through holes in the slab, located at radial perimeters around the column. The tensile strength of the CFRP was 128 ksi (883 MPa).

5.1.3   Load Protocol

During the simulated seismic tests, test specimens were supported at the slab ends by spreader beams, attached to vertical struts and fixed to the slab floor using clevises to resist gravity loads. Lateral loads applied by a hydraulic actuator were resisted by a horizontal strut attached to a steel reaction frame, attached to the bottom of the test specimens' lower column section. Gravity loads were applied using a hydraulic jack in conjunction with a load-maintainer that kept the gravity load constant. The applied gravity load induced a shear stress of $0.133\sqrt{f_c^{'}}$ MPa ($1.6\sqrt{f_c^{'}}$ psi), which acted on the critical perimeter of the control specimens in the study. An actuator applied progressively increased lateral drift excursions to the top of the test specimens' column to simulated seismic loads. Each test specimen was instrumented to measure forces, displacements and strains.

5.1.4 Lateral Load Test Results

Control specimens C-63 and C-02 exhibited punching shear failures at lateral drift-ratios 2.26% and 2.44%, respectively, whereas the upgraded test specimens demonstrated ductile inelastic behavior in excess of 8% inter-story drift. Specimen C-63 resisted a maximum lateral load of 24.5 kN (5.5 kips), which corresponded to an unbalanced moment of 37.8 kN-m (334.5 kip-in). Specimen C-02 attained a maximum lateral load of 27 kN (6.1 kips) and an unbalanced moment of 41.3 kN-m (365.5 kip-in). The greatest lateral load was resisted by specimen B4-S, equal to 48 kN (213.5 kips) and an unbalanced moment of 73 kN-m (647 kip-in). Specimen A4-S resisted a lateral load of 41.2 kN (9.3 kips) and an unbalanced moment of 63 kN-m (558 kip-in).

5.1.5 Residual Gravity Load Carrying Capacity Results

The residual gravity load carrying capacity of each test specimen was tested after the simulated seismic tests. A concentric load was applied vertically to the specimens of the study using a hydraulic jack. Results from the tests showed that specimen A4-S had the greatest residual gravity load capacity, followed by specimens B4-S, C-02 and C-63. The behavior of specimen C-63 was found to be highly susceptible to progressive collapse because the bottom steel was not continuous.

5.2 CONCLUSIONS

Based on the results of the study, the following conclusions can be made:

(i) Applying CFRP stirrups in radial patterns around the slab-column interface of flat-plate structures is a feasible method of upgrading the connection for seismic loading conditions. When CFRP shear reinforcement was provided at the slab-column connection, punching shear failure was prevented and the failure

mode changed to flexure. This enabled the upgraded specimens to display ductile behavior, whereas the control specimens exhibited punching shear failures.

To assure ductile failure modes, the CFRP stirrups were designed incorporating the current ACI eccentric shear stress model, defined in section 11.12.6 of ACI 318-02. However, when calculating the required shear capacity at the critical section, probable unbalanced moment capacity of the slab was used instead of a calculated unbalanced moment. The probable unbalanced moment capacity was calculated by adding the positive and negative moment capacity of the effective width in the column strip of the slab, which included the affects of strain-hardening of the longitudinal reinforcement. Typical design moments are calculated using probable earthquake loads.

(ii) Upgrading the flat-plate slab-column connections using CFRP stirrups significantly increased the drift capacity of the connection. Results from testing show that specimens A4-S and B4-S both had increases in lateral drift capacity of 177% over control specimen C-02. Specimen C-02 exhibited a punching shear failure at a lateral drift of 2.44%, whereas specimens A4-S and B4-S both attained lateral drift ratios of 8.33%.

It should be noted that these drift ratios achieved by specimens A4-S and B4-S are unrealistic when they are compared with code limits and reasonable drift levels in real flat-plate structures. However, if this method of upgrading flat-plate slab-column connections can result in large inter-story drift capacities while subjected to large gravity loads, the performance of these upgraded connections should be adequate in less demanding conditions.

(iii) The connection rotation capacity of the upgraded test specimens was also improved with the addition of CFRP stirrups. An increase in rotational capacity of over 200% was shown in test specimen B4-S. Specimen A4-S had measured increases in rotational capacity of 130%, which were limited by the saturation of

rotation instruments. It is believed that if rotation instruments were able to record data through the duration of the test, the increase in connection rotation capacity of specimen A4-S would be similar to B4-S.

(iv) Strengthening the region adjacent to the column faces shifted the critical perimeter of the slab-connections of the upgraded specimens, which prevented punching shear failure and allowed these specimens to deform inelastically, in a stable manner. The upgraded test specimens therefore dissipated considerably more amounts of energy than the control specimens. This was shown by significant increases in all of the ductility parameters calculated from the test results. The energy-damage indicator showed the greatest increase, being 8-10 times greater for the upgraded test specimens than control specimen C-02. The work-damage indicator of the upgraded test specimens was 4-times that of specimen C-02. Both cumulative displacement and rotation ductility ratios increased 3-4 times that of specimen C-02 and the displacement and rotation ductility factors were 2-3 times greater than the control specimen.

(v) The flexural strength of the upgraded test specimens was increased due to the horizontal components of the external CFRP stirrups and strain hardening of the flexural steel. This was evidenced by specimen A4-S exhibiting a 53% increase in flexural strength over specimen C-02 and specimen B4-S exhibiting a 77% increase in flexural strength. The configuration and geometry of the CFRP stirrups played a role in the amount of flexural strength increase that each upgraded test specimen achieved. However, the relationship between shear, flexure, and anchorage interaction could not be determined from the limited results of this study.

(vi) Analysis of the test results show that flat-plate slab-column connections upgraded with CFRP stirrups did not experience a radical change in the lateral stiffness. A maximum stiffness increase was measured to be 3%.

136

(vii) Stiffness degradation did not occur as rapidly in the upgraded test specimens, in comparison to the control specimens. As the lateral load excursions increased, the stiffness of the upgraded specimens did not degrade rapidly because the CFRP stirrups helped mitigate damage within the connection region. This area

(viii) Upgrading slab-column connections with CFRP stirrups had a beneficial impact on the residual gravity strength of the connection. The residual gravity load carrying capacity of specimen B4-S was 97% of the concentric punching shear capacity of specimen C-02. In addition, the amount of damage incurred from simulated seismic tests played a key role in the post-earthquake gravity load carrying capacity of flat-plate slab-column connections.

5.3 FUTURE WORK

The following recommendations can be made based on the findings of the study:

(i) The procedures for applying CFRP stirrups to slab-column connections have been established based on laboratory test specimens. These procedures were developed to upgrade existing slabs that were constructed with this application in mind. Further research should be conducted as to the application of the technique developed herein to structures in service, pertaining to:

- Coring holes in slabs where the location of flexural reinforcement is not known;
- Refining procedures for applying epoxy to carbon fiber strips to minimize clean-up;
- Overhead application of uncured CFRP stirrups, using formwork or ladders; and,
- Applying uncured CFRP strips in variable climate conditions.

(ii)   Additional testing is recommended to determine the effects of varying the amount and configuration of CFRP reinforcement on the seismic performance of the upgraded connection. This includes structures that have been previously subjected to lateral displacements and incurred variable amounts of damage. Furthermore, the shear resistance provided by damaged concrete in flat-plate slab-column connections due to seismic effects should be identified.

(iii)   Research should also be conducted determine the relationship of shear, flexure and anchorage interaction of the CFRP stirrups towards the increase in shear and flexural capacities. Identifying the effects of these forces will help identify critical load cases, which cause undersigned failure of the CFRP stirrups. Moreover, this research may assist in the development of strength reduction factors for this specific upgrade application.

References

[1] ACI Committee 318, "Building Code Requirements for Reinforced Concrete (ACI 318-63)." American Concrete Institute, Farmington Hills, MI, 1963.

[2] ACI Committee 318, "Building Code Requirements for Reinforced Concrete (ACI 318-95)." American Concrete Institute, Farmington Hills, MI, 1963.

[3] ACI Committee 318, "Building Code Requirements for Reinforced Concrete (ACI 318-02)." American Concrete Institute, Farmington Hills, MI, 2002

[4] ACI-ASCE Committee 352, "Recommendations for Design of Slab-Column Connections in Monolithic reinforced Concrete Structures (ACI 352.1R-88)." ACI Structural Journal, V. 85, No. 6, Nov.-Dec. 1988, pp. 675-696.

[5] Allen, F.H. and Darvall, P., "Lateral Load Equivalent Frame." ACI Journal, *Proeedings* V. 74, No. 7, July 1977, pp. 294-299.

[6] Binici, Baris and Oguzhan Bayrak, "Punching Shear Strengthening of Reinforced Concrete Flat Plates Using Carbon Fiber Reinforced Polymers." *ASCE Journal of Structural Engineering*, Vol. 129, No. 9, Sept 2003.

[7] Cano, Mary T. and Richard Klingner, "Comparison of Analysis Procedures for Two-Way Slabs." ACI Structural Journal, V. 85, Nov.-Dec. 1988, pp. 597-608.

[8] Ebead, U. and H. Marzouk, "Strengthening of Two-Way Slabs Subjected to Moment and Cyclic Loading." *ACI Structural Journal*, Vol. 99, No. 4, July-Aug 2002, pp. 435-444.

[9] Ehsani, M.R. and J.K. Wight, "Confinement Steel Requirements For Connections in Ductile Frames." *ASCE Journal of Structural Engineering*, Vol. 116, No. 3, Mar. 1990, pp. 751-767.

[10] Farhey, Daniel N., Moshe A. Adin and David Z. Yankelevsky, "Repaired Reinforced Concrete Flat-Slab-Column Subassemblages Under Lateral Loading." *ASCE Journal of Structural Engineering*, Vol. 121, No. 11, Nov 1995, pp. 1710-1720.

[11] FEMA 310, "Handbook for the Seismic Evaluation of Buildings – A Prestandard." Federal Emergency Management Agency, Washington, D.C, Jan. 1998.

[12] FEMA 356, "Prestandard and Commentary for the Seismic Rehabilitation of Buildings." Federal Emergency Management Agency, Washington, D.C, Nov. 2002.

[13] Hassanzadeh, Ghassem and Haakan Sundqvist, "Strengthening of Bridge Slabs on Column." Nordic Concrete Research, No. 21, Jan. 1998.

[14] *International Building Code*. International Code Council, Falls Church, Virginia, 2000.

[15] Islam, Shafiqul and Robert Park, "Test on Slab-Column Connections with Shear and Unbalanced Flexure." *ASCE Journal of Structural Engineering*, Vol. 102, No. ST3, Mar 1976, pp. 549-568.

[16] *MathCad 2002 Professional*. MathSoft, Inc., Cambridge, MA, 2002.

[17] Megally, Sami and Amin Ghali, "Punching Shear Design of Earthquake-Resistant Slab-Column connections." *ACI Structural Journal*, Vol. 97, No. 5, Sept-Oct 2000, pp. 720-730.

[18] Mitchell, D., R. Tinaws and R.G. Redwod, "Damage to Buildings due to the 1989 Loma Prieta Earthquake-a Canadian Code Perspecitve." Canadian Journal of Civil Engineering, V. 17 No. 10, pp 813-834.

[19] Mitchell, D., R.H. Devall, M. Saatcioglu, R. Simpson, R. Tinawi and R. Tremblay, "Damage to Concrete Structures due to the 1994 Northridge Earthquake." Canadian Journal of Civil Engineering, V. 22, No. 4, pp 361-377.

[20] Moehle, Jack P., Michael E. Kreger, and Roberto Leon, "Background to Recommendations for Design of Reinforced Concrete Slab-Column Connections." *ACI Structural Journal*, Nov-Dec 1988, pp. 636-644.

[21] Morrison, Denby G., Ikuo Hirasawa and Mete A. Sozen, "Lateral Load Tests of Reinforced Concrete Slab-Column Connections." *ASCE Journal of Structural Engineering*, Vol. 109, No. 11, Nov1983, pp. 2698-2714.

[22] *NEHRP Recommended Provisions for Seismic Regulations for New Buildings and Other Structures*. Building Seismic safety Council for Federal Emergency Management Agency Committee 368, Washington, D.C., 2001.

[23] Pan, Austin A., and Jack P. Moehle, "Reinforced Concrete Flat-plates Under Lateral Loading: An Experimental Study Including Biaxial Effects." Report No. UCB/EERC-88/16, Oct. 1988.

[24] Pecknold, David A., "Slab effective Width for Equivalent Frame analysis." ACI Journal, *Proeedings* V. 72, No. 4, Apr. 1975, pp. 135-137.

[25] *RCCOLA Computer Program*. S. A. Mahin, Department of Civil Engineering, University of California, Berkeley, CA, 1977.

[26] Robertson, Ian N., Tadashi Kawai, James Lee, and Brian Enomoto, "Cyclic Testing of Slab-Column Connections with Shear Reinforcement." *ACI Structural Journal*, V. 99, No. 5, Sept. 2002, pp. 605-613.

[27] *SAP2000 Nonlinear*. Computers & Structures, Inc., Berkeley, CA, 2000.

[28] Vanderbilt, M. Daniel, and Corley, W. Gene, "Frame Analysis of Concrete Buildings." *Concrete International: Design & Construction*, V. 5, No. 12, Dec. 1983, pp. 33-43.

APPENDIX A

Design Calculations

A.1   PROTOTYPE STRUCTURAL DESIGN CALCULATIONS

The prototype structure of this study was a flat-plate concrete building, designed for office occupancy in a moderate seismic zone. The structure was designed according to ACI 318-2002 with loads defined by IBC 2000. An interior flat-plate slab-column assemblage within the prototype structure was then chosen to be constructed at half scale to complete the experimental phase of the study. *Mathcad Professional 2002* spreadsheets were used to perform design calculations. Design calculation spreadsheets are presented in this section.

A.1.1 Preliminary Design

The plan and elevation of the prototype structure are shown in Figure A.1:
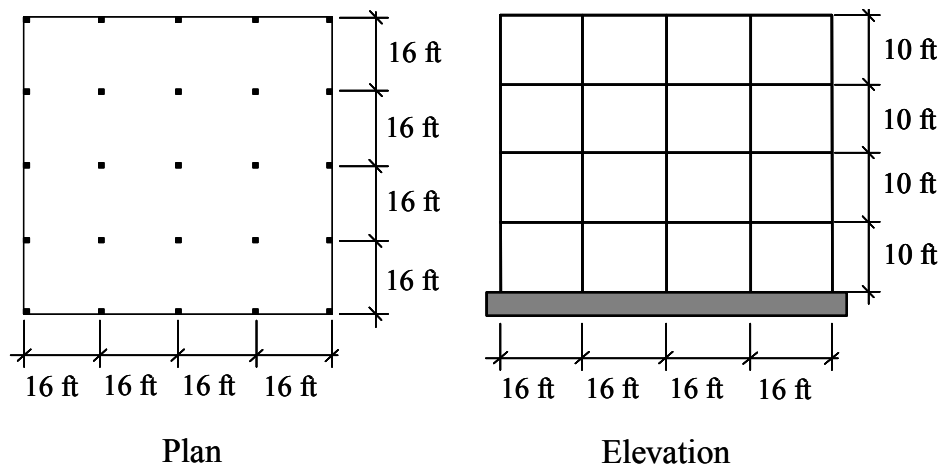
Figure A.1 Plan and Elevation of the Prototype Structure

Unit definitions:

$$psi := \frac{1 \cdot lbf}{in^2} \qquad psf := \frac{lbf}{ft^2} \qquad g = 386.088 \frac{in}{sec^2}$$

$$kip := 1000 \cdot lbf \qquad ksi := \frac{1 \cdot kip}{in^2}$$

Material Properties:

$$f_c := 4 \cdot ksi \qquad f_y := 60 \cdot ksi$$

Slab span length:

$$l := 16 \cdot ft$$

The prototype structure was designed to resist the following loads, in addition to self-weight:

$$LL := 50 \cdot psf \qquad \text{(Office Building Occupancy)}$$

$$Partition := 20 \cdot psf$$

A.1.1.1 Slab Thickness

The trial slab thickness was selected using the deflection criteria in table 9.5(c) in section 9.5.3 of ACI 318-02 for slabs without drop panels:

$$h := \frac{l}{33} \qquad \text{(Interior panel)}$$

$$h = 5.818 \, in$$

Choose a slab thickness of 8".

A.1.1.2   Column Design

The main lateral force resisting system (LFRS) in the prototype structure was assumed to be a flat-slab moment frame. Therefore, the columns must be designed well below the balanced point to achieve a displacement ductility factor greater than 1:

ACI 318-02 column strength (section 10.3.6):

$$P_o = 0.85 \cdot A_g \cdot f_c + \rho_s \cdot A_g \cdot f_y$$

A 1% reinforing ratio and grade 60 steel are used:

$$P_o = A_g \cdot \left(0.85 \cdot f_c + .6\right)$$

The column axial load must be below the balanced point to achieve sufficient ductility. The required cross-sectional area can be approximated using a column load of 30% P_o, and the used of a square column:

$$P_u = 0.3 \cdot (0.65)\left(A_g\right) \cdot \left(0.85 \cdot f_c + .6\right)$$

$$A_g = \frac{P_u}{0.166 \cdot f_c + 0.117}$$

For an interior column (8" slab thickness assumed):

$$P_u := [1.2 \cdot (100 \cdot psf + Partition) + 1.6 \cdot LL] \cdot l^2 \qquad P_u = 57.344\, kip$$

$$A_g := \frac{4 \cdot P_u}{0.166 \cdot f_c + 0.117 \cdot ksi} \qquad\qquad A_g = 293.695\, in^2$$

Required column dimension:

$$c := \sqrt{A_g} \qquad\qquad c = 17.138\, in$$

Choose 20" x 20" square columns $\qquad\qquad c := 20 \cdot in$

144

Required area of steel:

$$A_s := 0.01 \cdot c^2 \qquad\qquad A_s = 4\,in^2$$

Use 8 - #7 reinforcing bars:

$$\rho := \frac{8 \cdot 0.66 \cdot in^2}{c^2} \cdot 100 \qquad\qquad \rho = 1.32$$

Equation 11.12.2.1(c) of ACI 318-02 governed the flat-slab shear-strength for the interior, square columns. Concentric punching shear checked:

$$V_u := [1.2 \cdot (100 \cdot psf + Partition) + 1.6 \cdot LL] \cdot l^2 \qquad V_u = 57.344\,kip$$

$$d := h - 0.75 \cdot in - 0.5 \cdot in \qquad\qquad b_o := 4 \cdot (c + d)$$

$$V_c := \frac{4 \cdot \sqrt{4000} \cdot b_o \cdot d}{1000} \cdot ksi \qquad\qquad V_c = 113.571\,kip$$

A.1.2 Gravity and Lateral Load Design Moments

Gravity moments were calculated using the ACI Direct Design Method (section 13.6) and seismic lateral loads were determined using IBC 2000. Wind loads were not calculated because the study specifically focused on simulated seismic loads. Lateral load frame analysis was performed on *SAP2000*. A two-dimensional, interior-frame, was modeled using the columns and an effective width of the slab [ ] from the preliminary calculations. Design moments were then calculated using the appropriate IBC load combinations.

A.1.2.1 Gravity Loads

Applicable load combinations:

1.4D   1.2D + 1.0E + 0.5L

1.2D + 1.6L   0.9D + 1.0E

ACI Direct Design Method Prerequisites (13.6.1):

1. 3 continuous spans.
2. Rectangular panels: length ratio is 1/1 (< 2).
3. Successive length are equal.
4. No offsets.
5. LL/DL = 0.4 (< 2).
6. No panel with beams on all sides

Loads:

$DL := 120 \cdot psf$ $LL := 50 \cdot psf$

Total static moment:

$l = 16 \, ft$ $l_n := l - \dfrac{20}{12} \cdot ft$

$M_{DL} := \dfrac{DL \cdot l \cdot l_n^2}{8}$ $M_{DL} = 591.68 \, kip \cdot in$

$M_{LL} := \dfrac{LL \cdot l \cdot l_n^2}{8}$ $M_{LL} = 246.533 \, kip \cdot in$

Moment distribution factors:

$\dfrac{\alpha_1 \cdot l_2}{l_1} = 0$ $\beta_t = 0$

Table A.1 lists the ACI 318-02 DDM positive and negative moments distribution factors applied to the interior frame (section 13.6.3). Load combinations were calculated after moments from seismic loads were determined.

Table A.1 Positive and Negative Moment Distribution Factors

Slab Moments	Interior Span		Exterior Span		
	Positive	Negative	Negative (ext)	Positive	Negative (int)
Total	$.35M_0$	$.65M_0$	$.26M_0$	$.52M_0$	$.70M_0$
Column Strip	$.21M_0$	$.49M_0$	$.26M_0$	$.31M_0$	$.53M_0$
Middle Strip	$.14M_0$	$.16M_0$	0	$.21M_0$	$.17M_0$

A.1.2.2 Seismic Loads

Prototype structure was desinged for moderate seismic loads (St. Louis ar

Occupancy Category I   Site Class B

$S_s := 0.75 \cdot g$ $S_1 := 0.22 \cdot g$

From IBC 2000 table 1615.1.2(1) and1615.1.2(2), Site Class B:

$F_a := 1.0$ $F_v := 1.0$

$S_{Ds} := \frac{2}{3} \cdot (F_a \cdot S_s)$ $S_{D1} := \frac{2}{3} \cdot (F_v \cdot S_1)$

$S_{Ds} = 0.5 \, g$ $S_{D1} = 0.147 \, g$

Seismic design category determined from IBC 2000 table 1616.3(1) and 1615.(3), Site Class B.

$S_{Ds} < 0.5 \cdot g$ $S_{D1} < 0.2 \cdot g$

Design Category C $I_e := 1.0$

No geometric or mass irregularities existed in the layout of the prototype structure, so the Equivalent Lateral Force procedure may be used.

Natural period of the prototype structure calculated (1617.4.2.1):

$h_n := 40$ $c_t := 0.03$

$T_a := c_t \cdot h_n^{(0.75)} \cdot \sec$ (100% lateral load resisted by r/c moment-frame system)

$T_{a2} := 0.1 \cdot 4 \cdot \sec$ $T_a = 0.477 \sec$

$T_n := 0.4$ $T_{a2} = 0.4 \sec$

Design Base Shear (1617.4.4):

$V = C_s \cdot W$

Where:

$$C_s = \frac{S_{Ds}}{\left(\dfrac{R}{I_e}\right)}$$ But, $0.044 \cdot S_{Ds} \cdot I_e < C_s < \dfrac{S_{D1}}{\left(\dfrac{R}{I_e}\right) \cdot T}$

Flat-plate moment frame were assumed to be an intermediate concrete moment resisting frame. No system limitations for seismic design category C for this frame type (IBC 2000 table 1617.6).

$R := 5$ $C_s := \dfrac{S_{Ds}}{\left(\dfrac{R}{I_e}\right)}$ $C_s = 0.1\,g$

148

$$C_{s\_upper} := \frac{S_{D1}}{\left(\dfrac{R}{I_e}\right) \cdot T_n}$$

$$C_{s\_upper} = 0.073 \, g$$

$$C_{s\_lower} := 0.044 \cdot S_{Ds} \cdot I_e \qquad\qquad C_{s\_lower} = 0.022 \, g$$

$$C_s := C_{s\_upper}$$

Dead load of the structure determined(per floor):

$$w_{slab} := (100 \cdot psf + Partition) \cdot (64 \cdot ft)^2 \qquad w_{slab} = 491.52 \, kip$$

Total floor weight of 525 kips.

$$w := 525 \cdot kip$$

Design base shear:

$$V := C_s \cdot 4 \cdot \frac{w}{g}$$

$$V = 154 \, kip$$

Vertica seismic forces distributed (16174.3):

$$F_x = C_{vs} \cdot V \qquad\qquad\qquad C_{vx} = \frac{w_x \cdot h_x^k}{\displaystyle\sum_{i=1}^{n} w_i \cdot h_i^k}$$

$$V_x = \sum_{i=1}^{n} F_i$$

$$k := 1.28 \qquad\qquad\qquad \text{(interpolation)}$$

Let:

$i := 1..4$

Floor height and weight listed in order, from the 1st floor.

$$h_i := 10 \cdot i \cdot \text{ft} \qquad\qquad\qquad w_i := 500 \cdot \text{kip}$$

$$C_{v_i} := \frac{w_i \cdot (h_i)^k}{\displaystyle\sum_{j=1}^{4} w_j \cdot (h_j)^k} \qquad\qquad C_v^T = (\,0.075 \quad 0.181 \quad 0.304 \quad 0.44\,)$$

$$F_i := C_{v_i} \cdot V \qquad\qquad F^T = (\,11.487 \quad 27.896 \quad 46.875 \quad 67.742\,)\,\text{kip}$$

$$V_i := \sum_{i=i}^{4} F_{(i)} \qquad\qquad V^T = (\,154 \quad 142.513 \quad 114.617 \quad 67.742\,)\,\text{kip}$$

Lateral forces equally to distributed between 4 frames (exterior frames had half the dead load of the interior frames):

$$F_{\text{frame\_int}_i} := \frac{1}{4} \cdot F_i \qquad\qquad F_{\text{frame\_int}} = \begin{pmatrix} 2.872 \\ 6.974 \\ 11.719 \\ 16.936 \end{pmatrix} \text{kip}$$

A.1.3 Lateral Load Analysis

As previously stated, a two-dimensional model of an interior frame in the prototype structure was created using SAP2000. Columns were modeled according to the dimensions calculated in the preliminary design. "Beams" used in the model consisted of an effective width of the slab, and the previously calculated thickness. The effective width parameter chosen for analysis was developed by Pecknold (Pecknold, David A., "Slab Effective Width for

150

Equivalent Frame Analysis," ACI Journal, *Proceedings,* V. 72, No.4 Apr. 1975, pp. 135-137), which used the effective width ratio found in figure 4, page 137. Figure A.2 shows a picture of the two-dimensional frame created in *SAP2000*.
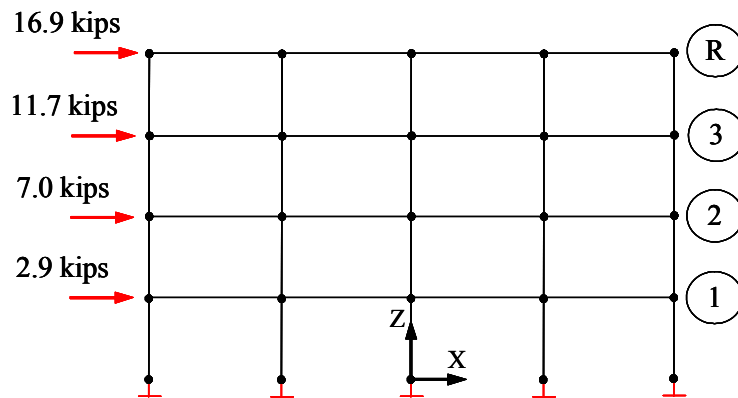
Figure A.2 Two-Dimensional SAP2000 Prototype Structure Frame

Effective width parameter:

$$\alpha := 0.77 \qquad\qquad l_{eff} := \alpha \cdot l$$

$$l_{eff} = 12.32 \, ft$$

Individual frame element forces are found at the end of the section. Maximum moments located along the second floor of an interior frame were used in the design. Slab moments acting on floor 2 of the frame are listed below:

$$M_{E\_ext\_negative} := 460 \cdot kip \cdot in \qquad\qquad M_{E\_int\_positive} := 424 \cdot kip \cdot in$$

$$M_{E\_ext\_mid} := 11 \cdot kip \cdot in \qquad\qquad M_{E\_int\_negative} := 424 \cdot kip \cdot in$$

$$M_{E\_ext\_positive} := 438 \cdot kip \cdot in$$

IBC 2000 earthquake load parameters:

$$E_1 = \rho \cdot Q_E + 0.2 \cdot S_{Ds} \cdot D \qquad\qquad E_2 = \rho \cdot Q_E - 0.2 \cdot S_{Ds} \cdot D$$

$$\rho = 2 - \frac{20}{r_{maxi}\sqrt{A_i}}$$

(ρ_{maxi} is defined in IBC 1617.2.2)

Table A.2 shows the reliability factor calculations:

Table A.2 Reliability Factor Calculations

Story	Total Story Shear (kips)	ρ_{max} calculation				
		V1 + 0.7V2	0.7V2 + 0.7V3	0.7V3 + 0.7V4	0.7V4 + V5	ρ_i
2	38.5	12.60	11.87	11.86	12.56	0.327
3	35.63	11.03	11.96	11.96	11.02	0.336
4	28.66	8.85	9.65	9.64	8.84	0.337
Roof	16.94	5.02	6.15	6.13	4.98	0.363

$$r_{max} := 0.36281 \qquad\qquad A := 64 \cdot 64$$

$$\rho := 2 - \frac{20}{r_{max} \cdot \sqrt{A}} \qquad\qquad \rho = 1.139$$

A.1.4 Slab Design

Load combinations were calculated and distributed to column and middle strips using an Excel spreadsheet. Table A.3 summarizes the maximum and minimum calculated interior span moments. Positive moments are assumed to act on the tension face of the slab. In the table, "Pos" headings are assumed to be moments acting at mid-slab-span, and "Neg" headings are moments acting at the

column faces. A negative numbers listed under a "Pos" or "Neg" headings indicated the moment was reversed.

Table A.3 Maximum and Minimum Interior Span Moments

Interior Span				
Moments	Column Strip		Middle Strip	
(kip-in)	Pos	Neg	Pos	Neg
Maximum	231.9	918.4	154.6	179.5
Minimum	111.8	-252.6	-	-

A.1.4.1 Interior Span Slab Flexural Steel

Material properties:

$$f_y := 60 \cdot ksi \qquad\qquad f_c := 4.5 \cdot ksi \qquad\qquad h := 8 \cdot in$$

Column strip negative moment:

$$M_{cs\_neg} := \frac{918.4}{8} \cdot kip \cdot \frac{in}{ft} \qquad\qquad M_{cs\_neg} = 114.8 \, kip \cdot \frac{in}{ft}$$

$$As_{cs\_neg\_reqd} := \frac{M_{cs\_neg}}{f_y \cdot .9 \cdot h \cdot .9} \qquad\qquad As_{cs\_neg\_reqd} = 0.295 \, \frac{in^2}{ft}$$

No. 5 bars at 10" tried(detailing follows):

$$d := h - 0.75 \cdot in - .625 \cdot in \qquad\qquad As_{cs\_neg} := 0.372 \cdot \frac{in^2}{ft}$$

$$a := \frac{As_{cs\_neg} \cdot f_y}{0.85 \cdot f_c} \qquad\qquad a = 0.486 \, in$$

$$Mn_{cs\_neg} := 0.9 As_{cs\_neg} \cdot f_y \cdot \left(d - \frac{a}{2}\right)$$

$$\rho_{cs\_neg} := \frac{As_{cs\_neg}}{d}$$

$$Mn_{cs\_neg} = 128.199 \, kip \cdot \frac{in}{ft}$$

$$\rho_{cs\_neg} = 4.679 \times 10^{-3}$$

Column strip positive moment (occured at column face):

$$M_{cs\_pos} := \frac{252.6}{8} \cdot kip \cdot \frac{in}{ft}$$

$$M_{cs\_pos} = 31.575 \, kip \cdot \frac{in}{ft}$$

$$As_{cs\_neg\_reqd} := \frac{M_{cs\_pos}}{f_y \cdot .9 \cdot h \cdot .9}$$

$$As_{cs\_neg\_reqd} = 0.295 \, \frac{in^2}{ft}$$

No. 5 bars at 18" (maximum spacing) used:

$$d := h - 0.75 \cdot in - .625 \cdot in$$

$$As_{cs\_pos} := 0.207 \cdot \frac{in^2}{ft}$$

$$a := \frac{As_{cs\_pos} \cdot f_y}{0.85 \cdot f_c}$$

$$a = 0.271 \, in$$

$$Mn_{cs\_pos} := 0.9 As_{cs\_pos} \cdot f_y \cdot \left(d - \frac{a}{2}\right)$$

$$Mn_{cs\_pos} = 72.542 \, kip \cdot \frac{in}{ft}$$

Middle strip negative moment:

$$M_{ms\_neg} := \frac{179.5}{8} \cdot kip \cdot \frac{in}{ft}$$

$$M_{ms\_neg} = 22.438 \, kip \cdot \frac{in}{ft}$$

No. 5 bars at 18" used:

$$Mn_{ms\_neg} := Mn_{cs\_pos}$$

$$Mn_{ms\_neg} = 72.542 \, kip \cdot \frac{in}{ft}$$

154

Middle strip positive moment:

$$M_{cs\_pos} := \frac{154.6}{8} \cdot kip \cdot \frac{in}{ft} \qquad\qquad M_{cs\_pos} = 19.325\,kip \cdot \frac{in}{ft}$$

Again, No. 5 bars at 18" used:

$$Mn_{ms\_pos} := Mn_{cs\_pos} \qquad\qquad Mn_{ms\_pos} = 72.542\,kip \cdot \frac{in}{ft}$$

Punching shear strength checked including the effects of unbalanced moment (ACI 318-02 section 11.12.6):

$$d := h - 0.75 \cdot in - 0.5 \cdot in \qquad\qquad b_o := 4 \cdot (c + d)$$

$$V_u = 57.344\,kip \qquad\qquad v_{u\_conc} := \frac{V_u}{b_o \cdot d}$$

$$v_{u\_conc} = 79.396\,psi$$

Two sources of unbalanced moment existed: live loads and earthquake loads:

$$M_{ub\_live} := 0.07 \frac{LL \cdot l \cdot l_n{}^2}{2} \qquad\qquad M_{ub\_live} = 69.029\,kip \cdot in$$

$$M_{ub\_eq} := 918.4 \cdot kip \cdot in + 252.6 \cdot kip \cdot in$$

$$M_{ub\_eq} = 1.171 \times 10^3\,kip \cdot in$$

Earthquake unbalanced moments controlled.

$$Jc := \frac{b_1 \cdot d \cdot \left(b_1 + 3 \cdot b_2\right) + d^3}{3}$$

For a square column, $b_1 = b_2$:

$$b_1 := 20 \cdot in + d \qquad\qquad\qquad b_2 := b_1$$

$$Jc := \frac{b_1 \cdot d \cdot \left(b_1 + 3 \cdot b_2\right) + d^3}{3} \qquad\qquad Jc = 6.543 \times 10^3\, in^3$$

$$\gamma_v := 0.4 \qquad\qquad\qquad\qquad \text{(square column)}$$

$$v_{u\_mom} := \frac{\gamma_v \cdot M_{ub\_eq}}{Jc} \qquad\qquad\qquad v_{u\_mom} = 71.593\, psi$$

Total acrued shear stress:

$$v_u := v_{u\_conc} + v_{u\_mom} \qquad\qquad v_u = 150.989\, psi$$

Shear resistance was previously calculated:

$$V_c = 113.571\, kip \qquad\qquad\qquad v_c := 0.75 \frac{V_c}{b_o \cdot d}$$

$$v_c = 117.934\, psi$$

The provided shear resistance did not meet the shear demand calculated from combined gravity and earthquake loads. ACI Chapter 21 flat-plate, gravity shear limit checked ($0.4*V_o$):

$$\text{Ratio} := \frac{V_u}{V_c} \qquad\qquad \text{Ratio} = 0.505$$

Live load was included in the calculation of the punching shear strength. ACI chapter 21 gravity load limit rechecked:

$$v_{u\_conc} := \frac{0.4 \cdot V_c}{b_o \cdot d}$$

$$v_u := v_{u\_conc} + v_{u\_mom} \qquad\qquad v_u = 134.491\,\text{psi}$$

The prototype structure was assumed to be an existing structure. Deficient interior connections will have to be upgraded to meet the shear demand of a moderate level seismic event. However, the structure was detailed according to ACI Chapter 21 provisions:

ACI 21.12.6:

1. 50% of the negative reinforcement of the column strip must be placed in a zone (c + 3h) from the column centerline.
2. 25% of the negative reinforcement of the column strip must be continuous.
3. 50% of the positive reinforcement in the middle strip and all of the reinforcement in the column strip must be continuous.

A.1.4.2 Prototype Structure Interior Frame Details

<div align="center">(a)   (b)</div>
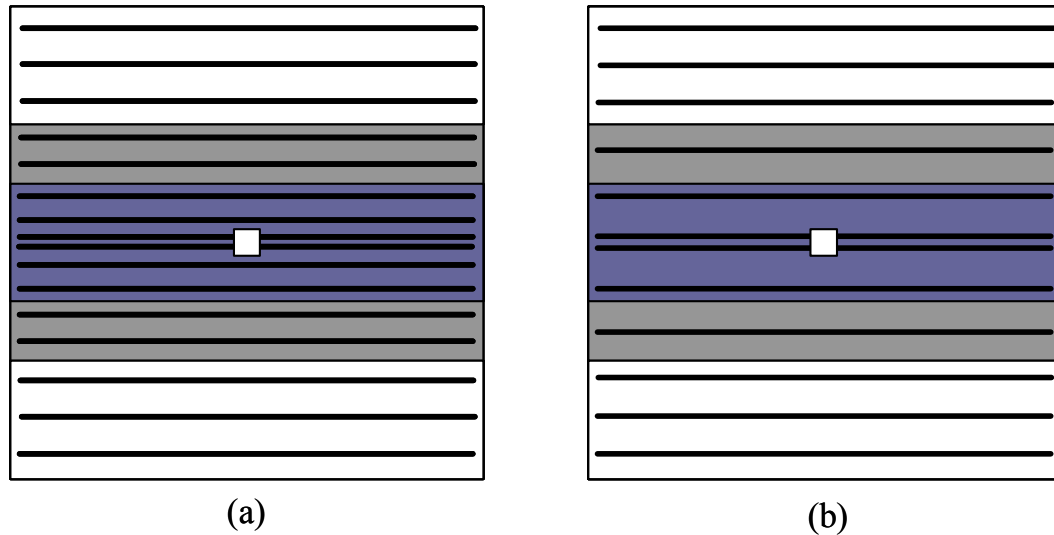
Figure A.3 Prototype Structure Steel Reinforcing Bar Details: (a) Top Mat of Steel; and, (b) Bottom Mat of Steel

Top and bottom mat longitudinal reinforcing bar details are displayed Figure A.3 (a) and (b). Symmetric reinforcement in the perpendicular direction was not drawn for clarity. The blue regions show the effective width of the column strip, where the remaining column strip is displayed gray. The middle strip regions are shown in white. A rebar schedule and reinforcement ratios for the interior spans of the prototype structure is listed in Table A.4.

Table A.4 Prototype Structure Interior Span Rebar Schedule

STEEL LOCATION	SLAB ZONE	DIMENSION (in)*	ρ (%)	NUMBER OF BARS
TOP STEEL	COLUMN STRIP	96	0.99	10
	C + 3H	44	1.30	6
	ONE-HALF REMAINING AREA	26	0.73	2
	MIDDLE STRIP	96	0.60	6
	ONE-HALFAREA	48	0.60	3
BOTTOM STEEL	COLUMN STRIP	96	0.60	6
	MIDDLE STRIP	96	0.60	6
	ONE-HALFAREA	48	0.60	3

A.1.5 Column Design

The preliminary column design was checked for adequacy using the sectional analysis program RCCOLA. The interaction diagram for the preliminary column design is shown in Figure A.4 . The applied axial load and moment are calculated:

Preliminary column section:

20" x 20" square columns, with 8 - #7 reinforcing bar

$$P_{u\_col} := 4 \cdot \left[[1.2 \cdot (100 \cdot psf + Partition) + 1.6 \cdot LL] \cdot l^2 \right]$$

$$P_{u\_col} = 229.376 \, kip$$

$$M_{u\_col} := 196.62 \cdot kip \cdot in + 0.6 \cdot M_{ub\_eq}$$

$$M_{u\_col} = 899.22 \, kip \cdot in$$

Applied_Load := (230 900)
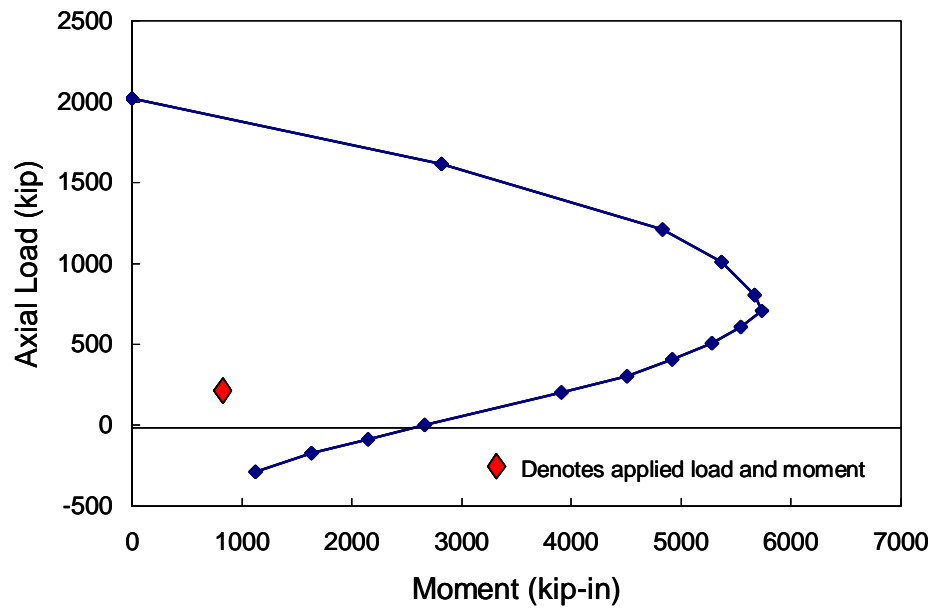
Figure A.4 Prototype Column Axial Load-Moment Interaction Diagram

The preliminary column is sufficient

A.1.6 SAP2000 Analysis Results

This section lists the *SAP2000* lateral load analysis results.   The column elements two-dimensional model are shown in Figure A.5 and the beam numbers are shown in Figure A.6.
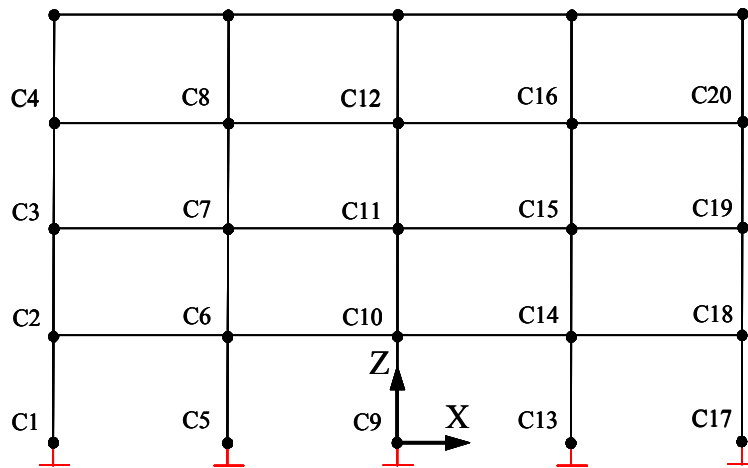
Figure A.5 Column Elements of SAP2000 Frame
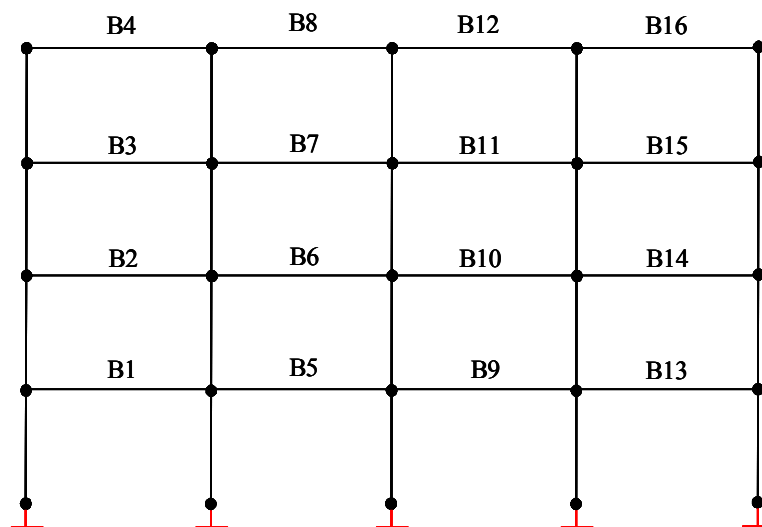
Figure A.6 Beam Elements of SAP2000 Frame

Beam forces from lateral load analysis are listed in Table A.5:

Table A.5 Beam Forces from SAP2000 Analysis

Beams						
Element Number	P (kip)	V2 (kip)	V3 (kip)	T (kip)	M2 (kip-in)	M3 (kip-in)
1						
	-1.37	4.48	0	0	0	442.4
	-1.37	4.48	0	0	0	227.31
	-1.37	4.48	0	0	0	12.23
	-1.37	4.48	0	0	0	-202.86
	-1.37	4.48	0	0	0	-417.95
2						
	-6.01	4.68	0	0	0	460.44
	-6.01	4.68	0	0	0	235.89
	-6.01	4.68	0	0	0	11.33
	-6.01	4.68	0	0	0	-213.22
	-6.01	4.68	0	0	0	-437.78
3						
	-9.61	3.5	0	0	0	343.69
	-9.61	3.5	0	0	0	175.65
	-9.61	3.5	0	0	0	7.61
	-9.61	3.5	0	0	0	-160.43
	-9.61	3.5	0	0	0	-328.47
4						
	-15.08	1.96	0	0	0	196.62
	-15.08	1.96	0	0	0	102.76
	-15.08	1.96	0	0	0	8.9
	-15.08	1.96	0	0	0	-84.95
	-15.08	1.96	0	0	0	-178.81
5						
	-1.46	4.17	0	0	0	399.6
	-1.46	4.17	0	0	0	199.57
	-1.46	4.17	0	0	0	-4.61E-01
	-1.46	4.17	0	0	0	-200.49
	-1.46	4.17	0	0	0	-400.52

Beams						
Element Number	P (kip)	V2 (kip)	V3 (kip)	T (kip)	M2 (kip-in)	M3 (kip-in)
6						
	-4.31	4.42	0	0	0	424.19
	-4.31	4.42	0	0	0	211.98
	-4.31	4.42	0	0	0	-2.36E-01
	-4.31	4.42	0	0	0	-212.45
	-4.31	4.42	0	0	0	-424.66
7						
	-7.11	3.37	0	0	0	323.46
	-7.11	3.37	0	0	0	161.78
	-7.11	3.37	0	0	0	9.53E-02
	-7.11	3.37	0	0	0	-161.59
	-7.11	3.37	0	0	0	-323.27
8						
	-10.65	1.8	0	0	0	172.6
	-10.65	1.8	0	0	0	86.18
	-10.65	1.8	0	0	0	-2.44E-01
	-10.65	1.8	0	0	0	-86.67
	-10.65	1.8	0	0	0	-173.09
9						
	-1.5	4.16	0	0	0	400.26
	-1.5	4.16	0	0	0	200.42
	-1.5	4.16	0	0	0	5.91E-01
	-1.5	4.16	0	0	0	-199.24
	-1.5	4.16	0	0	0	-399.08
10						
	-2.7	4.42	0	0	0	424.37
	-2.7	4.42	0	0	0	212.38
	-2.7	4.42	0	0	0	3.80E-01
	-2.7	4.42	0	0	0	-211.62
	-2.7	4.42	0	0	0	-423.61
11						
	-4.61	3.36	0	0	0	322.91
	-4.61	3.36	0	0	0	161.5
	-4.61	3.36	0	0	0	8.13E-02
	-4.61	3.36	0	0	0	-161.34
	-4.61	3.36	0	0	0	-322.75

Beams						
Element Number	P (kip)	V2 (kip)	V3 (kip)	T (kip)	M2 (kip-in)	M3 (kip-in)
12						
	-6.3	1.8	0	0	0	172.83
	-6.3	1.8	0	0	0	86.6
	-6.3	1.8	0	0	0	3.72E-01
	-6.3	1.8	0	0	0	-85.86
	-6.3	1.8	0	0	0	-172.09
13						
	-1.61	4.47	0	0	0	416.83
	-1.61	4.47	0	0	0	202.39
	-1.61	4.47	0	0	0	-12.04
	-1.61	4.47	0	0	0	-226.47
	-1.61	4.47	0	0	0	-440.9
14						
	9.62E-02	4.66	0	0	0	436.58
	9.62E-02	4.66	0	0	0	212.72
	9.62E-02	4.66	0	0	0	-11.14
	9.62E-02	4.66	0	0	0	-235
	9.62E-02	4.66	0	0	0	-458.86
15						
	-2.1	3.48	0	0	0	327.02
	-2.1	3.48	0	0	0	159.82
	-2.1	3.48	0	0	0	-7.38
	-2.1	3.48	0	0	0	-174.57
	-2.1	3.48	0	0	0	-341.77
16						
	-1.9	1.94	0	0	0	177.65
	-1.9	1.94	0	0	0	84.49
	-1.9	1.94	0	0	0	-8.67
	-1.9	1.94	0	0	0	-101.83
	-1.9	1.94	0	0	0	-194.99

Column forces from lateral load analysis are listed in Table A.5

Table A.6 Column Forces from SAP2000 Analysis

Columns						
Element N	P (kip)	V2 (kip)	V3 (kip)	T (kip)	M2 (kip-in)	M3 (kip-in)
1						
	14.62	6.63	0	0	0	664.76
	14.62	6.63	0	0	0	266.77
	14.62	6.63	0	0	0	-131.23
2						
	10.13	5	0	0	0	311.18
	10.13	5	0	0	0	11.06
	10.13	5	0	0	0	-289.07
3						
	5.46	4.01	0	0	0	171.37
	5.46	4.01	0	0	0	-69.25
	5.46	4.01	0	0	0	-309.88
4						
	1.96	1.92	0	0	0	33.81
	1.96	1.92	0	0	0	-81.4
	1.96	1.92	0	0	0	-196.62
5						
	-14.56	6.6	0	0	0	661.72
	-14.56	6.6	0	0	0	265.69
	-14.56	6.6	0	0	0	-130.34
5						
	5.81E-02	8.53	0	0	0	737.05
	5.81E-02	8.53	0	0	0	225.46
	5.81E-02	8.53	0	0	0	-286.13
6						
	4.44E-02	8.62	0	0	0	531.42
	4.44E-02	8.62	0	0	0	14.08
	4.44E-02	8.62	0	0	0	-503.26

Columns						
Element N	P (kip)	V2 (kip)	V3 (kip)	T (kip)	M2 (kip-in)	M3 (kip-in)
7						
	8.73E-02	6.92	0	0	0	358.71
	8.73E-02	6.92	0	0	0	-56.68
	8.73E-02	6.92	0	0	0	-472.07
8						
	5.49E-02	4.43	0	0	0	179.86
	5.49E-02	4.43	0	0	0	-85.77
	5.49E-02	4.43	0	0	0	-351.41
9						
	8.16E-03	8.43	0	0	0	733.06
	8.16E-03	8.43	0	0	0	227.02
	8.16E-03	8.43	0	0	0	-279.03
10						
	4.08E-03	8.47	0	0	0	521.75
	4.08E-03	8.47	0	0	0	13.32
	4.08E-03	8.47	0	0	0	-495.11
11						
	5.58E-04	6.86	0	0	0	353.93
	5.58E-04	6.86	0	0	0	-57.8
	5.58E-04	6.86	0	0	0	-469.53
12						
	2.80E-05	4.35	0	0	0	176.66
	2.80E-05	4.35	0	0	0	-84.63
	2.80E-05	4.35	0	0	0	-345.92
13						
	1.62E-02	8.51	0	0	0	735.36
	1.62E-02	8.51	0	0	0	225.02
	1.62E-02	8.51	0	0	0	-285.32
14						
	1.20E-02	8.61	0	0	0	530.58
	1.20E-02	8.61	0	0	0	14.03
	1.20E-02	8.61	0	0	0	-502.52

Columns					
Element N	P (kip)	V2 (kip)	V3 (kip)	T (kip)	M2 (kip-in)	M3 (kip-in)
15						
	6.48E-02	6.91	0	0	0	357.68
	6.48E-02	6.91	0	0	0	-56.79
	6.48E-02	6.91	0	0	0	-471.25
16						
	4.44E-02	4.4	0	0	0	178.52
	4.44E-02	4.4	0	0	0	-85.61
	4.44E-02	4.4	0	0	0	-349.74
18						
	-10.09	4.99	0	0	0	310.56
	-10.09	4.99	0	0	0	10.99
	-10.09	4.99	0	0	0	-288.57
19						
	-5.42	4	0	0	0	170.29
	-5.42	4	0	0	0	-69.5
	-5.42	4	0	0	0	-309.29
20						
	-1.94	1.9	0	0	0	32.49
	-1.94	1.9	0	0	0	-81.25
	-1.94	1.9	0	0	0	-194.99

A.1.7 Design Moments

This section lists the design moments calculations for the interior span of the prototype structure. All moments were compiled using *Excel*, where load combinations were tabulated. Table A.7 lists the calculated gravity loads, and Table A.8 lists the earthquake moments from computer analysis. The load combinations are calculated in Table A.9. Table A.10 lists the final interior slab design moments.

Table A.7 Gravity Load Moments

Slab Moments	Dead Load (kip-in)*	Interior Span (kip-in)		Live Load (kip-in)	Interior Span	
		Positive	Negative		Positive	Negative
Total		207.1	384.6		86.3	160.2
Column Strip	591.7	124.2	288.4	246.5	51.8	120.2
Middle Strip		82.8	96.1		34.5	40.1

Table A.8 Earthquake Moments

Slab Moments	Interior Span		
	Neg/Pos	E (+)	E (-)
Total		512.2	454.5
Column Strip	424.0	512.2	454.5
Middle Strip		0.0	0.0

Table A.9 Load Combinations

Combo	Interior Span				
	Column Strip			Middle Strip	
	Pos	Neg	Neg (+E)	Pos	Neg
1.4D	173.9	403.8	0.0	116.0	134.6
1.2D+1.6L	231.9	538.4	0.0	154.6	179.5
1.2D+E+.5L	175.0	918.4	-106.0	0.0	0.0
1.2D-E+.5L	175.0	860.7	-48.3	0.0	0.0
.9D+E	111.8	771.8	-252.6	0.0	0.0
.9D-E	111.8	714.1	-194.9	0.0	0.0

Table A.10 Design Moments

Moments (kip-in)	Interior Span			
	Column Strip		Middle Strip	
	Pos	Neg	Pos	Neg
Maximum	231.9	918.4	154.6	179.5
Minimum	111.8	-252.6	-	-

A.2 TEST SPECIMEN STIFFNESS ANALYSIS

The design loads for the prototype structure were formulated using a combination of the ACI direct design method moments and a SAP 2000 frame. The direct design method was used to obtain the gravity load moments and an interior frame was modeled and analyzed using SAP 2000. The original SAP analysis model the interior frame using the gross column properties and and effective width of the slab, using the results of Pecknold. Results from each of these analyses were tabulated and load combinations were calculated using Microsoft Excel and the flat-plate system was designed accordingly.

The elastic portions of the lateral load-displacement backbone curves from the actual tests will be compared with two-dimensional frame models created using SAP2000. The SAP2000 analyses will model the flat-plate test specimen using the effective width, and the explicit transverse torsional member method. A unit lateral load will be applied to model to determine the flexibility of the system.

Geometric and Material properties of the test specimen:

$$L_S := 96 \cdot in \qquad\qquad L := 60 \cdot in \qquad\qquad h := 4.5 \cdot in$$

$$E_{steel} := 29000 \cdot ksi \qquad\qquad E_{concrete} := 57 \cdot \sqrt{4000} \cdot ksi$$

$$I_{column} := 534 \cdot in^4 \qquad\qquad f_{rupture} := \frac{7.5 \cdot \sqrt{4000}}{1000} \cdot ksi$$

A.2.1 Effective Width Calculations

The effective width parameter taken from Allen and Darvall, "Lateral Load Equivalent Frame," ACI Journal, *Proceedings,* V. 74, No.7 Apr. 1977, pp. 294-299 and Pecknold, David A., "Slab Effective Width for Equivalent Frame Analysis," ACI Journal, *Proceedings,* V. 72, No.4 Apr. 1975, pp. 135-137.

Effective width parameters:

$$\alpha_A := 0.51 \qquad\qquad\qquad \alpha_P := 0.77$$

Material and intertial properties can then be defined:

$$EI_s := E_{concrete} \cdot \frac{\alpha_A \cdot L_s \cdot h^3}{12} \qquad\qquad EI_c := E_{steel} \cdot I_{column}$$

$$EI_s = 1.34 \times 10^6 \, kip \cdot in^2 \qquad\qquad EI_c = 1.549 \times 10^7 \, kip \cdot in^2$$

However, prior to loading the test specimen laterally, a gravity load was applied, which cracked the slab. It is therefore recommended to take one-third the slab stiffness, due to cracking. Figure A.7 shows the flexibility model used in the computer analysis

$$EI_s := 0.33 \, E_{concrete} \cdot \frac{\alpha_A \cdot L_s \cdot h^3}{12}$$
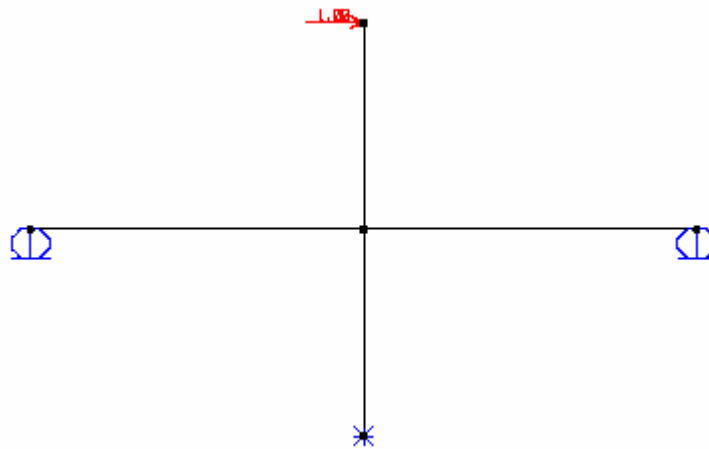
Figure A.7 SAP 2000 Flexibiltiy Model

SAP2000 Analysis results:

$$f_{effective\_width} := 0.0668 \frac{in}{kip}$$

Check results verses hand calculation using the stiffness method:

$$\Delta := P \cdot \left[\frac{1}{12 \cdot EI_c} \cdot \frac{L^2}{EI_s} \cdot \left(EI_c \cdot L_s + EI_s \cdot L \right) \right]^{\blacksquare}$$

$$f := \frac{1}{12 \cdot EI_c} \cdot \frac{L^2}{EI_s} \cdot \left(EI_c \cdot L_s + EI_s \cdot L \right) \qquad\qquad f = 0.066 \frac{in}{kip} \qquad\qquad (O.K.)$$

Results based on Pecknold's method:

$$f_{eff\_pecknold} := 0.042 \cdot \frac{in}{kip}$$

It should be noted that the prototype analysis and design called for a concrete column. A concrete column was modeled using gross and cracked section properties of the scaled test specimen. The cracked section was assumed to be 50% of the gross section. SAP2000 flexibility analysis:

$$f_{eff\_conc\_gross} := 0.06784 \frac{in}{kip} \qquad\qquad f_{eff\_conc\_cracked} := 0.07318 \frac{in}{kip}$$

Percentage difference:

$$P_{gross\_steel} := \frac{f_{eff\_conc\_gross} - f_{effective\_width}}{f_{effective\_width}} \cdot 100$$

$$P_{gross\_steel} = 1.557$$

$$P_{cracked\_steel} := \frac{f_{eff\_conc\_cracked} - f_{effective\_width}}{f_{effective\_width}} \cdot 100$$

$$P_{cracked\_steel} = 9.551$$

The concrete column influences the system to be 11% more flexible. However, the slab has the greater influence as to the overall flexibility of the system. Cracking models represent an approximate percentage reduction of the total section. The differences will therefore be assumed negligible as the most load redistribution will occur transversely across the length of the slab. Check lateral load to crack the concrete column:

$$P_{col\_flex\_crack} := \frac{(12 \cdot in)^3}{6} \cdot f_{rupture} \cdot \frac{1}{60 \cdot in} \qquad P_{col\_flex\_crack} = 2.277 kip$$

At this lateral load, slab cracks cause the specimen to degrade from the elastic range.

A.2.2 Explicit Transverse Torsional Memeber Method

A three dimensional model of the flat-plate system was created using the slab, columns and torsional members, as defined in the ACI Equivalent Frame Method. This is shown in Figure A.8. Half of the slab-beam stiffness is applied to each beam, and half of the torsional stiffness is applied to each transverse member. Torsional stiffness is distributed to the transverse members by solving for the torsional constant, J, and assigning that value to the torsional member's section properties.
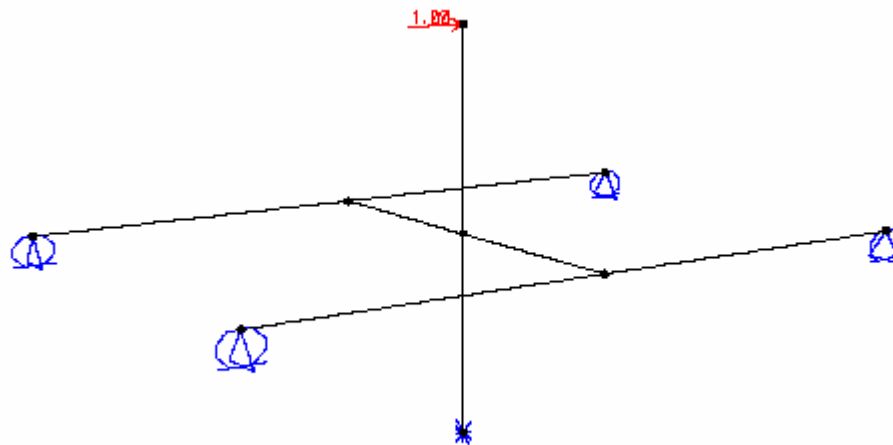
Figure A.8 Transverse Torsional Method Flexibility Model

Stiffness of the torsional members:

$$K_t := \sum_n \frac{9 \cdot E_c \cdot C}{l_2 \cdot \left(1 - \frac{c}{l_2}\right)^3} \blacksquare \qquad\qquad C := \left(1 - 0.62 \cdot \frac{x}{y}\right) \cdot \frac{x^3 \cdot y}{3} \blacksquare$$

Torsional constant for the test specimen:

$$c := 12 \cdot in \qquad l_2 := L_s \qquad x := 4.5 \cdot in \qquad y := c$$

$$C := \left(1 - 0.62 \cdot \frac{x}{y}\right) \cdot \frac{x^3 \cdot y}{3} \qquad\qquad C = 279.754 in^4$$

$$K_t := 2 \frac{9 \cdot E_{concrete} \cdot C}{l_2 \cdot \left(1 - \frac{c}{l_2}\right)^3} \qquad\qquad K_t = 2.823 \times 10^5 \, kip \cdot \frac{in}{rad}$$

$$\frac{K_t}{2} = 1.411 \times 10^5 \, kip \cdot in \qquad G := 1593.2 \cdot ksi \qquad L := 30 \cdot in$$

$$J := \frac{K_t \cdot L}{2 \cdot G} \qquad\qquad J = 2.658 \times 10^3 \, in^4$$

SAP2000 analysis results:

$$f_{explicit} := 0.0734 \frac{in}{kip}$$

A.3　TEST SPECIMEN STRENGTH ANALYSIS

This section calculates the lateral strength of the control specimens based on ACI 318-02 provisions and FEMA 356 Provisions. The lateral strength of the control specimens will be checked based on unbalanced moment capacity and shear capacity.

A.3.1　Moment Capacity of Slab Based on ACI 318-2002

Define specimen properties:

$$f_c := 4.0 \cdot ksi \qquad f_y := 60 \cdot ksi \qquad \gamma_f := .6 \qquad \gamma_v := .4$$

$$h := 4.5 \cdot in \qquad d := 3.25 \cdot in \qquad c := 12 \cdot in \qquad b_1 := (c + d)$$

$$b_0 := (c + d) \cdot 4 \qquad\qquad b_0 = 61 \, in$$

$$Jc := \frac{b_1 \cdot d \cdot (4 \cdot b_1) + d^3}{3} \qquad\qquad Jc = 1.019 \times 10^3 \, in^3$$

Moment capacity of flat-plate slab is based on the effective width (c + 3h). Define w = c + 3h:

$$w := c + 3 \cdot h \qquad\qquad w = 25.5 \, in$$

Area of steel within effective width, all bars in the test specimens are #4:

$$As_t := 4 \cdot .196 \cdot in^2 \qquad\qquad As_t = 0.784 \, in^2$$

$$As_b := 2 \cdot .196 \cdot in^2 \qquad\qquad As_b = 0.392 \, in^2$$

174

Moment capacity of negative steel:

$$a := \frac{As_t \cdot f_y}{.85 \cdot f_c \cdot w} \qquad a = 0.543 \, in$$

$$Mn_t := As_t \cdot f_y \cdot \left(d - \frac{a}{2}\right) \qquad Mn_t = 140.119 \, kip \cdot in$$

Moment capacity of positive steel:

$$a := \frac{As_b \cdot f_y}{.85 \cdot f_c \cdot w} \qquad a = 0.271 \, in$$

$$Mn_b := As_b \cdot f_y \cdot \left(d - \frac{a}{2}\right) \qquad Mn_b = 73.25 \, kip \cdot in$$

Total Unbalanced Moment Capacity:

$$M_{ub} := \frac{Mn_t + Mn_b}{\gamma_f} \qquad M_{ub} = 355.615 \, kip \cdot in$$

Lateral Capacity of Slab Based on Test Setup:

$$F_{flex} := \frac{M_{ub}}{60 \cdot in} \qquad F_{flex} = 5.927 \, kip$$

Check the moment capacity the slab including negative steel near the edge of the effective width (c + 3h).

$$As_t := 6 \cdot .196 \cdot in^2 \qquad As_t = 1.176 \, in^2$$

Moment capacity of negative steel:

$$a := \frac{As_t \cdot f_y}{.85 \cdot f_c \cdot w} \qquad a = 0.271 \, in$$

$$Mn_t := As_t \cdot f_y \cdot \left(d - \frac{a}{2}\right) \qquad Mn_t = 200.608 \, kip \cdot in$$

Total Unbalanced Moment Capacity (positive steel unchanged):

$$M_{ub2} := \frac{Mn_t + Mn_b}{\gamma_f} \qquad\qquad M_{ub2} = 456.429\,\text{kip·in}$$

Lateral Capacity of Slab Based on Test Setup:

$$F_{flex2} := \frac{M_{ub2}}{60 \cdot \text{in}} \qquad\qquad F_{flex2} = 7.607\,\text{kip}$$

A.3.2 Shear Capacity of Slab Based on ACI 318-2002

Concrete shear strength is controlled by equation 11-35 of section 11.12.2.1 of ACI 318-02:

$$V_c := \frac{4 \cdot \sqrt{4000}}{1000} \cdot \text{ksi·b}_0 \cdot d \qquad\qquad V_c = 50.154\,\text{kip}$$

ACI 318 limits the shear acting on the critical section of a flat plate slab (chpt. 21 provisions) to 0.4:

$$V_u := .40 \cdot V_c \qquad\qquad V_u = 20.061\,\text{kip}$$

Moment acting on slab to cause a punching failure:

$$M_{shear} := \left(\frac{V_c - V_u}{b_0 \cdot d}\right) \cdot \frac{Jc}{\gamma_v} \qquad\qquad M_{shear} = 386.764\,\text{kip·in}$$

Control specimen shear capacity:

$$F_{shear} := \frac{M_{shear}}{60 \cdot \text{in}} \qquad\qquad F_{shear} = 6.446\,\text{kip}$$

A.3.3 Moment Capacity of Slab Based on FEMA 356/Nov 2000

Chapter 6 of FEMA 356 covers stiffness and strength evaluation of concrete structures. 6.5.4.3 discusses strength evaluation of slab-column moment frames. Moment capacity is to be calculated in accordance with ACI 318, with the following modification:

$$\text{effective width} = c + 5$$

The lateral capacity of the system is therefore increased over that of the previous ACI calculations. An equivalent amount of top steel contributes to the flexural capacity, but four positive reinforcing bars resist unbalanced moment as well:

$$As_b := 4 \cdot .196 \cdot in^2 \qquad\qquad As_b = 0.784\, in^2$$

$$a := \frac{As_b \cdot f_y}{.85 \cdot f_c \cdot w} \qquad\qquad a = 0.543\, in$$

$$Mn_b := As_b \cdot f_y \cdot \left(d - \frac{a}{2}\right) \qquad\qquad Mn_b = 140.119\, kip \cdot in$$

$$M_{ub2} := \frac{Mn_t + Mn_b}{\gamma_f} \qquad\qquad \boxed{M_{ub2} = 567.878\, kip \cdot in}$$

$$F_{flex2} := \frac{M_{ub2}}{60 \cdot in} \qquad\qquad \boxed{F_{flex2} = 9.465\, kip}$$

A.3.4 Shear Capacity of Slab Based on FEMA 356

FEMA 6.5.4.3 states the shear capacity due to unbalanced moment should be calculated using ACI 318, without any modifications. The lateral capacity has therefore been calculated as:

$$M_{shear} = 386.764\,kip{\cdot}in \qquad F_{shear} = 6.446\,kip$$

A.4 CFRP STIRRUP CONNECTION UPGRADE DESIGN

Shear reinforcement must be provided to upgrade the test specimen connection so the specimen will not punch when loaded laterally. This will be accomplished by increasing the ACI critical perimeter until the slab's concrete shear strength can resist the shear stress from combined gravity shear and unbalance moment. To increase the critical perimeter, carbon fiber reinforce polymer shear stirrups will be added in perimeters around the slab-column interface. Two different stirrup layouts will be designed.

When subjected to lateral loads, punching is controlled by the amount of unbalanced moment acting on the flat-plate connection because gravity shear is constant. Therefore, the shear stress acting on the critical perimeter cannot exceed a stress corresponding to the maxim probable moment capacity of the slab. (Whether or not the behavior is ductile is then a matter of detailing) Calculate the critical perimeter should be calculated based on the probable moment capacity of the section.

Control specimen properties:

$$f_c := 4.5{\cdot}ksi \qquad f_y := 60{\cdot}ksi \qquad f_u := 1.25{\cdot}f_y \qquad \gamma_f := .6 \qquad \gamma_v := .4$$

$$h := 4.5{\cdot}in \qquad d := 3.25{\cdot}in \qquad c := 12{\cdot}in \qquad b_1 := (c + d)$$

178

$$b_0 := (c + d) \cdot 4 \qquad\qquad b_0 = 61 \, in$$

$$Jc := \frac{b_1 \cdot d \cdot (4 \cdot b_1) + d^3}{3} \qquad\qquad Jc = 1.019 \times 10^3 \, in^3$$

Must satisfy ACI 318-02 11.12.6.2 for combined gravity shear and unbalanced moment, using the probable slab moment resistance:

$$\frac{V_u}{b_0 \cdot d} + \frac{\gamma_v \cdot M_{probable}}{\left(\dfrac{J}{c}\right)} \leq v_c$$

Calculate the probable moment based on the effective width (c+3h), including bars at the edge of this region. See previous section for detailed calculations. All longitudinal bars are no. 4.

$$w := c + 3 \cdot h \qquad\qquad w = 25.5 \, in$$

$$As_t := 6 \cdot .196 \cdot in^2 \qquad\qquad As_t = 1.176 \, in^2$$

$$As_b := 2 \cdot .196 \cdot in^2 \qquad\qquad As_b = 0.392 \, in^2$$

Probable moment capacity of negative ste

$$a := \frac{As_t \cdot f_u}{.85 \cdot f_c \cdot w} \qquad\qquad a = 0.904 \, in$$

$$Mprob_t := As_t \cdot f_y \cdot \left(d - \frac{a}{2}\right) \qquad\qquad Mprob_t = 197.417 \, kip \cdot in$$

Moment capacity of positive steel:

$$a := \frac{As_b \cdot f_u}{.85 \cdot f_c \cdot w} \qquad\qquad a = 0.301\,\text{in}$$

$$Mprob_b := As_b \cdot f_y \cdot \left(d - \frac{a}{2} \right) \qquad\qquad Mprob_b = 72.895\,\text{kip·in}$$

Total Unbalanced Moment Capacity

$$Mprob_{ub} := \frac{Mprob_t + Mprob_b}{\gamma_f} \qquad\qquad Mprob_{ub} = 450.521\,\text{kip·in}$$

A.4.1 Determine the Number of CFRP Stirrups Perimeters

Concentric flat-slab punching tests were performed by Binicci and Bayrak at the University of Texas. In these tests the first perimeter of CFRP shear stirrups we positioned at a distance of d/4 from the column face and additional shear reinforcement was provided at a distance d/2. Shear stress is then calculated at a distance d/2 from the outermost CFRP shear stirrup perimeter.

Determine the required critical perimeter, b0, by iterating the number of reinforcing perimeters at the distances defined by Binicci and Bayrak. Try 3, 4, and 5 reinforcing perimeters:

Gravity shear and shear resistance was determined in A.3.2:

$$V_g := 20.061 \cdot \text{kip}$$

Shear resistance of concrete is defined in section 11.12.6.2 of ACI 318-02 as:

$$v_c := 2 \cdot \sqrt{4000} \cdot \text{psi} \qquad\qquad v_c = 126.491\,\text{psi}$$

180

Three reinforcing perimeters:

$$b0_3 := \left(c + \frac{7d}{2} \right) \cdot 4$$

$$b0_3 = 93.5 \, in$$

$$b1_3 := \left(c + \frac{7d}{2} \right)$$

$$Jc_3 := \frac{b1_3 \cdot d \cdot \left(4 \cdot b1_3 \right) + d^3}{3}$$

Shear Stress:

$$v_{probable3} := \frac{V_g}{b0_3 \cdot d} + \frac{\gamma_v \cdot Mprob_{ub}}{\left(Jc_3 \right)}$$

$$v_{probable3} = 141.762 \, psi$$

Three reinforcing perimeters is not sufficient, try 4:

$$b0_4 := \left(c + \frac{9d}{2} \right) \cdot 4$$

$$b0_4 = 106.5 \, in$$

$$b1_4 := \left(c + \frac{9d}{2} \right)$$

$$Jc_4 := \frac{b1_4 \cdot d \cdot \left(4 \cdot b1_4 \right) + d^3}{3}$$

Shear Stress:

$$v_{probable4} := \frac{V_g}{b0_4 \cdot d} + \frac{\gamma_v \cdot Mprob_{ub}}{\left(Jc_4 \right)}$$

$$v_{probable4} = 116.405 \, psi$$

Four reinforcing perimeters are sufficient, calculate 5:

$$b0_5 := \left(c + \frac{11d}{2} \right) \cdot 4$$

$$b0_5 = 119.5 \, in$$

$$b1_5 := \left(c + \frac{11d}{2} \right)$$

$$Jc_5 := \frac{b1_5 \cdot d \cdot \left(4 \cdot b1_5 \right) + d^3}{3}$$

Shear Stress:

$$v_{probable5} := \frac{V_g}{b0_5 \cdot d} + \frac{\gamma_v \cdot Mprob_{ub}}{(Jc_5)}$$

$$v_{probable5} = 98.111 \, psi$$

Use four reinforcing perimeters to upgrade the test specimen connections, using the spacing defined by Binicci and Bayrak.

A.4.2 CFRP Shear Stirrup Design

Each shear stirrup layout has a total of 8 cored holes per-perimeter (Figure A.9). To determine cross-sectional areas, design FRP-stirrups to resist the excess shear stress calculated using the probable moment resistance.

Layout A4-S   Layout B4-S
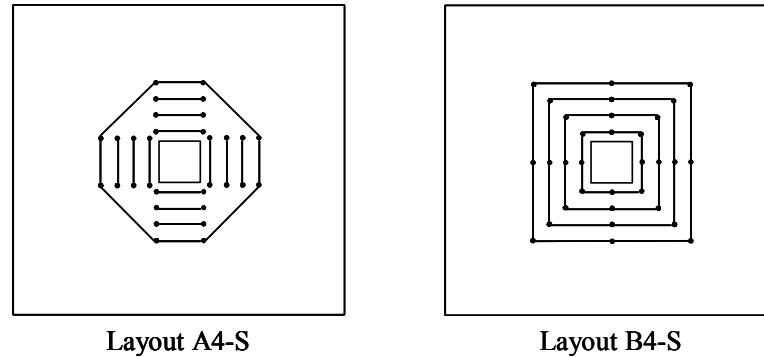
Figure A.9 Connection Upgrade Layouts

Shear resisted by the CFRP stirrups:

$$v_{frp} \geq \frac{V_u}{b_0 \cdot d} + \frac{\gamma_v \cdot M_u}{\left(\dfrac{J}{c}\right)} - v_c$$

182

$$v_{frp} := \frac{V_g}{b_0 \cdot d} + \frac{\gamma_v \cdot Mprob_{ub}}{Jc} - v_c \qquad\qquad v_{frp} = 0.152\,ksi$$

CFRP properties are reported by FYFE Co. Use a safety factor of 1/3, as defined by Binicci and Bayrak:

$$f_u := 127 \cdot ksi \qquad\qquad \beta := \frac{1}{3} \qquad\qquad t := \frac{1}{16} \cdot in$$

Total shear to be resisted by the CFRP Stirrups:

$$V_{excess} := v_{frp} \cdot b_0 \cdot d \qquad\qquad V_{excess} = 30.037\,kip$$

Required width of fiber, per 8 hole layout:

$$w_{frp} := \frac{V_{excess}}{f_u \cdot \beta \cdot t \cdot 8} \qquad\qquad w_{frp} = 1.419\,in$$

Choose two CFRP stirrups having widths of 0.75 inches, per hole. For upgrade pattern A4-S, CFRP strips must be cut to a length such that the strip passes two- times through each hole. Upgrade pattern B4-S provides two stirrups per hole using single-pass CFRP strips. Details of the CFRP shear reinforcement through the cored holes are shown in Figure A.10 and Figure A.11.
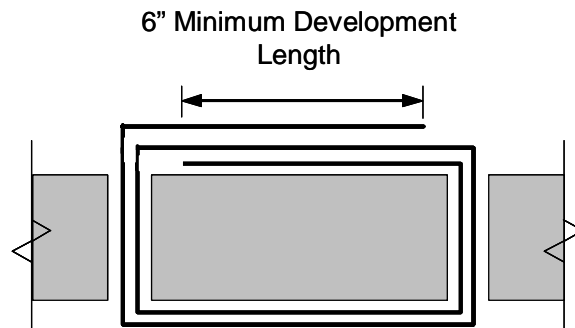
Figure A.10 Connection Upgrade A4 CFRP Shear Stirrup Detail

183

6" Minimum Development
Length
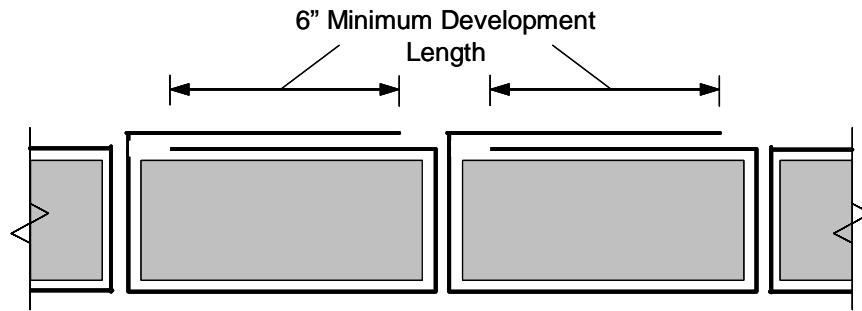
Figure A.11 Connection Upgrade B4 CFRP Shear Stirrup Detail

Table A.11 shows the required CFRP strip lengths for connection upgrades A4 and B4.

Table A.11 Required Carbon Fiber Strip Lengths for Upgrade Designs A4-S and B4-S

Upgrade A4		Upgrad B4	
Perimeter (from column)	Length (in)	Perimeter (from column)	Length (in)
1 through 4	86	1	30
		2	36
		3	40
Diagonal at 4	32	4	44

184

APPENDIX B

Structural Drawings

B.1 **S**TRUCTURAL **D**ETAILS FOR THE **T**EST **F**RAME AND **S**ETUP

Figure B.1 through Figure B.7 show the details for the test frame and setup, including all connections. Slab details are shown in Figure B.8 and Figure B.9.

North

W12×152
W10×88
MTS HYDRAULIC ACTUATOR
6.00"
3'
1'-10.48"
10.94"
S 1
2'-6.00"
S 3
W10×88
TEST SPECIMEN
LL3x3x5/16
W14×257
S 1
Ø1.38"
S 2
2'-6.00"
8'-10.11"
2'-11.00"
6'-11.625"
2'-11.50"
6'-4.11"
3.00"
C6x13
VERTICAL
JACK
4'-6.69"
W14×426
3'-0.61"
W12×39
(TYP)
1'-0.19"

4'   4'   4'   4'

NORTH ELEVATION TEST SETUP

SLAB-COLUMN CONNECTION TESTS

1
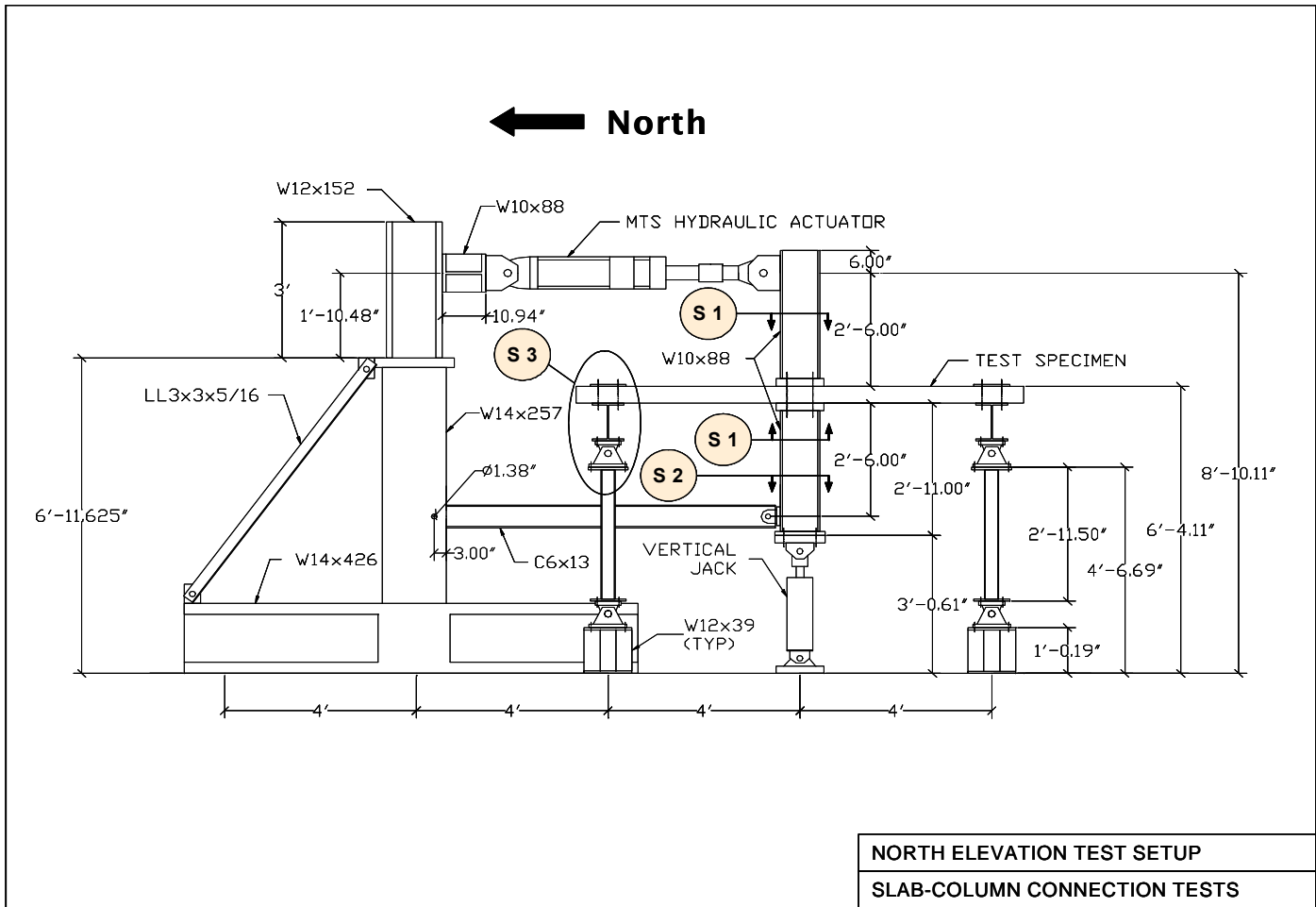
Figure B.1 North Elevation Test Setup

West

2'-8.00" 2'-8.00" 2'-8.00"

ALL TEST COMPONENTS AND
DIMENSIONS LISTED IN DRAWING
S1. OUT OF PLANE COMPONENTS
AND DIMENSIONS LISTED IN THIS
DRAWING.

S 4

S 5

W10×39

3" DIAMETER EXTRA
STRONG PIPE (TYP)

4X4 WOOD BLOCKS
(TYP)

4' 4'

WEST ELEVATION TEST SETUP

SLAB-COLUMN CONNECTION TESTS
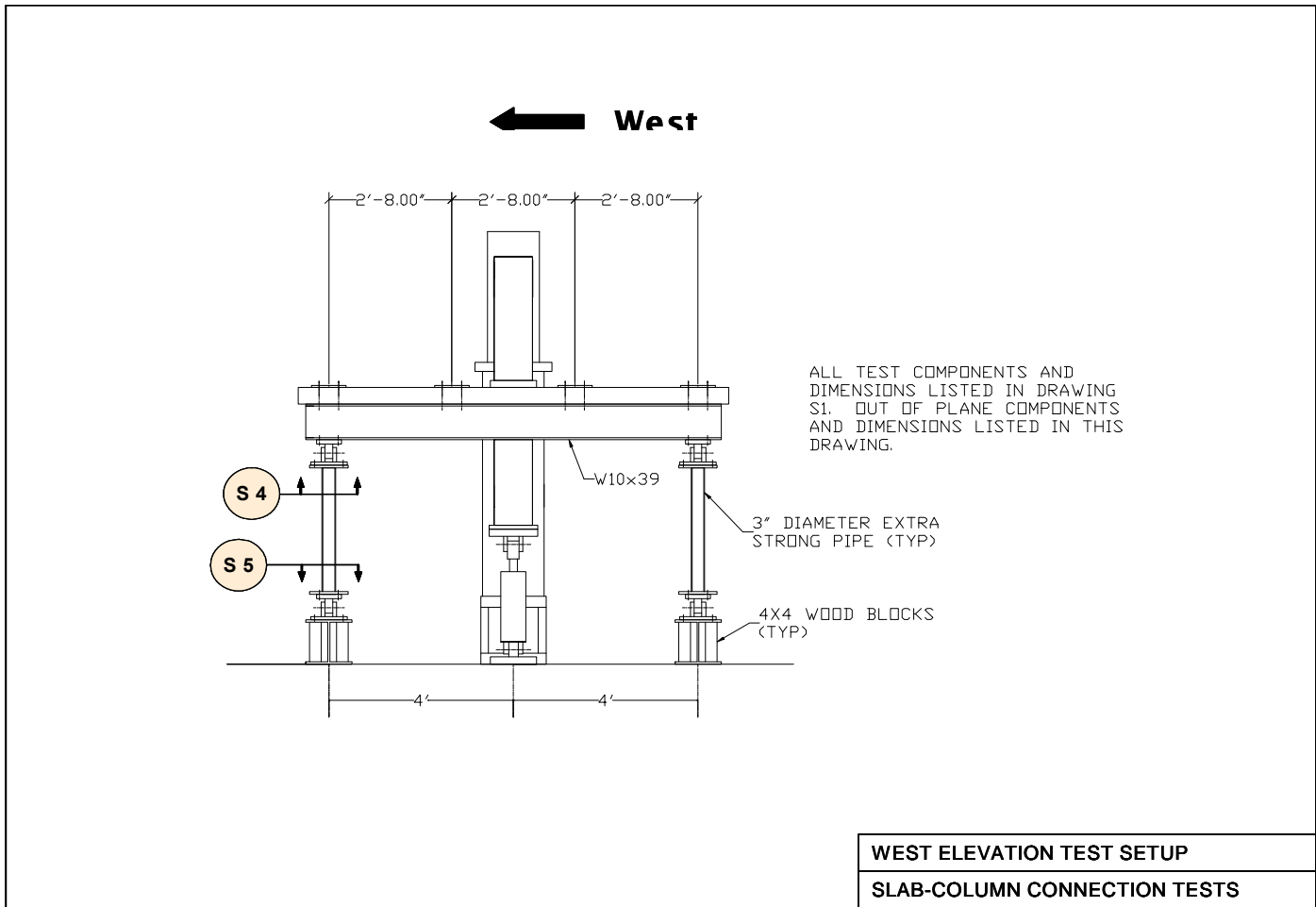
Figure B.2 West Elevation Test Setup

1'

$1\frac{1}{2}''$

$3''$

$3''$

$3''$

$1\frac{1}{2}''$

2"

$2\frac{13}{16}''$

BASE PLATE

ASTM GRADE 36 STEEL

WELD SCHEDULE

70 KSI FILLET WELDS
CENTER COLUMN ON BASE PLATE
TOP FLANGE: 3 PASSES PER SIDE
WEB: 1 PASS PER SIDE

COLUMN

ASTM GRADE 50 STEEL
W 10×88

BOLTS

ASTM A490 BOLTS
7/8" DIAMETER

DETAIL S1

SLAB-COLUMN CONNECTION TESTS
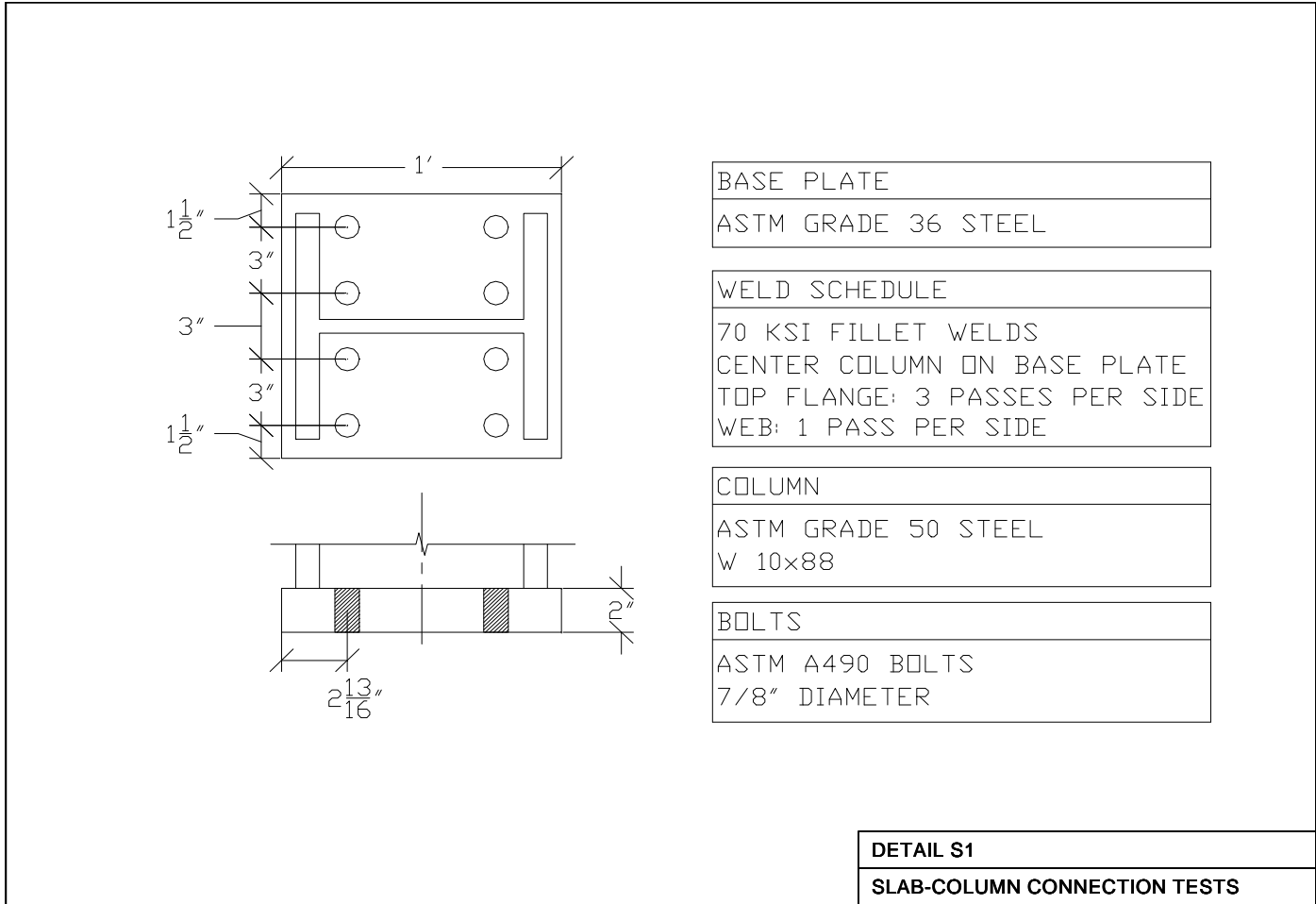
Figure B.3 Column Detail

LABORATORY
EYE BRACKET
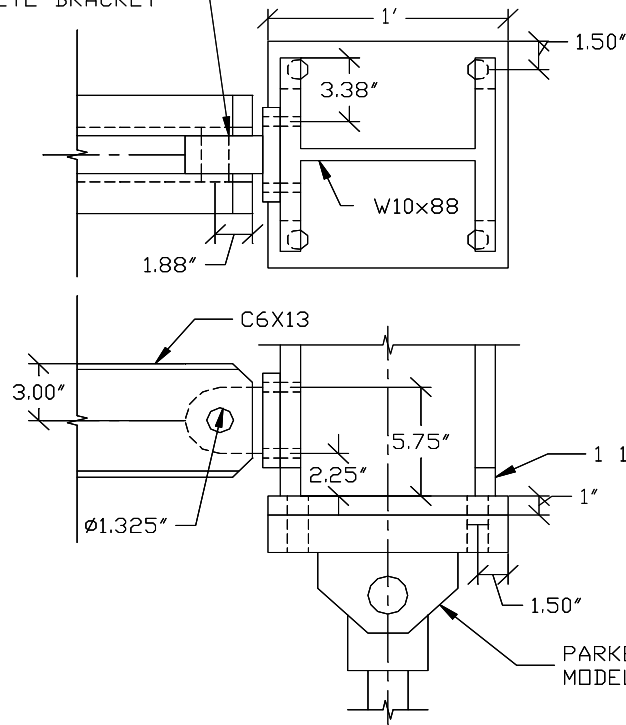
1'

1.50"

3.38"

W10×88

1.88"

| BASE PLATE |
| ASTM GRADE 36 STEEL |

| WELD SCHEDULE |
| 70 KSI FILLET WELDS
CENTER COLUMN ON BASE PLATE
TOP FLANGE: 3 PASSES PER SIDE
WEB: 1 PASS PER SIDE |

| BOLTS |
| ASTM A490 BOLTS
VERTICAL JACK: 7/8" DIAMETER
HORZ. STRUT: 1/2" DIAMETER |

C6X13

3.00"

5.75"

2.25"

ø1.325"

1 1/2" CHAMFER (TYP)

1"

1.50"

PARKER SERIES 3H CLEVIS BRACKET.
MODEL NUMBER 69213.

1

DETAIL S2

SLAB-COLUMN CONNECTION TESTS

Figure B.4 Lateral Strut Connection Detail

8.00"

4.50"

2.00"

0.50"

10"×10" STEEL PLATE

1.50"

1.53"

PARKER SERIES 3H HEAVY DUTY
HYDRAULIC CLYLINDER: CLEVIS
BRACKET MODEL NUMBER 69209,
EYE BRACKET MODEL NUMBER 85362,
PIN MODEL NUMBER 68372.

W10×39

SEE 10" STRUT BASE PLATE
DETAIL FOR DIMENSIONS.

DETAIL S3

SLAB-COLUMN CONNECTION TESTS

Figure B.5 Strut to Spreader Beam to Slab Connection

10"

1.25"

7.50"

1.25"

0.75"

BASE PLATE
ASTM GRADE 36 STEEL

WELD SCHEDULE
70 KSI FILLET WELDS CENTER COLUMN ON BASE PLATE 1 PASS AROUND TUBE

COLUMN
ASTM GRADE 50 STEEL 3" DIAMETER, EXTRA STRONG PIPE

BOLTS
ASTM A490 BOLTS 7/8" DIAMETER

DETAIL S4
SLAB-COLUMN CONNECTION TESTS

Figure B.6 Top Strut Base-Plate Detail

9"

2"

4.95"

2"

0.50"

BASE PLATE
ASTM GRADE 36 STEEL

WELD SCHEDULE
70 KSI FILLET WELDS CENTER COLUMN ON BASE PLATE 1 PASS AROUND TUBE

COLUMN
ASTM GRADE 50 STEEL 3" DIAMETER, EXTRA STRONG PIPE

BOLTS
ASTM A490 BOLTS 7/8" DIAMETER

DETAIL S5
SLAB-COLUMN CONNECTION TESTS
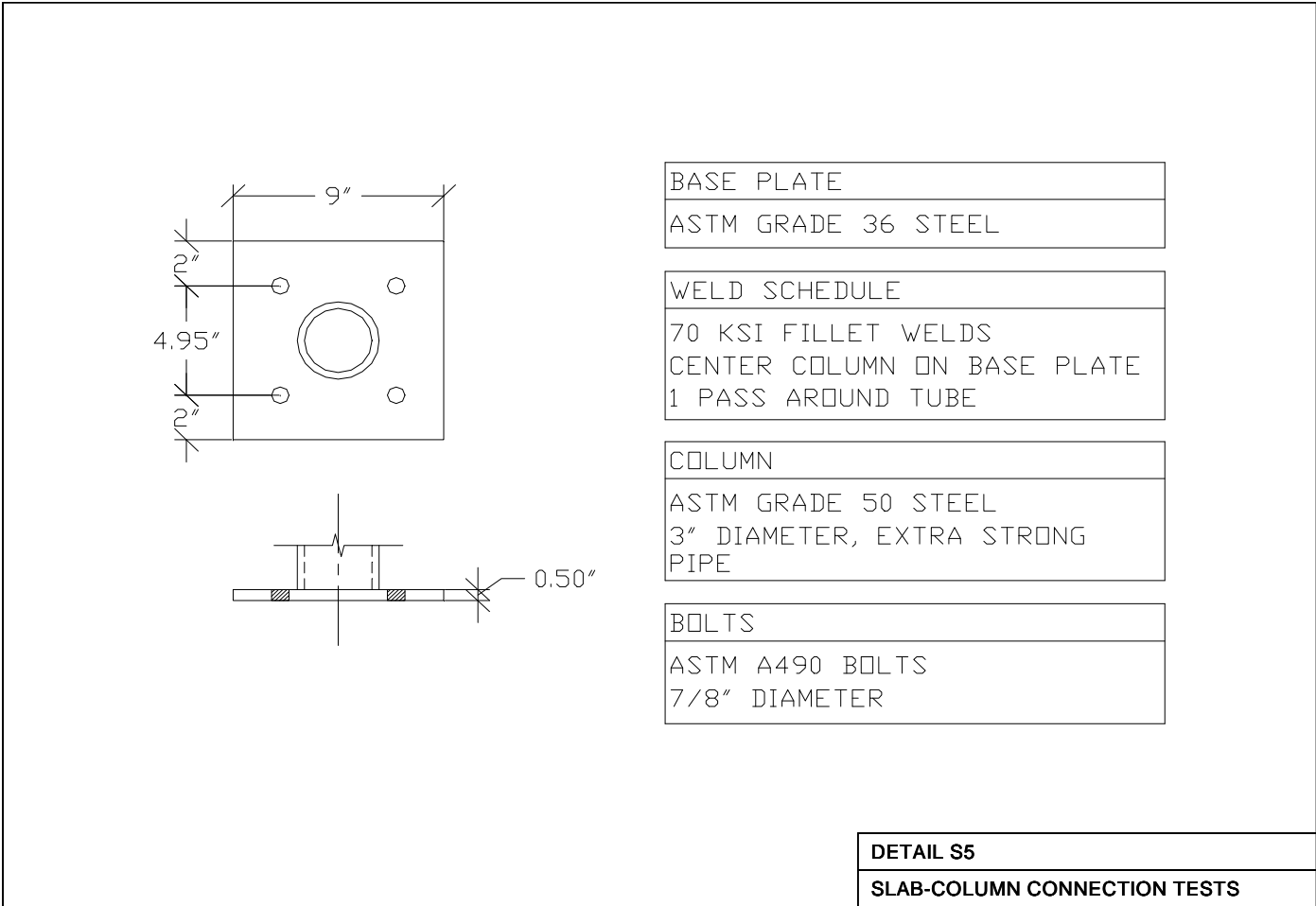
Figure B.7 Bottom Strut Base-Plate Detail

B.2 SLAB DETAILS

TOP STEEL   BOTTOM STEEL

MIDDLE STRIP   COLUMN STRIP   MIDDLE STRIP MIDDLE STRIP   COLUMN STRIP   MIDDLE STRIP

C+3H

9'-4.00" 8'

8'

9'-4.00"

REBAR SCHEDULE

ALL REINFORCING BARS SPECIFIED AS ASTM GRADE 60 STEEL
ALL REINFORCING BARS ARE #4 DIAMETER BARS
REINFORCING BAR LAYOUT IS THE SAME IN PERPENDICULAR DIRECTIONS

STEEL LOCATION	SLAB ZONE	DIMENSION (IN)	ρ (%)	NUMBER OF BARS	BAR SPACING
TOP STEEL	COLUMN STRIP	48	1.03	8	SEE BELOW
	ACI EFFECTIVE WIDTH	26	1.42	6	2 BARS @ 4" ABOUT CENTERLINE REMAING BARS EVENLY SPACED IN ZONE
	ONE-HALF REMAINING ZONE	11	0.56	1	BAR EVENLY SPACED IN ZONE
	MIDDLE STRIP	48	0.51	4	SEE BELOW
	ONE-HALFAREA	24	0.51	2	BARS EVENLY SPACED IN ZONE
BOTTOM STEEL	COLUMN STRIP	48	0.51	4	2 BARS @ 4" ABOUT CENTERLINE REMAINING BARS EVENLY SPACED IN ZONE
	MIDDLE STRIP	48	0.51	4	SEE BELOW
	ONE-HALFZONE	24	0.51	2	BARS EVENLY SPACED IN ZONE

TYPICAL REINFORCING BAR LAYOUT

SLAB-COLUMN CONNECTION TESTS

Figure B.8 Specimens C-02, A4-S and B4-S Details

193

REBAR SCHEDULE

ALL REINFORCING BARS SPECIFIED AS ASTM GRADE 60 STEEL
ALL REINFORCING BARS ARE #4 DIAMETER BARS
REINFORCING BAR LAYOUT IS THE SAME IN PERPENDICULAR DIRECTIONS

STEEL LOCATION	SLAB ZONE	DIMENSION (IN)	ρ (%)	NUMBER OF BARS	BAR SPACING
TOP STEEL	COLUMN STRIP	48	1.03	8	SEE BELOW
	ACI EFFECTIVE WIDTH	26	1.42	6	2 BARS @ 4" ABOUT CENTERLINE REMAING BARS EVENLY SPACED IN ZONE
	ONE-HALF REMAINING ZONE	11	0.56	1	BAR EVENLY SPACED IN ZONE
	MIDDLE STRIP	48	0.51	4	SEE BELOW
	ONE-HALFAREA	24	0.51	2	BARS EVENLY SPACED IN ZONE
BOTTOM STEEL	COLUMN STRIP	48	0.51	4	2 BARS @ 4" ABOUT CENTERLINE REMAING BARS EVENLY SPACED IN ZONE
	MIDDLE STRIP	48	0.51	4	SEE BELOW
	ONE-HALFZONE	24	0.51	2	BARS EVENLY SPACED IN ZONE

SPECIMEN 5 REINFORCING BAR LAYOUT

SLAB-COLUMN CONNECTION TESTS
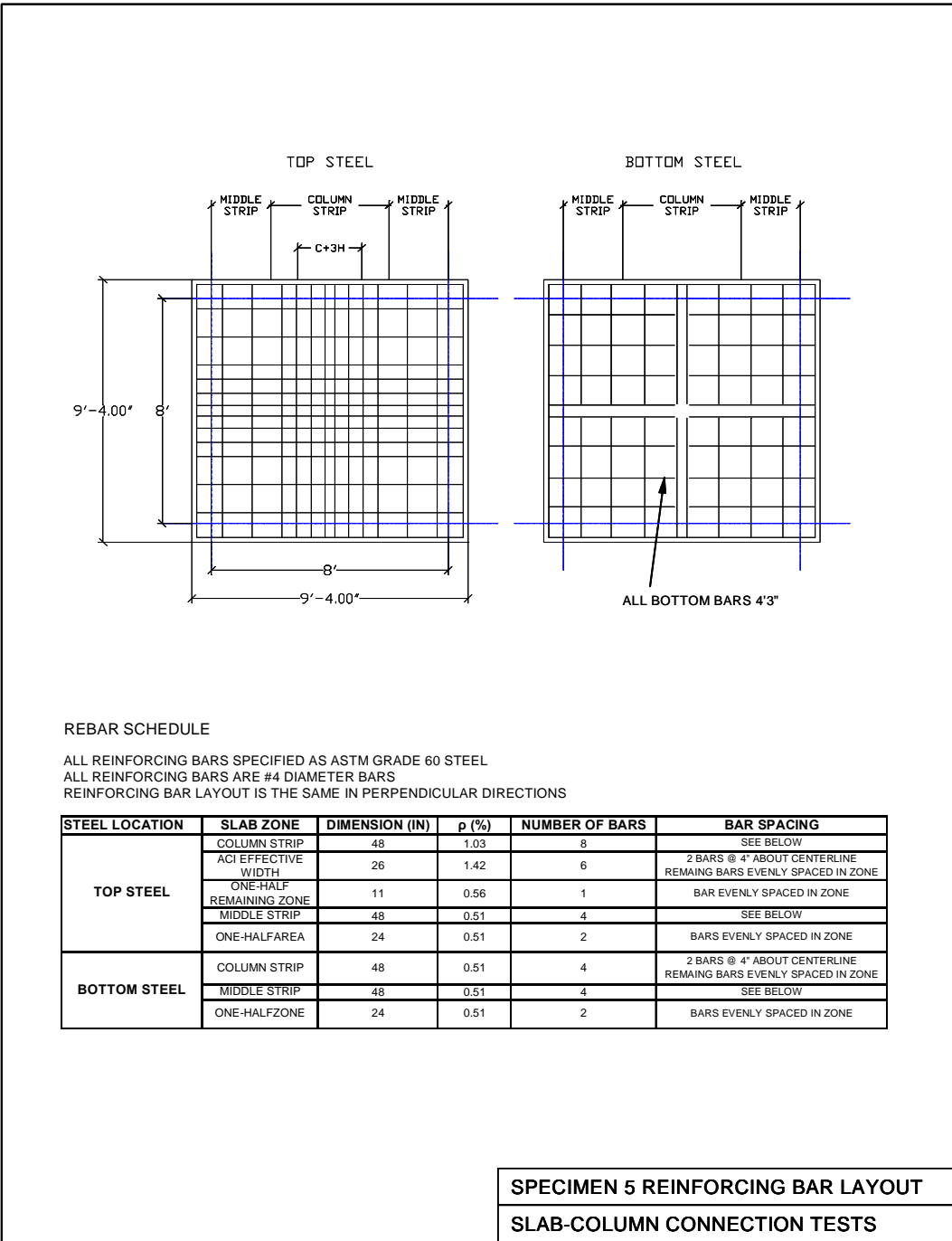
Figure B.9 Specimen C-63 Details

194

APPENDIX C

Chapter 4 Plots

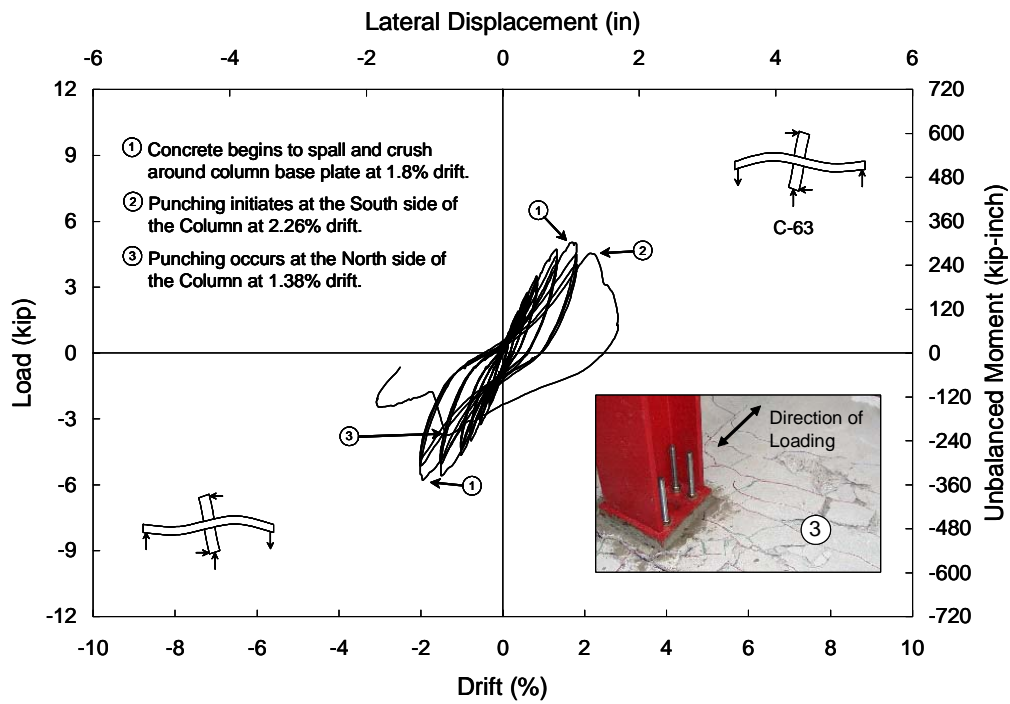## C.1   LOAD VERSUS DRIFT, ENGLISH UNITS

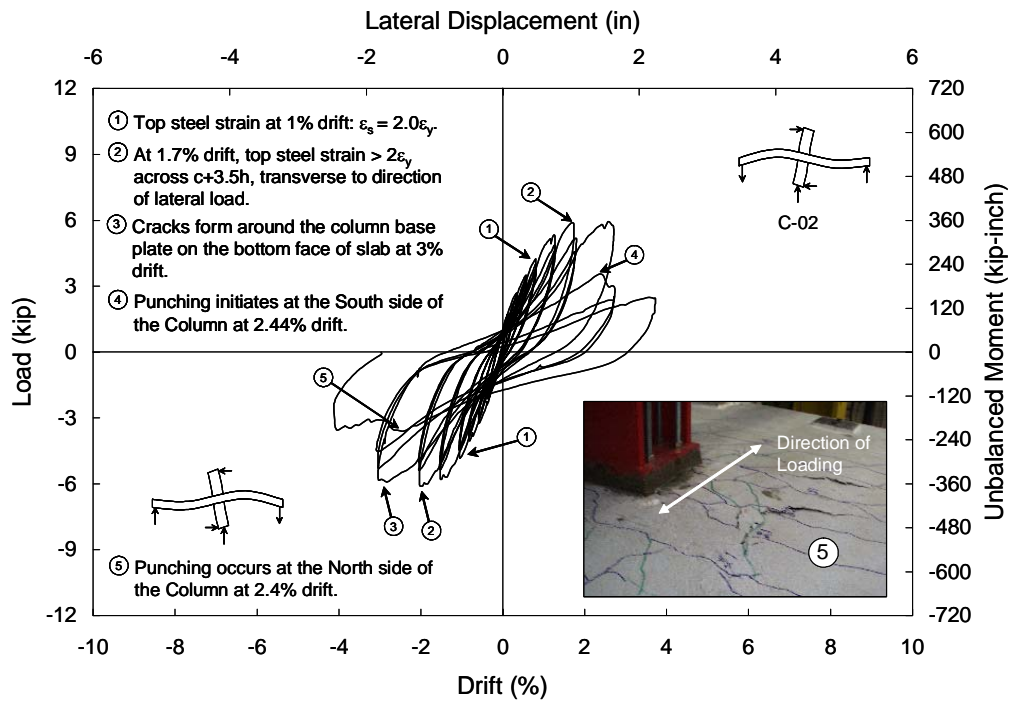*Figure C.1 Specimen C-63 Load versus Drift*

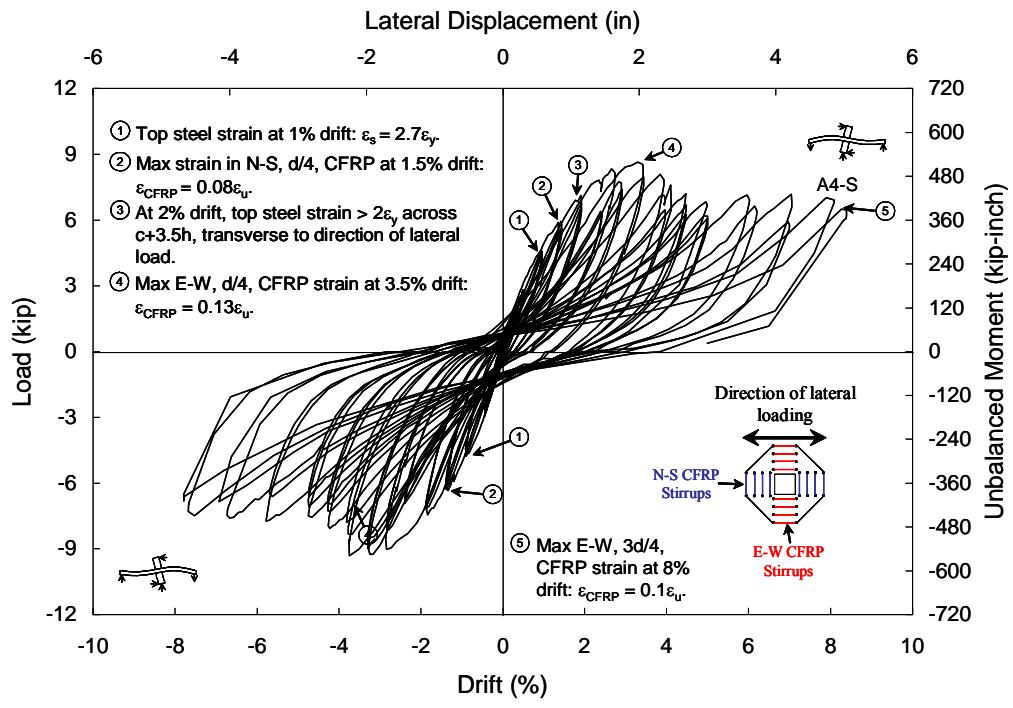*Figure C.2 Specimen C-02 Load versus Drift*
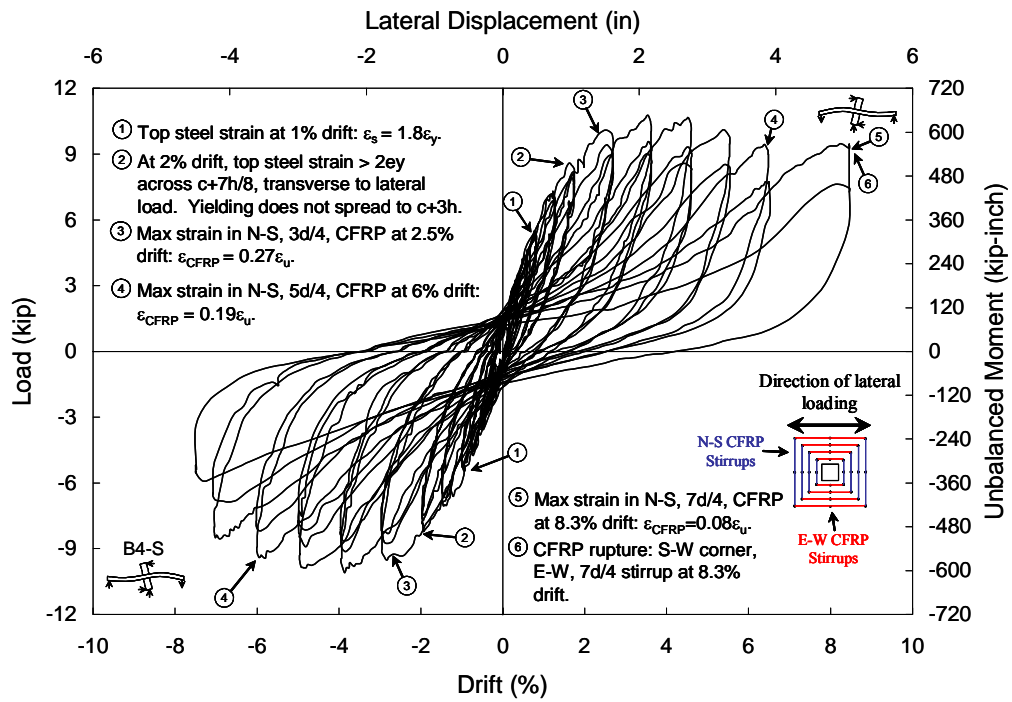
Figure C.3 Specimen A4-S Load versus Drift

Figure C.4 Specimen B4-S Load versus Drift

C.2 RESIDUAL GRAVITY LOAD CARRYING CAPACITY TESTS
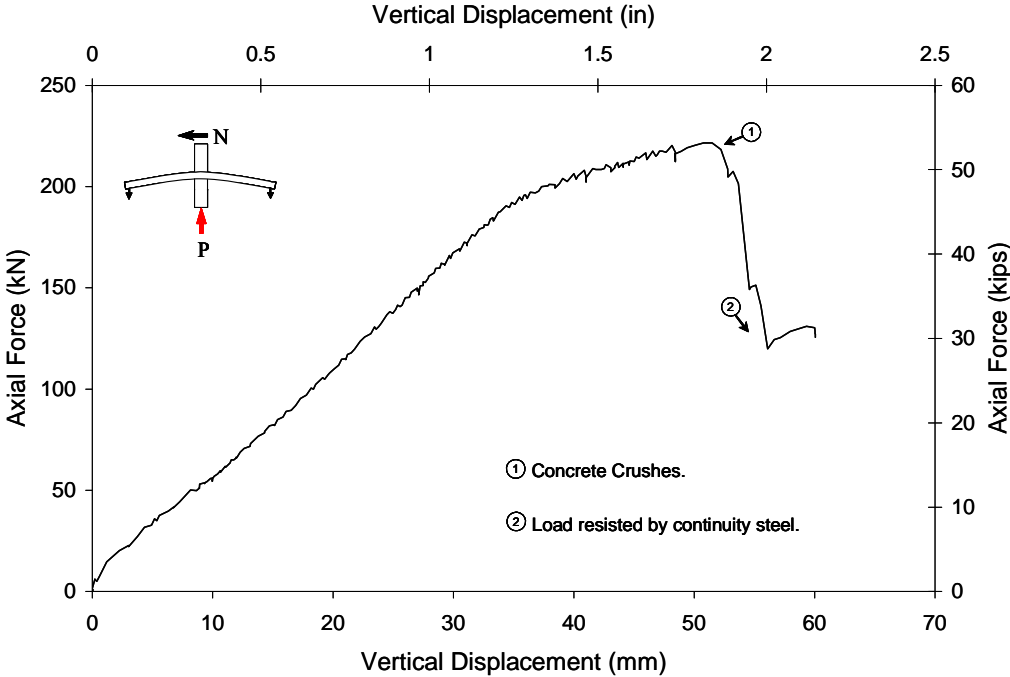
Figure C.5 Specimen C-63 Residual Gravity Load Test
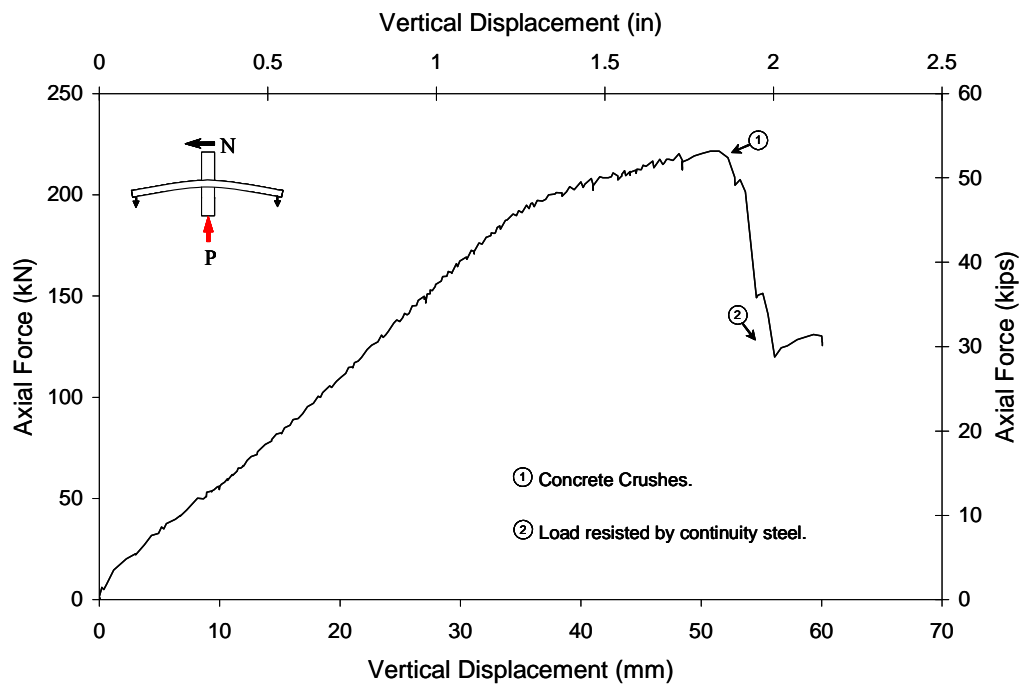
Figure C.6 Specimen C-02 Residual Gravity Load Test
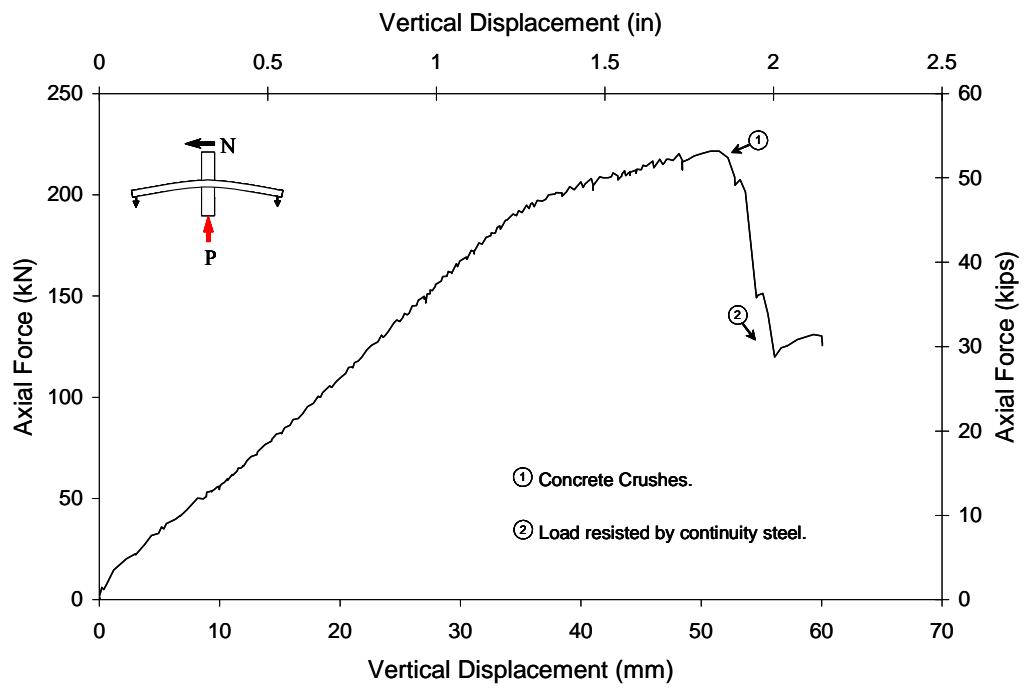
Figure C.7 Specimen A4-S Residual Gravity Load Test
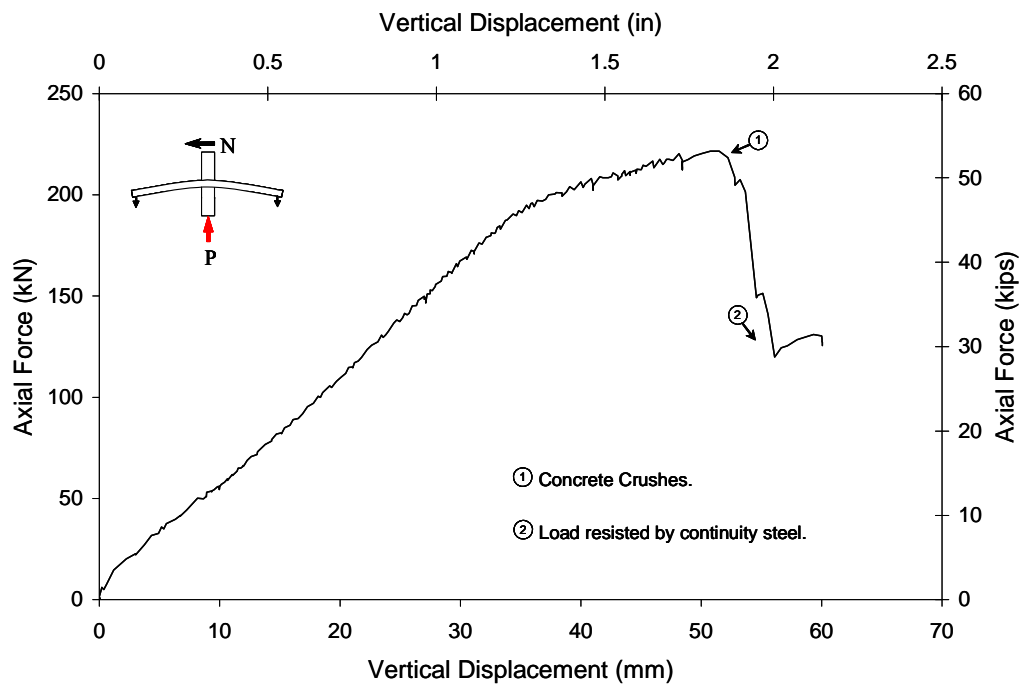
Figure C.8 Specimen B4-S Residual Gravity Load Test

APPENDIX D

Ductility Calculations

D.1   **C++ C**ODE

```
//              Hysterysis Parameters
#include <iostream.h>
#include <math.h>
#include <fstream.h>
#include <iomanip.h>
int main ()
{
        double V1, V2;   //i and i+1 momentK
        double D1, D2;         //i and i=1 rotationK
        double Ai;      //ith area
        double Vmax,    //max'K and min'K
               DVmax,
               Vmin,
               DVmin,
               Dmax,
               VDmax,
               Dmin,
               VDmin,
               delta,
               K;

        int i;                  //cycle number
```

```cpp
    double H;                    //hyKteriKiK
    ifstream infile( "control.txt", ios::in);
    ofstream outfile( "test1.txt", ios::out);
    infile >> V1;          //readK moment and rotationK from data file
    infile >> D1;
    infile >> V2;
    infile >> D2;
    i=1;
    H=0;

    outfile << setw(15) << "cycle" << setw(15) << "Vmax" <<
setw(15) << "D(Vmax)" << setw(15) << "Vmin" << setw(15) << "D(Vmin)" <<
setw(15) <<"Dmax"<< setw(15) << "V(Dmax)" << setw(15) <<  "Dmin"<<
setw(15) << "V(Dmin)"<< setw(15) << "delta" << setw(15) << "K" << setw(15)
<< "H" <<endl<<endl;

        Vmax = 0;
        DVmax = 0;
        Vmin = 0;
        DVmin = 0;
        Dmax = 0;
        VDmax = 0;
        Dmin = 0;
        VDmin = 0;
        while (!infile.fail()){
            Ai=.5*(V1+V2)*(D2-D1);
            H = H + Ai;


            if (V2 > Vmax){
```

204

```cpp
                              Vmax = V2;
                              DVmax = D2;
                      }
                      if (V2 < Vmin){
                              Vmin = V2;
                              DVmin = D2;
                      }
                      if (D2 > Dmax){
                              Dmax = D2;
                              VDmax = V2;
                      }
                      if (D2 < Dmin){
                              Dmin = D2;
                              VDmin = V2;
                      }
                      if (V2 == 0){
                              delta = 0.5*(Dmax + fabs(Dmin));
                              K = 0.5*((VDmax/Dmax) + fabs((VDmin/Dmin)));
                              outfile << setprecision(6) << setw(15) << i;
                              outfile << setprecision(6) << setw(15) << Vmax<<
setprecision(6) << setw(15) << DVmax;
                              outfile << setprecision(6) << setw(15) << Vmin<<
setprecision(6) << setw(15) << DVmin;
                              outfile << setprecision(6) << setw(15) << Dmax<<
setprecision(6) << setw(15) << VDmax;
                              outfile << setprecision(6) << setw(15) << Dmin<<
setprecision(6) << setw(15) << VDmin;
```

205

```cpp
                              outfile << setprecision(6) << setw(15) << delta;
                              outfile << setprecision(6) << setw(15) << K;
                              outfile << setprecision(6) << setw(15) << H<<endl;
                              Vmax = 0;
                              Vmin = 0;
                              Dmax = 0;
                              Dmin = 0;
                              i=i+1;
                              H = 0;
                              V1 = V2;
                              D1 = D2;
                              infile >> V2;
                              infile >> D2;
                    }
                    else{
                              V1 = V2;
                              D1 = D2;
                              infile >> V2;
                              infile >> D2;
                    }
          }
     return 0;
     }
```

D.2 LOAD-DISPLACEMENT DUCTILITY FACTORS

All data compiled from C++ programs was input into matricies in *MathCad 2001*. A copy of the spreadsheet used to calculate specimen C-63 ductility parameters are presented. Results for the other specimens are presented.

D.2.1 Specimen C-63

Define variables used in ductility calculations:

$$n := \text{rows}\left(HP_1\right) \qquad i := 1, 2 .. n \qquad m := \text{rows}(\text{Back})$$

$$V_{max_i} := HP1_{i,1} \cdot kip \qquad \qquad \Delta_{max_i} := HP1_{i,2} \cdot in$$

$$Kt1_i := HP1_{i,3} \cdot \frac{kip}{in} \qquad \qquad w1_i := HP1_{i,4} \cdot kip \cdot in$$

$$V_{backbone_j} := Back_{j,1} \qquad \qquad \Delta_{backbone_j} := Back_{j,2}$$

$$\Delta_{Max} := \max\left(\Delta_{max}\right) \qquad \qquad \Delta_{Max} = 1.769 in$$

Define initial stiffness:

$$K_1 := \frac{V_{backbone_2}}{\Delta_{backbone_2}} \cdot \frac{kip}{in} \qquad \qquad K_1 = 12.641\frac{kip}{in}$$

Define corresponding displacement:

$$V_{Max} := \max\left(V_{max}\right) \qquad \qquad V_{Max} = 5.415 kip$$

$$\Delta_1 := \frac{V_{Max}}{K_1} \qquad \qquad \Delta_1 = 0.428 in$$

80% reduction in lateral load:

$$V_{80} := 0.8 \cdot V_{Max} \qquad\qquad V_{80} = 4.332 kip$$

Average Backbone Curve

Legend:
- Backbone (red)
- 0.8V (blue)
- K1 (black)
- delta 1 (cyan)
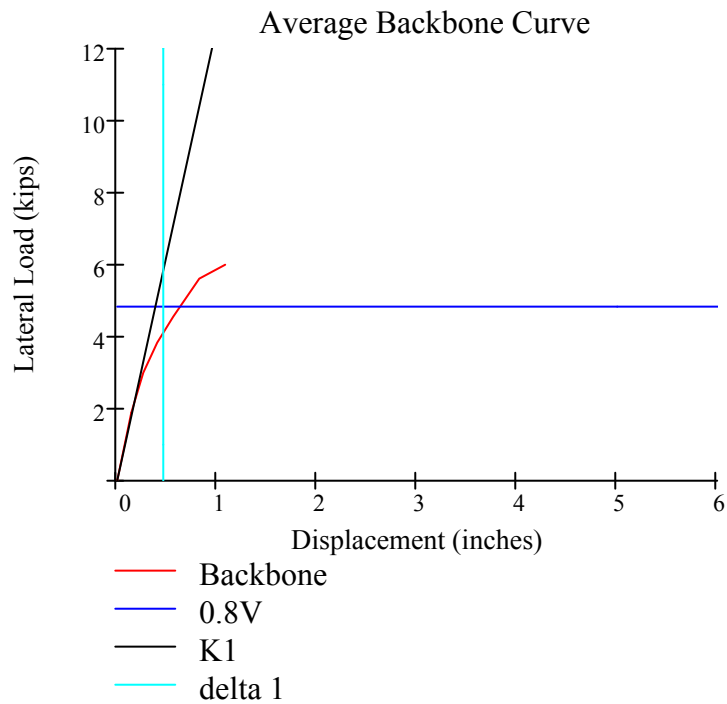
Displacement at 80% lateral load reduction:

$$\Delta_{80} := 1.1 \cdot in$$

Define ductility parameters:

$$\mu_{\Delta\_80} := \frac{\Delta_{80}}{\Delta_1} \qquad\qquad N_\Delta := \sum_{i=1}^{n} \frac{\Delta_{max_i}}{\Delta_1}$$

$$W := \frac{1}{V_{Max} \cdot \Delta_1} \cdot \sum_{i=1}^{n} w1_i \cdot \left(\frac{Kt1_i}{K_1}\right) \cdot \left(\frac{\Delta_{max_i}}{\Delta_1}\right)^2$$

208

Ductility parameters corresponding to the 80% loss in lateral load:

$$k := \begin{vmatrix} l \leftarrow \text{rows}\left(HP_1\right) \\ \text{for } a \in 1..l \\ \quad \text{return } a \text{ if } \Delta_{\max_a} > \Delta_{80} \end{vmatrix}$$

$$k := n - 1$$

$$N_{\Delta\_80} := \sum_{i=1}^{k} \frac{\Delta_{\max_i}}{\Delta_1}$$

$$W_{80} := \frac{1}{V_{Max} \cdot \Delta_1} \cdot \sum_{i=1}^{n} w_{1_i} \cdot \left(\frac{Kt_{1_i}}{K_1}\right) \cdot \left(\frac{\Delta_{\max_i}}{\Delta_1}\right)^2$$

Total moment-rotation ductility parameters:

$$N_{\Delta\_Total} := \sum_{i=1}^{k} \frac{\Delta_{\max_i}}{\Delta_1}$$

$$W_{Total} := \frac{1}{V_{Max} \cdot \Delta_1} \cdot \sum_{i=1}^{n} w_{1_i} \cdot \left(\frac{Kt_{1_i}}{K_1}\right) \cdot \left(\frac{\Delta_{\max_i}}{\Delta_1}\right)^2$$

C-63 ductility parameters:

$K_1 = 12.641\dfrac{\text{kip}}{\text{in}}$
$\qquad\qquad \mu_{\Delta\_80} = 2.568$

$V_{80} = 4.332\text{kip}$
$\qquad\qquad V_{Max} = 5.415\text{kip}$

$\Delta_{80} = 1.1\text{in}$
$\qquad\qquad \Delta_{Max} = 1.769\text{in}$

$N_{\Delta\_80} = 23.867$
$\qquad\qquad W_{80} = 26.741$

$N_{\Delta\_Total} = 23.867$
$\qquad\qquad W_{Total} = 26.741$

D.2.2 Specimen C-02

$K_1 = 11.469\dfrac{\text{kip}}{\text{in}}$
$\qquad\qquad \mu_{\Delta\_80} = 3.065$

$V_{80} = 4.79\text{kip}$
$\qquad\qquad V_{Max} = 5.987\text{kip}$

$\Delta_{80} = 1.6\text{in}$
$\qquad\qquad \Delta_{Max} = 1.74\text{in}$

$N_{\Delta\_80} = 29.482$
$\qquad\qquad W_{80} = 32.817$

$N_{\Delta\_Total} = 29.482$
$\qquad\qquad W_{Total} = 32.817$

D.2.3 Specimen A4-S

$$K_1 = 11.041 \frac{kip}{in} \qquad \mu_{\Delta\_80} = 5.926$$

$$V_{80} = 7.154 kip \qquad V_{Max} = 8.943 kip$$

$$\Delta_{80} = 4.8 in \qquad \Delta_{Max} = 4.854 in$$

$$N_{\Delta\_80} = 86.014 \qquad W_{80} = 118.853$$

$$N_{\Delta\_Total} = 86.014 \qquad W_{Total} = 118.853$$

D.2.4 Specimen B4-S

$$K_1 = 13.829 \frac{kip}{in} \qquad \mu_{\Delta\_80} = 5.9$$

$$V_{80} = 8.345 kip \qquad V_{Max} = 10.431 kip$$

$$\Delta_{80} = 4.45 in \qquad \Delta_{Max} = 4.793 in$$

$$N_{\Delta\_80} = 66.803 \qquad W_{80} = 107.515$$

$$N_{\Delta\_Total} = 73.157 \qquad W_{Total} = 118.146$$

D.3 MOMENT-ROTATION DUCTILITY PARAMETERS

Again, all data compiled from C++ programs was input into matricies in *MathCad 2001*. A copy of the spreadsheet used to calculate specimen C-63 ductility parameters are presented. Results for the other specimens are presented.

D.3.1 Specimen C-63

Define variables used in ductility calculations:

$$n := \text{rows}(HP_1) \qquad i := 1,2..n \qquad m := \text{rows}(Back) \qquad j := 1,2..m$$

$$d := 3.25 \cdot in \qquad\qquad b_o := 4 \cdot (12 \cdot in + d)$$

$$M_{max_i} := HP_{1_{i,1}} \cdot kip \cdot in \qquad\qquad \theta_{max_i} := HP_{1_{i,2}} \cdot rad$$

$$St_{1_i} := HP_{1_{i,3}} \cdot \frac{kip \cdot in}{rad} \qquad\qquad e_{1_i} := HP_{1_{i,4}} \cdot kip \cdot in \cdot rad$$

$$M_{backbone_j} := Back_{j,1} \qquad\qquad \theta_{backbone_j} := Back_{j,2}$$

$$\theta_{Max} := \max(\theta_{max}) \qquad\qquad \theta_{Max} = 0.024 rad$$

Define initial stiffness:

$$S_1 := \frac{M_{backbone_2}}{\theta_{backbone_2}} \cdot kip \cdot in \qquad\qquad S_1 = 5.51 \times 10^4 \, kip \cdot in$$

212

Define corresponding rotation:

$$M_{Max} := max(M_{max})$$ $$M_{Max} = 324.89 \text{kip·in}$$

$$\theta_1 := \frac{M_{Max}}{S_1}$$ $$\theta_1 = 5.897 \times 10^{-3} \text{rad}$$

80% reduction in unbalanced moment:

$$M_{80} := 0.8 \cdot M_{Max}$$ $$M_{80} = 259.912 \text{kip·in}$$

Average Backbone Curve

Backbone
0.8M
S1
theta 1
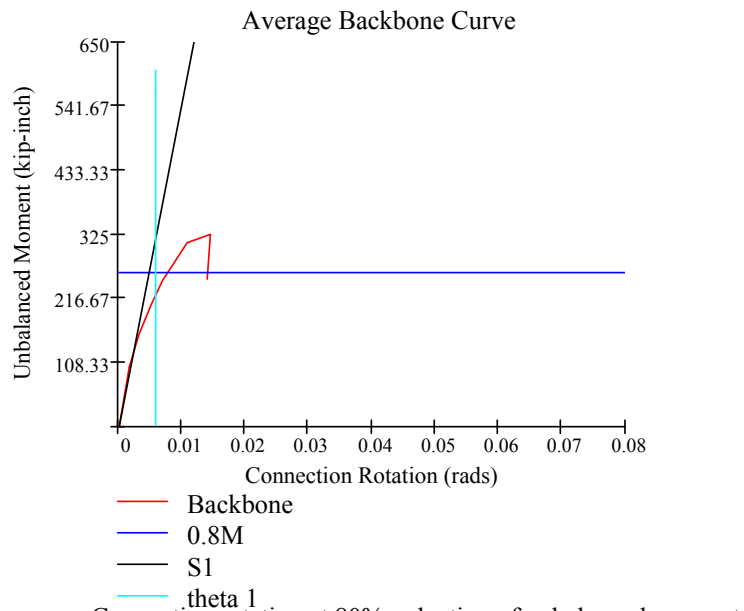
Connection rotation at 80% reduction of unbalanced moment:

$$\theta_{80} := 0.016 \cdot \text{rad}$$

Define ductility parameters:

$$\mu_{\theta\_80} := \frac{\theta_{80}}{\theta_1}$$ $$N_\theta := \sum_{i=1}^{n} \frac{\theta_{max_i}}{\theta_1}$$

$$E := \frac{1}{M_{Max} \cdot \theta_1} \cdot \sum_{i=1}^{n} e_{1_i} \cdot \frac{b_o}{d} \cdot \left(\frac{St_{1_i}}{S_1}\right) \cdot \left(\frac{\theta_{max_i}}{\theta_1}\right)^2$$

213

Ductility parameters corresponding to the 80% loss in unbalanced mom

$$k := \begin{array}{|l} 1 \leftarrow \text{rows}\left(HP_1\right) \\ \quad \text{for } a \in 1..1 \\ \quad\quad \text{return a if } \theta_{max_a} > \theta_{80} \end{array} \qquad\qquad k := n$$

$$N_{\theta\_80} := \sum_{i=1}^{k} \frac{\theta_{max_i}}{\theta_1}$$

$$E_{80} := \frac{1}{M_{Max} \cdot \theta_1} \cdot \sum_{i=1}^{k} e_{1_i} \cdot \frac{b_o}{d} \cdot \left(\frac{St_{1_i}}{S_1}\right) \cdot \left(\frac{\theta_{max_i}}{\theta_1}\right)^2$$

Total unbalanced moment-connection rotation ductility parameters:

$$N_{\theta\_Total} := \sum_{i=1}^{k} \frac{\theta_{max_i}}{\theta_1}$$

$$E_{Total} := \frac{1}{M_{Max} \cdot \theta_1} \cdot \sum_{i=1}^{k} e_{1_i} \cdot \frac{b_o}{d} \cdot \left(\frac{St_{1_i}}{S_1}\right) \cdot \left(\frac{\theta_{max_i}}{\theta_1}\right)^2$$

C-63 ductility parameters:

$$S_1 = 5.51 \times 10^4 \text{kip} \cdot \frac{\text{in}}{\text{rad}} \qquad \mu_{\theta\_80} = 2.713$$

$$M_{80} = 259.912 \text{kip·in} \qquad M_{Max} = 324.89 \text{kip·in}$$

$$\theta_{80} = 0.016 \text{rad} \qquad \theta_{Max} = 0.024 \text{rad}$$

$$N_{\theta\_80} = 25.821 \qquad E_{80} = 429.773$$

$$N_{\theta\_Total} = 25.821 \qquad E_{Total} = 429.773$$

D.3.2 Specimen C-02 Ductility Parameters

$$S_1 = 5.212 \times 10^4 \text{kip} \cdot \frac{\text{in}}{\text{rad}} \qquad \mu_{\theta\_80} = 3.192$$

$$M_{80} = 287.392 \text{kip·in} \qquad M_{Max} = 359.24 \text{kip·in}$$

$$\theta_{80} = 0.022 \text{rad} \qquad \theta_{Max} = 0.024 \text{rad}$$

$$N_{\theta\_80} = 29.034 \qquad E_{80} = 586.799$$

$$N_{\theta\_Total} = 29.034 \qquad E_{Total} = 586.799$$

D.3.3 Specimen A4-S Ductility Parameters

$$S_1 = 7.091 \times 10^4 \, \text{kip} \cdot \frac{\text{in}}{\text{rad}} \qquad \mu_{\theta\_80} = 7.269$$

$$M_{80} = 429.244 \text{kip·in} \qquad M_{Max} = 536.555 \text{kip·in}$$

$$\theta_{80} = 0.055 \text{rad} \qquad \theta_{Max} = 0.055 \text{rad}$$

$$N_{\theta\_80} = 97.909 \qquad E_{80} = 5.861 \times 10^3$$

$$N_{\theta\_Total} = 97.909 \qquad E_{Total} = 5.861 \times 10^3$$

D.3.4 Specimen B4-S Ductility Parameters

$$S_1 = 6.956 \times 10^4 \, \text{kip} \cdot \frac{\text{in}}{\text{rad}} \qquad \mu_{\theta\_80} = 6.891$$

$$M_{80} = 500.696 \text{kip·in} \qquad M_{Max} = 625.87 \text{kip·in}$$

$$\theta_{80} = 0.062 \text{rad} \qquad \theta_{Max} = 0.068 \text{rad}$$

$$N_{\theta\_80} = 77.066 \qquad E_{80} = 4.505 \times 10^3$$

$$N_{\theta\_Total} = 84.619 \qquad E_{Total} = 4.959 \times 10^3$$